TRANSMISSION LINE FAULT LOCATION USING UNSYNCHRONIZED MEASUREMENTS

by

Shoaib Hussain

A Thesis Presented to the Faculty of the
American University of Sharjah
College of Engineering
in Partial Fulfillment
of the Requirements
for the Degree of

Master of Science in
Electrical Engineering

Sharjah, United Arab Emirates

May 2013

Approval Signatures

We, the undersigned, approve the Master's Thesis of Shoaib Hussain.

Thesis Title: Transmission Line Fault Location Using Unsynchronized Measurements

Signature **Date of Signature**

_____ _____
Dr. Ahmed Osman Ahmed
Associate Professor
Department of Electrical Engineering
Thesis Advisor

_____ _____
Dr. Habibur Rehman
Associate Professor
Department of Electrical Engineering
Thesis Committee Member

_____ _____
Dr. Ahmed Gaouda
Associate Professor
Department of Electrical Engineering
UAE University
Thesis Committee Member

_____ _____
Dr. Mohamed El-Tarhuni
Head, Department of Electrical Engineering

_____ _____
Dr. Hany El Kadi
Associate Dean, College of Engineering

_____ _____
Dr. Leland Blank
Dean of College of Engineering

_____ _____
Dr. Khaled Assaleh
Director of Graduate Studies

Acknowledgements

All glory and gratitude is due to Allah, the Exalted, for providing me with the strength and determination to complete this thesis and infinite peace and blessings of Allah be upon His beloved Prophet Muhammad. In addition, I gratefully acknowledge my advisor Dr. Ahmed Osman Ahmed for his continuous help and unwavering support throughout the course of this research. Under his watchful guidance, I was able to grasp the most difficult concepts of this thesis easily. He was to help me whenever I struggled with a topic and was prompt in providing different solutions to an ongoing problem. I feel that I was really fortunate to have such a dedicated and inspiring advisor. Lastly, I am also extremely grateful to my parents, brother and sisters for their support in all my academic endeavors. It was their firm faith in me that inspired me to continue working harder and complete the thesis.

To my beloved parents, grand-parents, brother and sisters for their everlasting affections and unwavering faith in me

Abstract

Designing reliable and accurate fault locating algorithms is still considered a challenge despite the intense research and development efforts transcribed in literature. Modern power system networks have grown in complexity and the increased deregulation of utility markets have helped dedicated fault locator systems garner much attention. Traditional electro-mechanical distance relays can be considered the first in a series of attempts to realize the aim of fault distance location. However, these were designed to provide rapid and reliable indication of the general faulted area rather than furnish fault distance estimates with pin-point accuracy. On the other hand, fault locator systems are expressly designed to provide accurate, reliable and reproducible fault distance solutions that might work with single-ended or two-ended data measurements. The two-ended data measurement provides far more accurate results. However data synchronization between protective relays at both ends is another issue that demands careful consideration. More often than not, modern fault locating algorithms incorporate integrated communication capabilities with sophisticated computational routines to furnish fault location estimates within an acceptable range of accuracy. In this thesis, the solution to transmission line protection problem is modeled as a fault locating algorithm that utilizes unsynchronized measurements. Two new fault locating algorithms are designed for two fundamental power system topologies: multi-terminal or multi-tap transmission line systems and compensated power transmission lines. Compensated transmission lines might incorporate fixed series compensation (FSC) or shunt reactor compensation. Evaluations of the algorithms substantiate enhanced fault location accuracy and robustness against power system transients. Moreover, the accuracy of fault location solution and synchronization procedure is not dependent on the mode of operation of non-linear FSC devices and copes well with temporary turbulences caused by power system transients.

Search Terms: Fault Location, Distance Protection, Transmission Lines, Unsynchronized Measurements, Power System Transients, Multi-terminal Transmission Line, Compensated Transmission Line.

Table of Contents

Abstract 6

List of Figures 10

List of Tables 14

1. Introduction 15

1.1. Role of Protection in Modern Power Systems 15

1.2. Historical Background and Evolution of Protective Relays 16

1.3. Transmission Line Protection 17

1.4. Thesis Objectives 20

1.5. Thesis Organization 21

2. Literature Review 22

2.1. Zones of Protection and Reach Settings. 23

2.2. MHO Impedance Relays. 24

2.3. Distance Relay Implementation. 25

2.4. Modeling of Distance Relays. 25

2.4.1. Time-domain based Modeling of Distance Relays. 26

2.4.2. Distance Relay Functions using Phasors and Sequence Components. 27

2.5. Effect of Fault Resistance and Current In-feed 30

2.6. Impedance Trajectories due to Current In-feed and Fault Resistance. 31

2.7. Fourier Filtering and Discrete Fourier Transform 33

2.8. Voltage stability and Protective Relays. 35

2.8.1. Use of Voltage Stability Index (VSI) During Voltage Collapse 35

2.8.2. Relationship between Voltage Sag Location and Apparent Impedance 38

2.9. Application of Phasor Measurement Units (PMU) with Protective Relays. 40

2.10. Relay Performance and Fault Location without Charging Current Compensation (CCC). 41

2.10.1. Distance Relay Function. 41

2.10.2. Relay Performance With and Without Charging Current. 46

2.11. Fault Location on Transmission Lines. 49

2.11.1. Fault Location Schemes. 50

2.11.2. Transmission Line Models. 54

3. Problem Formulation and System Modeling 59

3.1. Fault Location Scheme for a Multi-Terminal Transmission Line System Using Unsynchronized Measurements 60

3.1.1. Data Synchronization Procedure. 61

3.1.2. Fault Location Scheme. 66

3.2. Fault Location on Series and Shunt-Compensated Lines Using Unsynchronized Measurements 69

3.2.1. Fixed Series Compensation Monitoring System 71

3.2.2. Fault Location Scheme. 74

4. Performance Evaluation and Simulation Results 85

4.1. Algorithm Evaluation for Multi-terminal System. 85

4.1.1. Synchronization and Fault Detection 86

4.1.2. Evaluation of Fault Locating Procedure. 88

4.1.3. Power System Transients and Fault Detection. 93

4.2. Algorithm Evaluation for Series and Shunt Compensated Lines. 99

4.2.1. Evaluation of Synchronization and Fault Locating Procedure 100

4.2.2. Two-phase-to-ground Fault with FSC Device Installed. 105

4.2.3. Symmetric Three-phase Fault with Shunt Reactor Installed. 107

5. Conclusion and Recommendations for Future Work..... 110

References 113

Vita..... 119

List of Figures

Fig. 2.1 - Plain impedance characteristic [3] 23

Fig. 2.2 - MHO Characteristic [4] 24

Fig. 2.3 - Single Source Model, 400 Km [4] 26

Fig. 2.4 - Models of the four fault types [16] 28

Fig. 2.5 - Sequence network connections: SLG 28

Fig. 2.6 - Two source system 30

Fig. 2.7 - Fault resistance and current in-feed [4] 31

Fig. 2.8 - Impedance phasors [4] 32

Fig. 2.9 - Impedance Trajectory for $R_f = 20$ [4] 32

Fig. 2.10 - Apparent impedance before & during fault [20] 36

Fig. 2.11 - VSI versus time [14] 38

Fig. 2.12 - Five bus system [15] 39

Fig. 2.13 - Two source system [58] 41

Fig. 2.14 - Sequence circuit diagram 42

Fig. 2.15 - Zones of MHO relay 45

Fig. 2.16 - Impedance Trajectory 46

Fig. 2.17 - Fault distance and resistance estimation 47

Fig. 2.18 - Fault flag 48

Fig. 2.19 - Over-reaching effect of distance relay 48

Fig. 2.20 - Fault location methods [1] 50

Fig. 2.21 - Fault location using GPS [48] 51

Fig. 2.22 - Compensated transmission lines 53

Fig. 2.23 - Lumped parameter model [21] 55

Fig. 2.24 - Section of a three phase transposed line [1] 55

Fig. 2.25 - Fault on lumped-parameter line [16] 56

Fig. 2.26 - (a) Positive, (b) Negative and (c) Zero sequence networks [16] 56

Fig. 2.27 - Distributed-parameter line model [37] 57

Fig. 2.28 - Distributed π model for i^{th} symmetrical component [38] 57

Fig. 3.1 - Five line multi-terminal system 61

Fig. 3.2 - Fault locator algorithm 66

Fig. 3.3 - Fault on line L_1 with assumed current directions 67

Fig. 3.4 - Generalized SC/MOV model [53] 70

Fig. 3.5 - Sample characteristic curve of an FSC 71

Fig. 3.6 - Single line diagram of FSC platform [57] 72

Fig. 3.7 - Data flow between FSC and monitoring system [57] 72

Fig. 3.8 - SC/MOV bank structure 73

Fig. 3.9 - Series-compensated line 74

Fig. 3.10 - Shunt-compensated transmission line 75

Fig. 3.11 - Unsymmetrical fault on right side of FSC unit 77

Fig. 3.12 - Fault on shunt-compensated line 82

Fig. 4.1 - Phase-A voltage and current waveforms 87

Fig. 4.2 - Calculated synchronization angles 87

Fig. 4.3 - Apparent deviation of synchronization angles 88

Fig. 4.4 - Distance *d*, phase-A, SLG fault 89

Fig. 4.5 - Actual Impedance Trajectory, SLG fault 89

Fig. 4.6 - Bus 1 Phase Currents 90

Fig. 4.7 - Distance *d*, A-B-G fault 90

Fig. 4.8 - Actual Impedance trajectory, L-L-G fault 91

Fig. 4.9 - Phase currents, bus 2 91

Fig. 4.10 - Distance *d*, 3-phase fault 92

Fig. 4.11 - Actual Impedance, 3-phase fault 92

Fig. 4.12 - Three phase currents, bus 3 93

Fig. 4.13 - Multi-terminal line with load 95

Fig. 4.14 - Bus 1 phase voltage waveforms during transients 96

Fig. 4.15 - Bus 1 phase current waveforms during transients 96

Fig. 4.16 - Synchronization angles during transients 97

Fig. 4.17 - Bus 1 phase current waveforms during transients and fault 98

Fig. 4.18 - Synchronization angles during transients and fault 98

Fig. 4.19 - FSC model in Simulink 100

Fig. 4.20 - Relative synchronization angle $\boldsymbol{\delta r}$, for fsc device 101

Fig. 4.21 - Synchronization angle solutions for $\boldsymbol{\delta}$ 102

Fig. 4.22 – a) Rejected distance estimate, b) Correct distance estimate 103

Fig. 4.23 - Correct synchronization angle solution for Bus M 104

Fig. 4.24 - Real and imaginary values of correct fault distance estimate, shunt compensated lines 105

Fig. 4.25 - Phase currents, bus M 106

Fig. 4.26 - Real and imaginary components of distance *d* 106

Fig. 4.27 – SC/MOV phase voltages and MOV phase currents 107

Fig. 4.28 - Phase currents, bus *M* 108

Fig. 4.29 - Fault distance estimate 108

List of Tables

Table 2.1 – Impedance magnitude and angle 39

Table 2.2 - Line Sequence Parameters 44

Table 2.3 - Modified line sequence parameters 47

Table 3.1 - Sequence components in various fault types 76

Table 4.1 - Line Impedance Parameters 85

Table 4.2 - Line lengths 86

Table 4.3 - Voltage sources in simulated system 86

Table 4.4 - Performance of fault locating scheme 93

Table 4.5 - Fault location estimate after transients 97

Table 4.6 - Line sequence parameters 99

Table 4.7 - FSC/MOV parameters 100

Table 4.8 - Performance of fault location scheme 109

Chapter 1

Introduction

Power system protection is a branch of power engineering concerned with the application of protective relaying and ensuring the reliability of system operation. The traditional building blocks of protection systems have been fuses, current and voltage transformers, protective relays and circuit breakers. The operational reliability of electric power systems and mass power transfer corridors is dependent on the reliability of attached protection systems to a large extent. Relaying technology has developed and changed rapidly over the last few decades but the principle objective has remained the same; that is to keep the power system stable by detecting and isolating only the faulted components or affected portions of the system whilst leaving the healthy network intact.

1.1. Role of Protection in Modern Power Systems

A typical electrical power system consists of generators, transformers and distribution transmission lines. Power systems are often subjected to temporary disturbances and occasionally, short circuits that at times represent an abnormally destructive operating condition [1]-[3]. The sudden and heavy influx of current associated with short circuits is likely to cause permanent damage to power system components if circuit breakers and protective relays are not installed to effectuate preventive measures. Once a fault is detected in a section of a power system, an automatic protective device is required to swiftly isolate the affected element to maintain the healthy portion of the power system in normal operation. If a short circuit is allowed to persist for a longer period of time, particularly on strongly sourced power systems, the heavy current flow might damage critical power corridors of the system. The large fault current might also exceed the thermal capacity of the conductors and cause a fire accident. Uncleared faults might spread to other parts of the system and cause a dip in voltage to a level untenable for electric generators to maintain synchronism. Thus, an uncleared heavy short circuit fault can lead to total operation failure that is often characterized by cascaded tripping of transmission lines [1].

The fundamental requirements of a protective system are selectivity, reliability, sensitivity, stability and fast operation. Selectivity is the ability of a protective system to differentiate between a fault in the protected system and normal operating condition. Additionally the relay should also be able to identify whether the fault lies within its designated zone of protection or outside the zone. Fine tuned selectivity also enables a relay to discriminate between faults and transient conditions such as power surges or a transformer's inrush current that superficially resembles a fault condition. Therefore, selectivity is lost when a relay can no longer discriminate between instances when instantaneous tripping is required and those for which no operation is justified [1]-[2].

Reliability of a protective system is the ability to act when a fault occurs in its zone of protection. The failure of a protective system might be caused due to the failure of one or more of the supporting elements. The important elements of a protective system include relay, circuit breakers and voltage and current transformers. A high degree of reliability can be achieved by periodic maintenance and testing of the installed protective elements [1]. Sensitivity of a protective system is the ability to operate when the voltage or current exceeds a certain threshold or the pick-up value. Current-based relays should not operate when the present current is below the pick-up value. A protective system should also remain stable and operational when a large current flows through its protective zone due to external faults. The external faults outside of its protective zone are supposed to be cleared by the concerned circuit breakers. The protective system acts as a back-up and operates only if the protective scheme of the zone in which the fault has occurred fails to clear the fault. A protective system should be designed to act fast enough to quickly isolate the affected segments of the power system in order to minimize material damage and maintain system stability. The stability and fast response criteria are of vital importance for modern power systems to ensure that faults are cleared without exceeding the critical clearing time [1].

1.2. Historical Background and Evolution of Protective Relays

Fuses are one of the earliest automatic protective devices that were used in the power industry for isolating faulty equipment. They were proven to be effective and

provided satisfactory performance for small power systems. However, they did suffer from the serious disadvantage of requiring frequent replacement along with being oblivious to directionality. A part of the inconvenience was overcome with the introduction of electro-magnetic protective relays and circuit breakers. These relays provided fast, simple and economical implementation of protection schemes that saw them become a main-stay in the industry. The electromagnetic relays successfully combined the over-current protection feature of fuses with the much sought-after directional protection for fast and accurate operation [1]. The popularity of electro-magnetic relays has continued to endure mostly because of their simplicity and low-cost maintenance. The growth in size and complexity of modern power system networks demanded fast, accurate and reliable protective schemes. The development of the transistor led to the rise of static solid-state relays. Solid-state relays provided the advantage of low burden on current and voltage transformers combined with faster operation, complete absence of mechanical inertia and contact wear-and-tear that plagued the traditional electro-mechanical relays. Break-through in semiconductor technology and the advent of microprocessors provided a greater leap in protection technology due to their limit-less range of applications. Microprocessors increased the overall flexibility of relays due to its programmable approach which meant that a number of relaying characteristics could be realized using the same interface [1].

1.3. Transmission Line Protection

A protection scheme might be used to protect equipment or a segment of a line. They usually incorporate one or more relays of the same or different types. Some of the important relay types include over-current, under-voltage, under-frequency, directional and impedance relays [4]-[6]. These relays are classified into categories depending on the function they are required to perform. The following are some of the most common protections schemes utilized for protecting modern power systems.

- Over-current protection
- Differential protection
- Phase comparison based protection
- Directional distance protection
- Dedicated fault locators with Digital Fault Recorder (DFR)

Over-current protection scheme is mainly used for protection of distributed lines, large motor systems and power system equipment. This scheme usually includes one or more over-current relays which operate when the current exceeds the pick-up value. Over-current relays need to be commissioned carefully to avoid problems with cold load pick-up. This is because the line current sometimes remains considerably higher than the steady-state load current due to sporadic spikes in power demand. The sustained high load current might be picked up by the over-current relay leading to false tripping. It is standard practice to include a safety margin when using over-current relays to preempt mal-operation [6].

The differential protection scheme is a unit protection system that is primarily used for the protection of generators, transformers, large sized motors and transmission lines. This scheme has its zone delimited by the location of current transformers (CTs) that are placed on both sides of each winding of a machine. The output of the secondary windings of CTs is applied to the relay coil. During normal condition or external fault, the current entering and leaving the winding is equal. But in the case of an internal fault, a current differential is formed which is compared to a restraint value by the relay. The comparison is carried out on the basis of a multi-slope percentage characteristic to render the relay immune to increased loading of the protected line or equipment [6].

Phase comparison protection utilizes phase comparison relays that are designed to respond to phase relation between the currents at all terminals of a protected line. The phase angle relation between line currents is checked by monitoring the time alignment between the measured currents. Phase protection schemes often make use of communication channels and are backed up by over-current and/or distance relays in case of loss communication [4], [6].

Distance relays have been used for protection of high voltage transmission lines for many years. They have steadily progressed from the electro-mechanical type to static analogue electronic type, and then on to the digital relay type that can be implemented entirely on digital signal processors (DSPs). The distance relays are usually designed to operate with three zones of protection in a time-stepped manner that cover the primary zone of protection and also provide remote back-up protection

for extended lengths of adjacent transmission lines. Zone 1 is usually set to cover 80-90 % of the primary transmission line to be protected and the zone 3 of the distance relay has the largest reach setting of the three zones covering up to 120% of the longest adjacent line. Zone 2 provides protection for a region that is intermediate between zones 1 and 3 [4].

A common problem associated with all zones of the distance relay is that of the under-reaching effect. Most distance relays are designed to work using sampled values of phase voltages and currents only of the buses they are attached to. That is, most distance relays and their algorithms work with only single-sided measurements without having a sense of currents being fed from other buses that contribute to the total fault current. A large in-feed current emanating from the opposite bus will cause the relay to under-reach since the impedance presented to the relay would be larger than its actual value [2], [4]. On the other hand, a large out-feed of the current would cause a distance relay to over-reach since the impedance calculated would be smaller than the actual value. Both these effects are explained in the sections that follow.

In-feed and out-feed are not the only factors that might cause a distance relay to mal-operate. Fault impedance, which is usually resistive in nature, also plays a part in fault determination. Based on the fault resistance value, and the magnitude and phases of all remote in-feed currents, the fault resistance might get magnified or diminished accordingly. Therefore, the complex impedance presented to the distance relay may fall in the wrong zone of protection or move entirely out of the protected zone in the R-X plane. Events related to voltage stability such as parts of power system nearing a voltage collapse or over-loading of the power system with heavily inductive load that causes voltage dips might result in the apparent impedance settling in any one of the three protective zones of the distance relay and thus cause a false tripping of the circuit breakers [2], [4].

Fault location on power system transmission lines is an area that has been researched intensively over the years and is a common theme that is closely associated with the application of distance relays to achieve zone protection, [8]-[14] and [16]-[61]. Fault locators, in contrast to distance protection, are expressly devised to pin-point the exact location of short-circuit faults on transmission lines which can

be crucial for expediting the process of repair and restoration of power system operation. Numerous fault detection and location schemes have been proposed in the literature that can be categorized in several types based on method of data measurement, power system network topology, synchronization of measured signals and domain preferences. Some of the algorithms presented use local terminal measurements, while others utilize measurements from two terminal-ends encapsulating the entire transmission line and form the basis for pilot relaying schemes.

1.4. Thesis Objectives

In this thesis, the solution to power system protection problem is modeled as a fault locating algorithm for aiding the operation of primary protection relays such as distance relays. In light of the short-comings associated with distance relays utilizing single-sided measurements to calculate the apparent impedance, fault locating algorithms are designed as pilot relaying schemes for two different fundamental power system topologies. The fault location algorithms are designed to mimic the real life system dynamics as closely as possible and enable feasible implementation on digital processors that coordinate relay operations.

The objectives of this thesis are to:

- Develop a digital fault location algorithm for long transmission lines operating at various voltage levels.
- Develop a fault location algorithm for multi-terminal transmission lines using unsynchronized measurements in which the natural shunt capacitance of transmission lines and the resulting charging currents are taken into account.
- Develop a fault location algorithm for series and shunt-compensated lines using unsynchronized measurements.
- Design robust fault locating algorithms that are able to perform under post-fault events of instability such as power system transients.

1.5. Thesis Organization

The rest of the thesis is organized as follows. In Chapter 2, a detailed literature is presented. The literature review focuses on the relaying characteristics of the standard MHO distance relay as well as modeling and its implementation. The effects of fault impedance, current in-feed and charging current on distance relays and fault locators are explained. Various fault locating schemes based on transmission line characteristics are also presented in the literature review.

In Chapter 3, models of the power system and problem formulation are presented. Chapter 3 also details the required synchronization procedures and the fault locating schemes both for the multi-terminal transmission lines and compensated transmission lines using unsynchronized measurements.

Chapter 4 illustrates the performance of the proposed algorithms by presenting detailed simulation results and analysis and finally, Chapter 5 concludes the thesis and suggests recommendations for future work.

Chapter 2

Literature Review

The advent of the microprocessor based protective systems incorporating new features and facilities has made immediate post-fault analysis of all transient phenomena a reality. The distance relaying functions can now be implemented as numerical algorithms on programmable digital signal processors and installed on remote high-voltage lines as stand-alone computers with or without communication capabilities. Micro-processor based relays allow protection engineers to immediately calculate the distance to the fault and store pre-fault and post-fault data on phase voltages and currents. This information can be extremely valuable to maintenance teams carrying out on-site inspection following the tripping of circuit breakers or clearance of faults on long distance transmission lines. The reduction in fault clearance times and fast fault location techniques mitigate the need for visual evidence of faults and provide savings on logistics in difficult terrains [1].

Distance relay based protection is a non-unit system of protection that provides economic and technical advantages when installed on critical high-voltage power transmission lines. Unlike over-current relays, the fault convergence of distance relays is independent of source impedance variations [1]-[2]. Distance protection based relays are also comparatively simple to apply and they provide protection for both its primary zone and other extended zones within a single scheme. The basic principle that all distance relays work on is the linear relationship between transmission line impedance and its length [3]. Since the impedance of a line is proportional to its length, a distance relay can be used to measure the impedance of a line to its set point or the reach point. The distance relay is designed to operate for faults occurring within the protected segment of a transmission line by measuring the impedance between relay and the point of the fault. If the apparent impedance calculated is less than the reach point setting, the relay assumes that a fault has occurred on the protected line and a trip command is issued to the connected circuit breaker. Since the calculated apparent impedance is dependent on the ratio of the voltage and current phasors, the complex impedance can then be plotted on an R-X diagram and compared against the loci of the protected zone impedance.

2.1. Zones of Protection and Reach Settings.

The reach settings and tripping times of the three zones enable correct coordination on a power system. A basic distance relay comprises of an instantaneous zone 1 protection and one or more time-delayed protection zones. More advanced numerical relays can have up to 5 zones and some are set to measure faults in the reverse direction [3]. For digital or numerical relays, the reach setting of zone 1 is set to cover about 85% of the primary protected line. A safety margin of about 15% is left to ensure that the zone 1 protection does not over-reach due to errors in the measurement of the voltage and current transformers. Zone 2 of the protection is set to cover the remaining 15% of the primary line. Zone 2 is usually set to cover the entire protected line along with 50% of the shortest adjacent line. Both the zone 1 and zone 2 of the distance relay are coordinated using a time delay to allow zone 1 to react before zone 2 does. Zone 3 usually has the largest reach setting of the three zones and is used to provide remote backup protection for adjacent lines. A diagram of the plain impedance characteristics is depicted in Fig. 2.1.

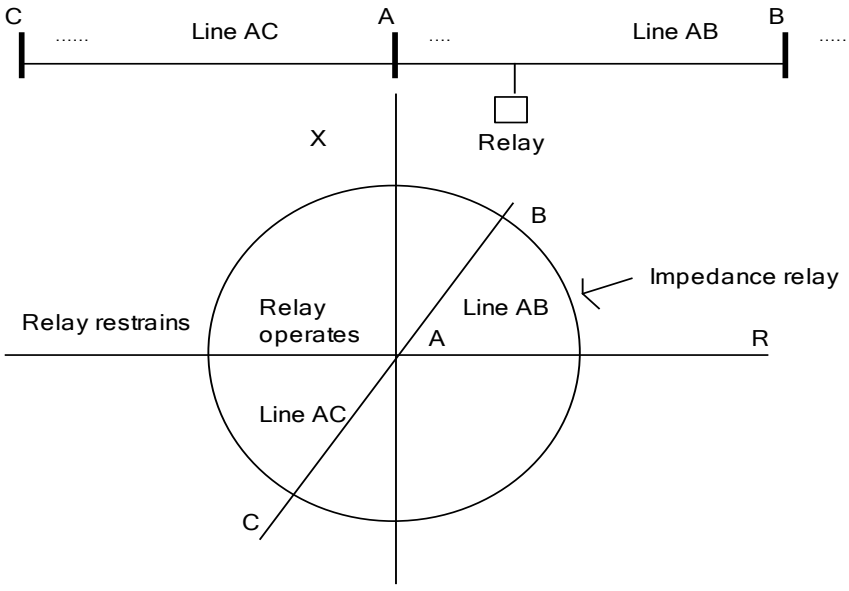

Fig. 2.1 - Plain impedance characteristic [3]

On an inter-connected power system, current in-feed from other sources causes the impedance presented to the distance relay to be larger than its actual value, and this needs to be taken into account while setting zone 3 reach. Non-directional impedance zones are sometimes used to provide protection for close-up faults. These plain

impedance relays do not take into account the phase angle between the voltage and current phasors. When their impedance characteristics are plotted on an R-X diagram, the loci forms a circle with the origin as its center. Since the measured impedance angle does not play a role in fault discrimination, this type of distance relay issues a trip command as long as the impedance magnitude falls within the perimeter of the protected zone impedance.

2.2. MHO Impedance Relays.

MHO impedance relays are called as such because its characteristics can be seen to be a straight line on the admittance diagram. It has qualities of both reach magnitude control and directional control that are missing in the plain impedance relay. MHO relays are still widely used in power systems that are protected by electro-mechanical relays as well as digital numerical relays. The impedance characteristics of an MHO relay when plotted on an R-X diagram is a circumference that passes through the origin. A typical MHO relay characteristic is shown in Fig. 2.2.

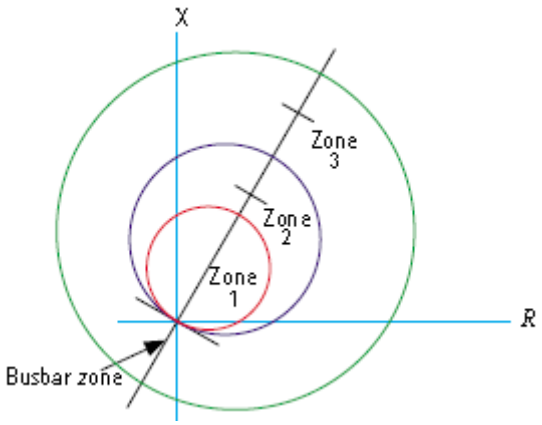

Fig. 2.2 - MHO Characteristic [4]

The above diagram illustrates that the MHO relay is inherently directional and operates for faults only in the forward direction that lie in any of the three protected zones. The MHO relay can be used to provide more or less of resistive coverage by controlling the angle of displacement of the diameter and the 'R' axis. This is done to compensate for faults that might have a fault resistance (R_f) value [4].

2.3. Distance Relay Implementation.

A distance relay protective function can provide protection for three distinct zones since the impedance to the fault point is a simple function of length. The impedance measured by a distance relay is dependent on several other factors as well:

- The magnitudes of current and voltage.
- The fault impedance loop being considered.
- The type of the fault itself.
- The symmetry of line itself, whether it is ideally transposed or not.
- The configuration of the transmission system, whether it is a single or multi-terminal circuit.
- The unseen in-feed current from remote sources that contribute to the fault current.

It should also be noted that protection against earth/ground faults may also require different characteristic settings when compared to phase faults. For a MHO relay with three distinct zones, a total of 18 impedance measurement units would be required to cover all the different fault types. For a phase-to-earth fault, the phase to ground voltage at the fault location is zero. However, the voltage drop to the fault is not the simple product of the phase current and the line impedance. The current in the fault loop depends on a number of factors such as number of earthing points, the method of grounding and the sequence impedances of the system.

2.4. Modeling of Distance Relays.

Ever since the classical publication on the use of symmetrical components for the transient analysis of symmetrical networks in [5], various venues in signal processing have been exploited to model the operation of distance relays. Symmetrical components remain at the heart of all analytical representations for poly-phase power systems [3]. The distance relay models suggested in the vast amount of literature can be broadly classified in to two categories:

i. Time-domain based models that use instantaneous values of sampled voltages and currents.

ii. Frequency-domain based modeling of distance relays that utilize filtered phasor representation of voltages and currents.

Time domain based models of distance relays include state-space representations such as those found in [1], [4], [7] and [8]. Other time domain methods include fault detection using travelling-wave formulation such as those described in [1], [6] and the use of recursive least square algorithms detailed in [11]. Frequency domain methods that involve extraction of the fundamental phasor quantities have been suggested and adopted much more extensively in the literature surveyed. The fundamental phasor quantities are calculated from the sampled data using well established techniques such as application of Kalman filters, Full and Half-cycled Discrete Fourier Transforms and variable window length Fourier techniques. These concepts are explored have been thoroughly explored in [12]-[22] and [24]-[27]. Novel frequency domain techniques such as application of Wavelet Transforms are described in great detail in [9], [10] and [23]. A concise overview of the most popular techniques is presented in this section.

2.4.1. Time-domain based Modeling of Distance Relays.

The design and operating behavior of a numerical distance relay that uses single-sided measurements of voltages and currents for calculating values of resistance and inductance up to the fault point is described in [4]. The distance relay modeled was used for a generic single-source radial system as shown in Fig. 2.3.

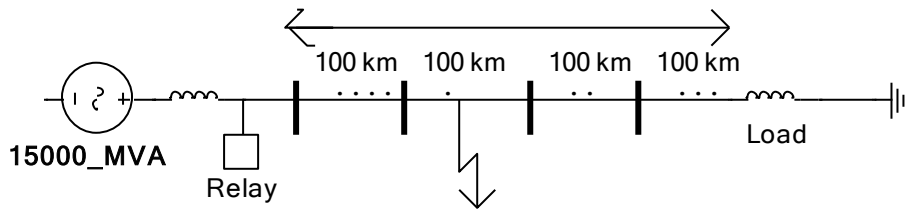

Fig. 2.3 - Single Source Model, 400 Km [4]

The relationship between the instantaneous samples of voltage and phase current is described by a simple first order ordinary differential equation:

$$R_i(t) + L\frac{d}{dt}(I_i) = v_i(t) \tag{2.1}$$

where L and R are the unknown values that are to be calculated using the measured samples of v_i and I_i .The relationship described above is valid provided that shunt capacitances are small enough to be ignored. Since there are two unknowns to be calculated, equation (2.1) and its first derivate can be used to form a system of two independent equations. Successive values of R and L can then be solved for each sample set of voltage and current using:

$$\begin{bmatrix} i(t) & \frac{d}{dt}i(t) \\ \frac{d}{dt}i(t) & \frac{d^2}{dt^2}i(t) \end{bmatrix} \begin{bmatrix} R \\ L \end{bmatrix} = \begin{bmatrix} v(t) \\ \frac{d}{dt}v(t) \end{bmatrix} \tag{2.2}$$

The calculated R and L values are based on the assumption that the fault voltage, V_f, is near zero and that the fault resistance is negligible. This method models the transmission line as having lumped resistance and inductance and does not consider the effects of mutual inductance and zero sequence currents. A more detailed model of a time-domain based distance relay using sequence components is described in [8] and is used as a basis for establishing later on as to why distance relay functions might fail when the natural shunt line capacitances are ignored.

2.4.2. Distance Relay Functions using Phasors and Sequence Components.

The performance equations for distance relays can be derived using the theory of symmetrical components [3]. One equation for each type of fault, namely phase to ground, phase to phase, three phase and double-phase-to-ground faults can be used for each of the three phases of the power system. Fig. 2.4 depicts models of each of the four fault types used for derivation of performance equations [16].

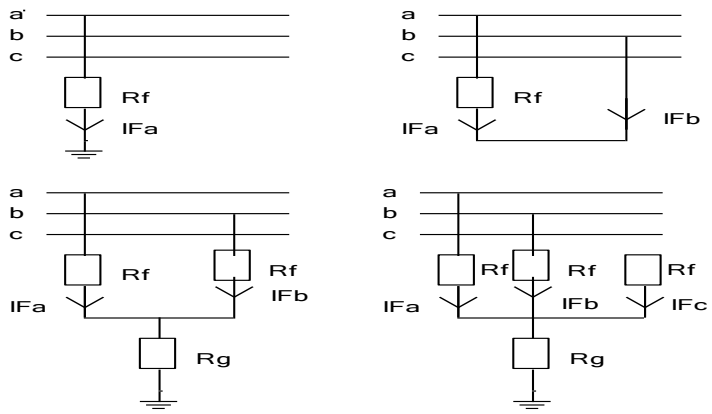

Fig. 2.4 - Models of the four fault types [16]

Distance relays operate based on the measured impedance at the relaying point. In the absence of any out-feed of current and for zero fault resistance, the measured impedance between relay and the fault point depends only on the length of the line segment joining the two [13]. The equivalent sequence circuits for a phase A to ground (SLG) fault is shown in Fig. 2.5 [2].

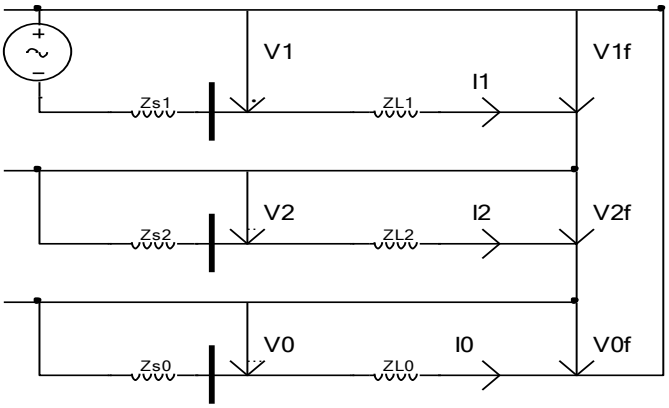

Fig. 2.5 - Sequence network connections: SLG

The voltage seen at the relay, Va, can be calculated as follows:

$$V_a = V_1 + V_2 + V_0 \tag{2.3}$$

Where,

$$V_1 = I_1 Z_{L1} + V_{1f}$$

$$V_2 = I_2 Z_{L1} + V_{2f}$$

$$V_0 = I_0 Z_{L0} + V_{0f} \tag{2.4}$$

Adding equations in (2.4) results in:

$$V_a = I_1 Z_{L1} + I_2 Z_{L1} + I_0 Z_{L0} + V_{1f} + V_{2f} + V_{0f} \tag{2.5}$$

Since the resistance R_f is assumed to be zero, equation (2.5) simplifies to:

$$V_a = (I_1 + I_2) Z_{L1} + I_0 Z_{L0} \tag{2.6}$$

It is clear from equation (2.6) that the voltage seen at relay side is not just made up of the voltage drop in the positive sequence impedance of the line like it is in a three phase fault, but also includes contribution from the zero sequence network that is proportional to zero sequence current and zero sequence impedance.

Using a similar methodology of sequence network representation, the voltage seen at the relay for a three phase fault is given by:

$$V_a = I_1 Z_{L1} + V_f \tag{2.7}$$

The term V_f is zero for when the fault resistance is zero. For a phase A to ground fault described by equation (2.6), the positive sequence impedance measure by the distance relay can be obtained with a little algebraic manipulation to yield:

$$Z_{L1} = \frac{V_a}{I_A + K_0 I_0} \tag{2.8}$$

Where K_0 is called the zero-sequence compensation factor and is given by:

$$K_0 = \frac{Z_{0L} - Z_{1L}}{Z_{1L}} \tag{2.9}$$

The voltage and current phasors are used to estimate the impedance seen between the relay and fault point. The impedance estimates can be determined using six relay elements; three for phase faults and three for ground/earth faults. Similar to the sequence network approach used earth and three phase faults, the positive sequence impedance seen by the relay during phase-to-phase faults can be expressed using a similar method. For a phase B-to-C fault, the positive sequence impedance is given by equation (2.10) below:

$$Z_{1BC} = \frac{V_B - V_C}{I_B - I_C} \tag{2.10}$$

The positive sequence representation for phase A-B and A-C can also be represented in a similar fashion using sequence components:

$$Z_{1AB} = \frac{V_A - B}{I_A - I_B} \tag{2.11}$$

$$Z_{1CA} = \frac{V_C - V_A}{I_C - I_A} \tag{2.12}$$

2.5. Effect of Fault Resistance and Current In-feed.

The effect of fault resistance on estimations of fault location on transmission lines is of particular interest to protection engineers since most distance relay functions are designed to work on single sided measurements. Earlier design of distance relays worked on the assumption of transmission lines being energized from one end only and fault resistances small enough to be ignored. Such fault locating procedures are now generally accepted to produce excessive errors [12]. Fault resistance is not the only source of error in fault location calculations, inter-connected system of buses can have multiple sources feeding a fault. The total complex impedance presented to a distance relay is a function of the cumulative in-feed current, the magnitude and phase of which is also in turn dependent on impedances of the sources feeding the fault. A typical interconnected system with two sources is shown in Fig. 2.6.

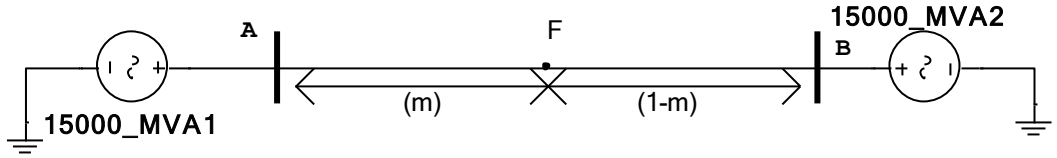

Fig. 2.6 - Two source system

For such a system with a distance relay attached at point A, the total resistance presented to the system is given as:

$$Z_T = mZ_L + K_r R_f \tag{2.13}$$

Where ‘m’ is the fractional distance to the point of fault and ‘K_r’ is a function of network current distribution factors, the location of fault and the type of short-circuit that occurs. It should also be noted that the coefficient ‘K_r’ is usually a complex number and therefore when multiplied with the fault resistance R_f, it makes the fault resistance appear as a complex impedance which might be inductive or capacitive depending on the angle of K_r.

2.6. Impedance Trajectories due to Current In-feed and Fault Resistance.

To explain the combined effect of fault resistance magnitude and the in-feed current, consider the system in Fig. 2.7 with sources and a phase to ground fault [4].

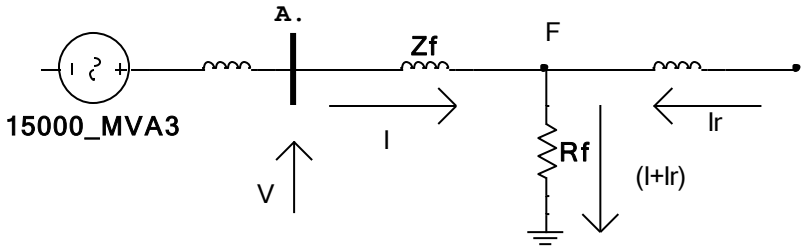

Fig. 2.7 - Fault resistance and current in-feed [4]

Both terminals of the transmission line are connected to a source and the fault current flowing through fault resistance might be greater than the current flowing between the points A and F. This means that the total impedance seen by the relay at point A is not the simple sum of Z_f and R_f. The error in calculation of the relay impedance is due to the current in-feed from the source at the opposite terminal. The total fault current is given by:

$$I_F = I + I_r \tag{2.14}$$

The voltage drop measured by the relay is therefore:

$$V_a = IZ_F + R_F(I + I_r) \tag{2.15}$$

As a result, the impedance measured by the relay is given by:

$$Z_a = \frac{V_a}{I} = Z_F + R_F\left(\frac{I_r}{I} + 1\right) \tag{2.16}$$

It is usually the case that the current I_r is not in phase with current I. The typical impedance phasors presented to the distance relay in such a scenario are described in Fig. 2.8.

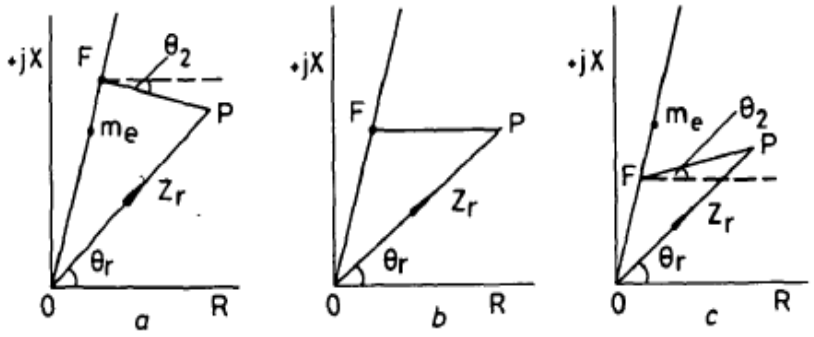

Fig. 2.8 - Impedance phasors [4]

In the diagram above, $Z_r = Z_F$, and m_e is the fractional distance to the earth fault at point F. Z_a is the equivalent impedance presented to the relay. θ_2 is the angle of the coefficient of R_F in equation (2.16). If the angle θ_2 is negative as shown in Fig. 2.8a, the total impedance seen has a lower magnitude than the sum of (Z_F +R_F) and the relay might over reach if the distance to the point F was outside of the protected zone in an R-X diagram. In Fig. 2.8c, θ_2 is positive and therefore causes a greater impedance to be seen by the relay than the actual and the relay might under-reach if line impedance to point F was inside the protected zone of the relay. Fig. 2.8b shows a scenario where the angle θ_2 is zero and the impedance seen by the relay is equal to the actual fault path impedance. The system shown in Fig. 2.7 was simulated using various values of fault resistance in [4] and the impedance trajectories were plotted against MHO relay characteristics as shown in Fig. 2.9.

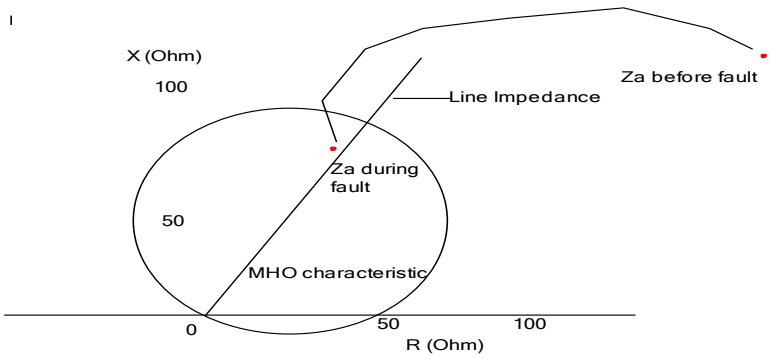

Fig. 2.9 - Impedance Trajectory for R_f = 20 [4]

It is shown that when fault resistance has a low non-zero value of 20Ω for a double fed circuit, the impedance trajectory barely settles inside the MHO characteristic circle. For a value of 40Ω, it was shown in [4] that the impedance trajectory settles just outside the protected impedance zone.

2.7. Fourier Filtering and Discrete Fourier Transform

Digital filtering algorithms are applied to obtain the required voltage and current phasor quantities for phasor based digital distance relays. The speed and accuracy with which the phasors are calculated plays an important role in fast fault detection and clearance times. When a fault occurs, the voltage and current waveforms become severely distorted due to the presence of higher harmonics and a significant decaying DC component [3], [24], [26] and [28]. The presence of higher harmonics makes the fast estimation of fundamental phasor quantities to be very difficult and ultimately affects the performance of the relays. A large variety of phasor estimations techniques have been presented in the reviewed literature and Discrete Fourier Transform based filtering remain the most popular and most widely used. This is because the computational cost of DFT is very low and it also provides good harmonic immunity. The DFT based algorithms can be classified as of two types; fixed window length algorithms and the relatively new adaptive window length algorithms. Fixed window length DFT algorithms remain the most widely adopted and comprise of Full Cycle DFT (FCDFT) and Half Cycle DFT (HCDFT) algorithms [22], [24]. The filtering capabilities of DFT based filters are dependent on the window length. A short data window gives an estimate of the phasor quantity very quickly but includes the possibility of an unstable output. Full length DFT computation gives a very stable output but comes at the cost of delayed response time. Despite the apparent short-coming of the full length DFT algorithm, it still remains popular since the delay induced in fault detection and the computation of fault location is at most one power cycle [1], [3]. The delay induced in the detection of fault can be compensated by using the FCDFT in conjunction with a fast fault detection algorithm and utilizing the DFT algorithm just for fault distance calculation. This method has been used to design most of the distance relay algorithms presented in literature.

The fundamental phasors from the full cycle DFT are calculated as follows:

Consider a phasor that represents the fundamental component with V_x and V_y being its real and imaginary parts. If N number of samples are taken per cycle of the fundamental component with Δt being the sampling time interval, then the real part of the fundamental phasor is given by the following summation:

$$V_x = \frac{2}{N}\sum_{i=0}^{N-1} v_i cos\left(\frac{2\pi i}{N}\right) \tag{2.17}$$

Where v_i is the i^{th} sample taken. Similarly, the imaginary part V_y of the fundamental phasor can be computed as follows:

$$V_y = \frac{2}{N}\sum_{i=0}^{N-1} v_i sin\left(\frac{2\pi i}{N}\right) \tag{2.18}$$

The phase angle of the fundamental phasor can be obtained by the following expression:

$$\delta = \tan^{-1}\left(\frac{V_y}{V_x}\right) \tag{2.19}$$

The coefficient (2/N) for the real and imaginary part is the scalar required to obtain the peak values of the fundamental frequency component, it can be readily replaced with (√2/N) to obtain the RMS values of the fundamental component [1]. Following the same derivation procedure shown above, the half-cycle DFT can also be evaluated in a similar manner. The real part, $V_{x1/2}$ of the fundamental phasor is given by the following expression:

$$V_{x1/2} = \frac{4}{N}\sum_{i=0}^{N/2-1} v_i cos\left(\frac{2\pi i}{N}\right) \tag{2.20}$$

The imaginary part, $V_{y1/2}$ of the fundamental phasor is given by:

$$V_{y1/2} = \frac{4}{N}\sum_{i=0}^{N/2-1} v_i sin\left(\frac{2\pi i}{N}\right) \tag{2.21}$$

The above expressions are used to compute the peak values of the fundamental phasor. The coefficients 4/N can be replaced with 4/√2N to obtain the RMS value of the phasor. The phase angle of the phasor can be computed in a similar manner as stated in equation (2.19). It can be seen in equations (2.20) and (2.21) that the half cycle window algorithm requires only half the number of samples than those required

for full window DFT. This algorithm appears to be the faster alternative but it has the possibility of being erroneous especially due to the presence of aperiodic components or odd and even harmonics [1], [25].

2.8. Voltage stability and Protective Relays.

According to the publication from IEEE joint task force on Stability, voltage stability is defined as the ability of a power system to maintain steady state voltages at all buses in the system after being subjected to a disturbance from a given initial operating condition [29]. It also refers to the system capability to maintain and restore equilibrium between the load demand and load supply from the power system. One possible outcome of voltage instability in a power system is the loss of service to load in an area. Other problems associated with voltage instability is the tripping of transmission lines by protective equipment such as over and under voltage relays and distance relays which have in the past contributed to cascaded power blackouts. Loss of synchronism in connected source generators is also a serious consequence of voltage instability. Voltage instability in a power system is observed when the reactive power available to a portion of a power grid falls below what is required by the connected transmission lines, power components such as transformers and the consumers. One possible mechanism of voltage collapse described in [30] is the stalling of industrial motors. Motors typically stall when the voltage drops below 70% of the nominal voltage at the motor terminals. At the reduced voltage levels the torque of motors falls below the load torque and the industrial motors slow down to a halt where they continue to consume large amounts of reactive power which further depresses the voltage on the power grids. One of the problems in predicting or detecting voltage collapse is that the voltage itself is not a good indicator of voltage instability. This has led to the development of stability indexes called System Status Indicators (SSI) and Voltage Stability Indexes (VSI) to gauge the possibility of an impending voltage collapse as discussed in [14] and [20].

2.8.1. Use of Voltage Stability Index (VSI) During Voltage Collapse

A new technique to prevent the false tripping of distance relays in the event of voltage instability is discussed in [14] and [20]. This is done by integrating the

adaptive setting of the zone 3 distance relay, rate of change of voltage at the buses and the use of VSI. The false tripping command issued by zone 3 element of distance relays has caused cascaded events and wide-area voltage collapse in the past. During voltage instability where the bus voltage is seen to dip, the impedance seen by the relay decreases and might enter zone 3 since it has the highest set reach point to provide backup protection. There is a need to develop an indicator that can differentiate between faults and other temporary events such as overloading and voltage instability. The impedance seen by the relay can be expressed as a function of active and reactive power measured at the relay bus. The impedance Z_a in terms of the complex power is given by:

$$Z_a = \left[\frac{P_{ij}}{P_{ij}^2+Q_{ij}^2} + j\frac{Q_{ij}}{P_{ij}^2+Q_{ij}^2}\right]|V_i|^2 = R_a + jX_a \tag{2.22}$$

The polar characteristics of the three zone distance relay are shown in Fig. 2.10.

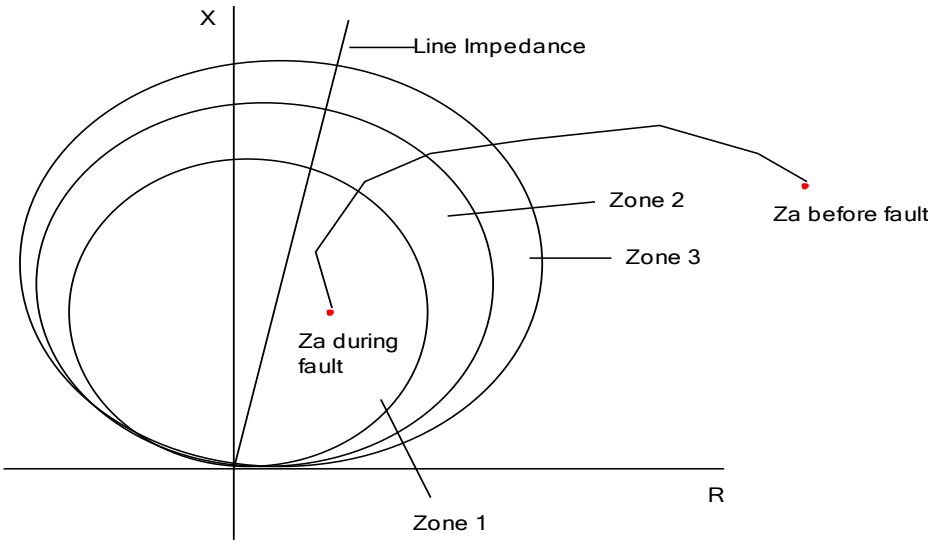

Fig. 2.10 - Apparent impedance before & during fault [20]

During the normal operating conditions of the power system, the measured impedance Z_a lies outside zone 3 of the relay. Once a fault occurs in one of the protective zones of the relay, the value of Z_a significantly reduces and enters one of the three zones. The VSI is developed on the idea that during a voltage collapse, any increment in the

apparent power S at the sending end does not produce any increment of apparent power at the receiving end [20]. The VSI is developed using apparent power relation with voltage and current magnitude.

$$|S| = |V||I| \tag{2.23}$$

Increase in apparent power also lead to an increase in voltage and current magnitude:

$$|S + \Delta S| = (|V| + \Delta|V|)(|I| + \Delta|I|) \tag{2.24}$$

Assuming $\Delta V \Delta I \sim 0$, (2.24) simplifies to:

$$|S + \Delta S| = |V||I| + \Delta|I||V| + \Delta|V||I| \tag{2.25}$$

Subtracting (2.25) from (2.24) and rearranging give:

$$\frac{\Delta S}{\Delta|I||V|} = \frac{\Delta|V||I|}{\Delta|I||V|} + 1 \tag{2.26}$$

The voltage stability index can now be expressed as:

$$VSI = \frac{\Delta|V||I|}{\Delta|I||V|} + 1 \tag{2.27}$$

From equation (2.27), the VSI would shoot to infinity if the operating conditions do not change and the current remains constant. To offset this possibility, a very small constant 'α' is added to the denominator.

$$VSI = \frac{\Delta|V||I|}{\Delta|I||V| + \alpha} + 1 \tag{2.28}$$

Where $\alpha = 10^{-10}$.

In [14], a multi-bus power system was simulated to see the performance of the VSI as an additional indicator to help the relay to differentiate between a fault and voltage collapse. Fig. 2.11 shows the VSI plotted against time and voltage at one of the buses nearing voltage collapse just after a fault.

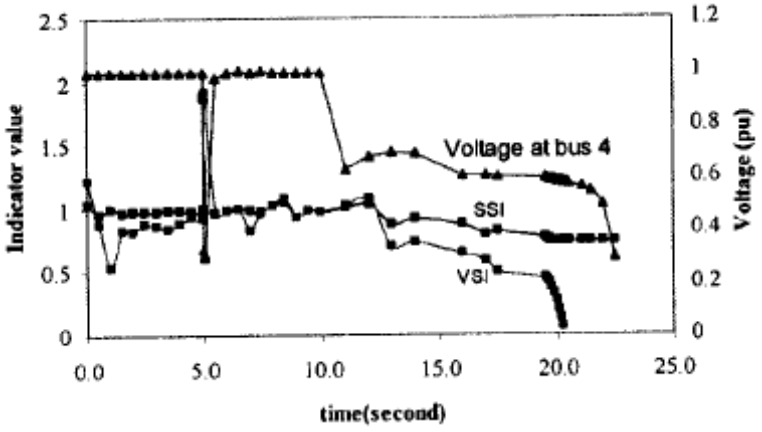

Fig. 2.11 - VSI versus time [14]

In Fig. 2.11, a fault was initiated after 5 seconds which is obvious from the bus voltage taking a sharp dip from 1pu to 0.2 pu. The threshold VSI value defined for this system was 0.2, which meant that for VSI less than 0.2, the system was nearing a voltage collapse and the distance relay trip signals should be blocked. It can be seen from the curves that VSI does not fall below 0.2 at the instant when a fault occurs and the bus voltage falls. This means that the fall in voltage was caused by a fault and not because of the bus nearing a voltage collapse. Voltage collapse conditions were purposely induced at the bus after 10 seconds to gauge the performance of VSI. The VSI responds as expected and falls below the threshold value of 0.2. At this point, all relay trip signals were blocked since no fault had occurred.

2.8.2. Relationship between Voltage Sag Location and Apparent Impedance

The information available to a distance relay can also be utilized for locating the source of voltage sag and indicate on which side of the measurement unit a voltage sag has occurred. A simple procedure is described in [15] for voltage sag source detection based on the principle of apparent impedance. The impedance seen by the relay in the event of a fault is given by:

$$Z_{seen} = \frac{V_a}{I_a} = z_{1f} + \Delta z \tag{2.29}$$

Where z_{1f} is the positive sequence impedance up to the fault point and Δz is a function of fault resistance and other in-feed currents. The above relation refers to impedance seen in the forward direction. However, in case of a fault occurring behind the relay,

the current direction is reversed and the resulting impedance will change both in magnitude and direction. Therefore, the magnitude and angle of the impedance can be used to identify faults occurring in front or behind the relays. A simple rule for detection of voltage sag occurring in front of a relay is described as follows:

$if\ |Z_{sag}| < |Z_{presag}|\ and\ \angle Z_{sag} > 0$, then the sag source is in front of the relay. Otherwise, the sag source is behind the relay.

The above condition was tested for a two terminal, radial and a multi-bus system to check for its validity. Fig. 2.12 shows the multi-bus system tested in [15].

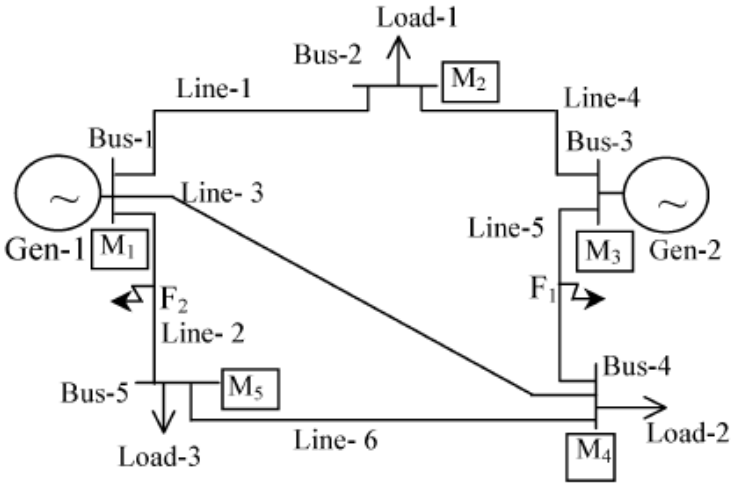

Fig. 2.12 - Five bus system [15]

The five bus system shown above was tested for voltage sag detection by inducing faults at points F_1 and F_2. The data collected from monitor M_5 was then used to identify whether voltage sag had occurred in front or behind it. The Table 2.1 shows the impedances for fault F_1 (in front of M_5) and F_2 (behind M_5).

Table 2.1 – Impedance magnitude and angle

Sag Position	Impedance Magnitude(Ω)	Impedance Angle(rad)
Presag	925.8	-1.3
In front of the monitor	451.9	1.2
Behind the monitor	67.8	-2.16

The two voltage sag situations were observed by monitor M_5. For the fault in front of the monitor, the impedance angle has a positive value and for the fault behind M_5, the impedance angle is negative. In both the cases, the impedance magnitude is also seen to decrease from the pre-sag magnitude. The test above proves the validity of the principle and can be used as an additional indicator to confirm whether a fault has occurred in the protected zone of the distance relay.

2.9. Application of Phasor Measurement Units (PMU) with Protective Relays.

A phasor measurement unit (PMU) is a device which measures electrical quantities of voltage and current using a common time reference for synchronization. In power applications, PMUs are also known as synchrophasors and play a very important role when incorporated in to protective relays. The outputs of PMUs provide truly synchronized measurements which enable synchronized comparison of two differing quantities in real time. Real time comparison of synchronized data can then be used for assessing power system conditions [31]. In relaying applications, transmission line faults occurring on Ultra/Extra High Voltage lines need to be located quickly to isolated the affected region and reduce outage time. Fault locators on distance relays produce the most reliable results when the measured system data is synchronized to a common reference point. Other fault locating methods that do not require phasor measurement units and can work on unsynchronized data have also been presented such as the one in [16]. However, this method requires that the synchronization phase angle be calculated first before the relay can calculate the fault distance. The algorithms developed in Chapter 3 are based on the assumption that synchronized measurements are not available to the relay through the use of PMUs, representing a more generalized case. This is due to the fact that the use of PMUs is still not as common as it could be, especially on mature (legacy) transmission line systems or where the installation of synchronized devices might hinder economic implementation of protective relays.

2.10. Relay Performance and Fault Location without Charging Current Compensation (CCC).

One of the challenges of the application of distance protection to long distance transmission lines is the influence of line capacitance. When a fault occurs on a long over-head line with sizeable shunt capacitance, large magnitude harmonic components of voltage and current evolve that are super-imposed on the fundamental frequency components [32]. Distance relaying function can be derived using both time-domain methods and phasor-based methods as stated in [1]. Both these methods offer certain advantages in terms of the time required for fault detection and the accuracy of fault distance calculation. The time domain method, which uses differential equations to express the relationship between phase voltage and phase current, provides fast fault detection. This is because the relay does not need to wait one complete cycle to determine voltage and current phasors using Fourier filtering for impedance determination. However, due to the presence of harmonics in the current waveform shortly after fault inception, the resistance and inductance values being calculated become very sensitive to lower harmonics. They may start oscillating while converging which makes uncompensated time-domain method unreliable for fault distance determination [1], [32]. It is therefore imperative to establish as to how the performance of a distance relay might be affected when relaying functions are devised assuming minimal charging current.

2.10.1. Distance Relay Function.

Consider a typical two-source system shown in the Fig. 2.13 with a single transmission line protected by relays ***A*** and ***B***. To better study the effects of charging current, a pilot-relaying scheme using synchronized measurements from both terminals of the protected line is considered.

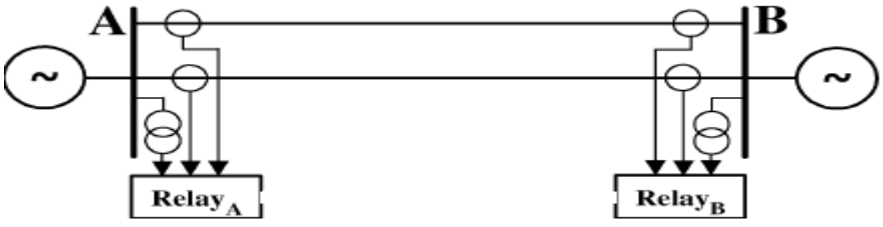

Fig. 2.13 - Two source system [58]

This is done to calculate the actual impedance between relay ***A*** and the point of fault and eliminate disturbances due to in-feed current and variable fault resistance. Time-domain based method is used to derive the relay function using differential equations. To achieve better accuracy, sequence components of the transmission line are used rather than lumped parameter values while the shunt capacitances are completely ignored. For a phase a-to-ground fault, the sequence circuit with distributed parameters is shown in Fig. 2.14.

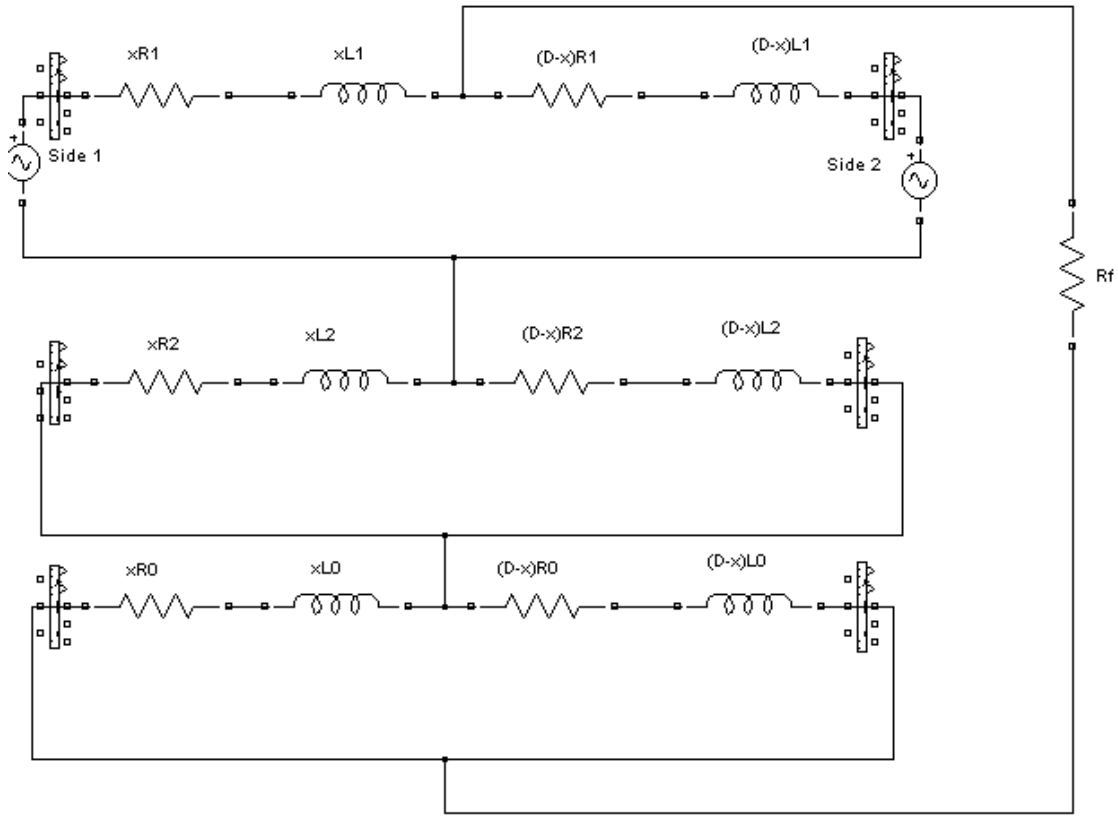

Fig. 2.14 - Sequence circuit diagram

It should be noted that:

x – fractional distance to the fault, $0 \leq x \leq 1$.

$R_1 = R_2$, $L_1 = L_2$ – positive and negative sequence resistance and inductance for entire line.

R_0, L_0 – zero sequence resistance and inductance for entire line.

R_f - fault resistance.

D = 1.

Terms and abbreviation for side 1 of system:

I_{1a} – side 1 phase A current

V_{1a} – side 1 phase A voltage

I_{10} – side 1 zero sequence current

V_{1af} – fault voltage on side 1 phase A

I_{1a}' – first derivative of side 1 phase A current

s – for s domain

Similar terms are used for side 2 of system as well.

For side 1 of system:

$$V_{1a}(s) = x[R_1 + sL_1]I_{1a}(s) + x[R_0 + sL_0 - R_1 - sL_1]I_{10}(s) + V_{1af}(s) \qquad (2.30)$$

For side 2 of system:

$$V_{2a}(s) = (1-x)[R_1 + sL_1]I_{2a}(s) + (1-x)[R_0 + sL_0 - R_1 - sL_1]I_{20}(s) + V_{2af}(s) \qquad (2.31)$$

$$V_{1af}(s) = V_{2af}(s) = 3(I_{10} + I_{20})R_f \qquad (2.32)$$

Subtracting (2.31) from (2.30) and rewriting terms with coefficient 'x' as given below:

$$R_1x = \overline{R_1}, L_1x = \overline{L_1}, and\ so\ on.$$

It should also be noted that for each differential element of the transmission line, the ratio between R_0 and R_1, and L_0 and L_1 is a constant. This can be used to reduce the numbers of variables in equation (2.30) and (2.31) to 2 from 4. The transmission lines

used in the test system are 3, three-phase pi-sections each of length 100km. The numerical values of the sequence parameters are given in Table 2.2.

Table 2.2 - Line Sequence Parameters

	Positive sequence/ Km	Zero sequence/ Km
Resistance	0.01273	0.3864
Inductance	0.9337×10^{-3}	4.1264×10^{-3}
Capacitance	12.74×10^{-12}	7.751×10^{-12}

Each parameter is multiplied by 300 for a 300km line. Using these parameters and defining two new constants where:

$$k_1 = \frac{R_0}{R_1},\ k_2 = \frac{L_0}{L_1} \tag{2.33}$$

Using the data above, and defining the coefficient 's' as d/dt in time-domain, subtracting (2.31) from (2.30) yields the following:

$$V_{1a} - V_{2a} - R_1[-I_{2a} + I_{20}] + R_0 I_{20} - L_1[-I'_{2a} + I'_{20}] + L_0 I'_{20} = \overline{R_1}[I_{1a} + k1-1I10+I2a+(k1-1)I20+L1[I1a'+(k2-1)I10'+I2a'+(k2-1)I20' \tag{2.34}$$

After algebraic manipulation, it can be seen that equation (34) has two variables only. To solve for the two unknowns, one more equation is required. This can be done by taking the derivative of equation (2.34) to obtain two independent equations which can be expressed in matrix form as shown:

$$\begin{bmatrix} A & B \\ A' & B' \end{bmatrix} \begin{bmatrix} \overline{R_1} \\ \overline{L_1} \end{bmatrix} = \begin{bmatrix} C \\ C' \end{bmatrix} \tag{2.35}$$

For each point in time, the system of equations can be solved to obtain a solution for R and L. Since the instantaneous values of resistance and inductance can now be

calculated, this method can be used to detect if the impedance has fallen to any one of the three zones of the distance relay. Once the numerical values of the positive sequence resistance and inductance are available, the presence of a fault can be determined by comparing complex impedance to the relay characteristic. The per-unit distance to the point of fault can then be easily calculated using phasors as:

$$xz_1 = \frac{V_{2a} - V_{1a} - z_1 I_{2a} - I_{20}[z_0 - z_1]}{-z_1 I_{1a} + [z_0 - z_1][-I_{10} - I_{20}] - z_1 I_{2a}} \tag{2.36}$$

Where xz_1 is a complex number. Once the value of xz_1 has been calculated, the following relation can be used to accurately estimate the point of the fault on the line:

$$d(km) = L \frac{|xz_1|}{|z_1|} \tag{2.37}$$

The zone elements of the MHO distance relay are shown in Fig. 2.15.

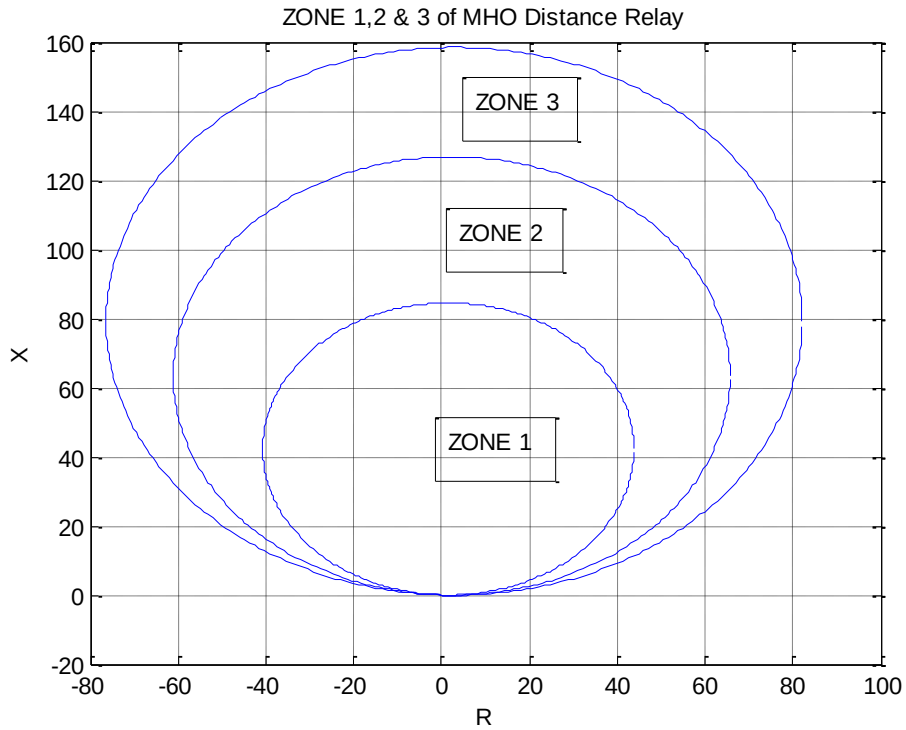

Fig. 2.15 - Zones of MHO relay

2.10.2. Relay Performance With and Without Charging Current.

Equation (2.35) is used to calculate values of R and L for each set of sampled data in time and compared against zone 1 reach settings in Fig. 2.15 to check if a fault has occurred. The resistance and inductance values calculated will not be used for distance calculations but only to gauge whether the impedance between the relay and the fault point has fallen within zone 1 reach. Once a fault is detected, a flag is raised and the algorithm uses Fourier filtering to calculate the phasor values of all required voltages and currents which are then used to calculate the accurate distance to the fault using equations (2.36) and (2.37).

The system was tested with a single-line to ground, high resistance fault of 100Ω placed after 0.1 seconds. The fault was placed at a distance of 200kms and the resulting waveforms were recorded. Plots for the calculated distance and impedance trajectory are shown Fig. 2.16. In this case the impedance settles in the outer boundary of zone 1.

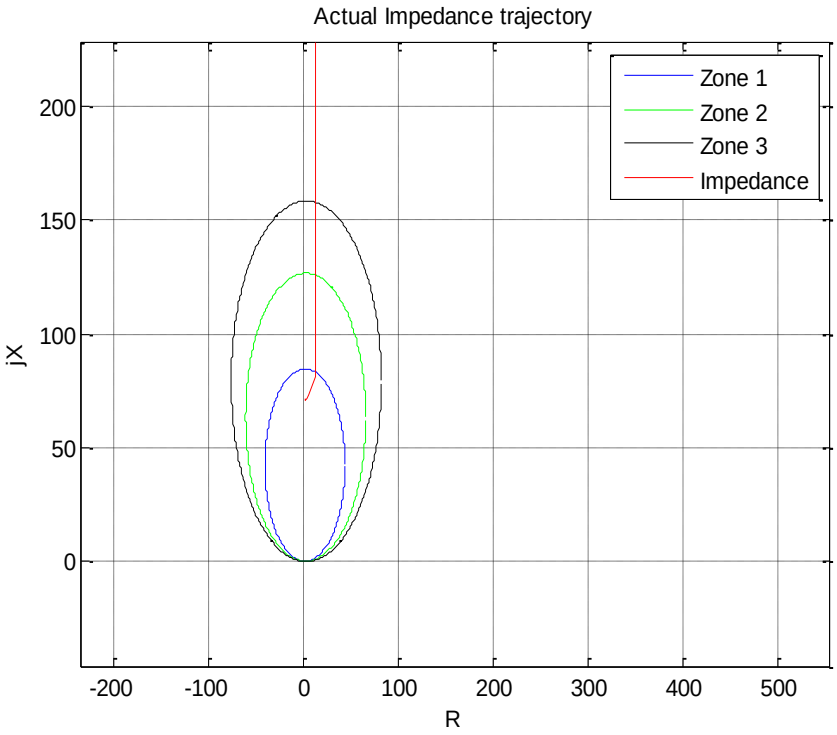

Fig. 2.16 - Impedance Trajectory

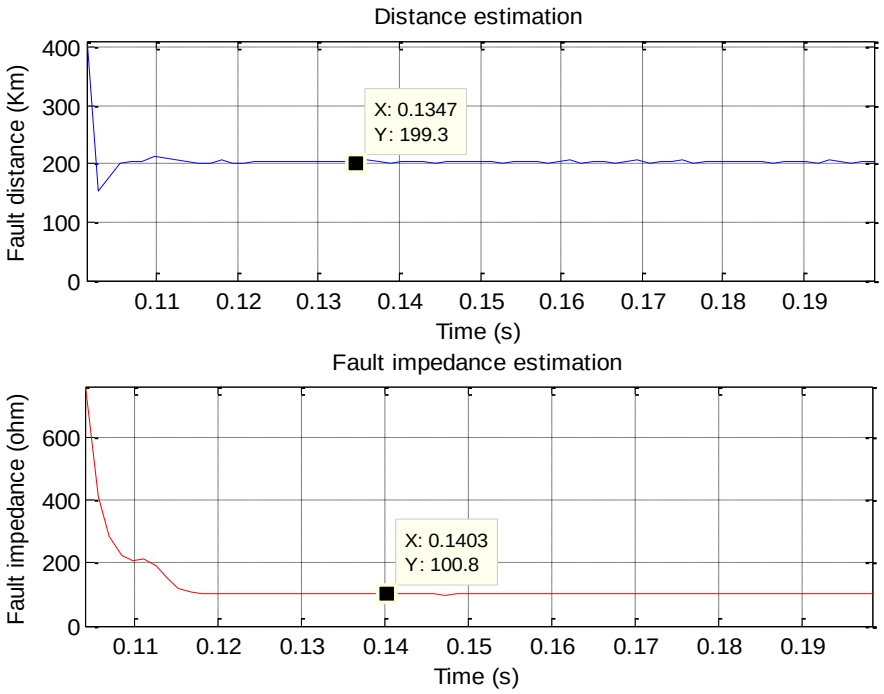

Fig. 2.17 - Fault distance and resistance estimation

Fig. 2.17 shows that the impedance to the point of fault, the per-unit distance and fault resistance can be accurately estimated when the line charging current is negligible. The system was tested again for a transmission with similar *R L* parameters but with significant distributed line capacitance. The new line parameters are given in Table 2.3.

Table 2.3 - Modified line sequence parameters

	Positive sequence/ Km	Zero sequence/ Km
Resistance	0.01273	0.3864
Inductance	0.9337×10^{-3}	4.1264×10^{-3}
Capacitance	12.74×10^{-9}	7.751×10^{-9}

The inclusion of line capacitance completely cripples the performance of the relay and the fault location algorithm. The relay erroneously signals the presence of a fault despite the fact no fault was placed on the system as evident from Fig. 2.18.

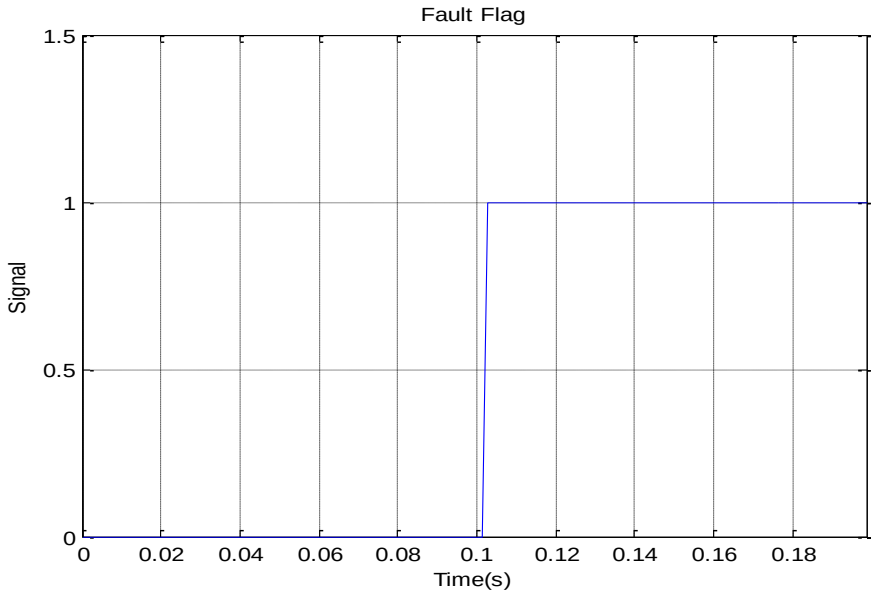

Fig. 2.18 - Fault flag

The distributed line capacitance causes significant oscillation of the calculated impedance. This oscillation caused the distance protection to over-reach due to the fact that a certain proportion of the line current measured by the relay sinks into the capacitance as charging current. The over-reaching phenomenon is illustrated in Fig. 2.19.

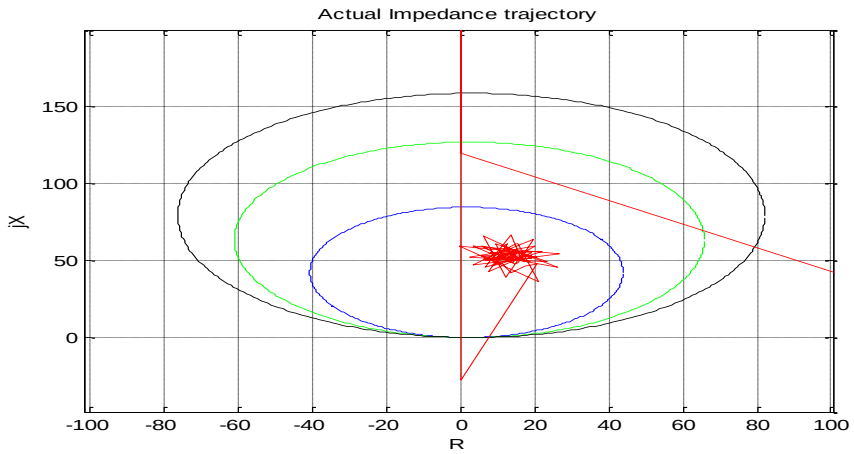

Fig. 2.19 - Over-reaching effect of distance relay

2.11. Fault Location on Transmission Lines.

Fault location on transmission line is an attractive and desirable feature in any protection scheme [32]-[47]. Distance relays installed for protection of transmission lines are able to furnish some information on the general area where a fault occurred, but are not purpose-built to pin-point the exact location. The distance to the point of fault can be calculated offline from the recorded data if required whereas the distance relaying function must be carried out online for fast response. The ability to locate a fault on a transmission line offers several incentives:

- Locating the fault accelerates transmission line restoration and maintains system stability.
- It improves system availability and potentially reduces operating costs.
- It saves the time and cost of sending out a repair crew to search for the fault point in bad weather or unfriendly terrain.

Numerous fault locating algorithms have been proposed in the literature that can be broadly categorized as:

- Single-ended algorithms.
- Two-ended algorithms.

Each of the two fault locating procedure types can be further sub-categorized as one of the following:

- Procedures based on the fundamental frequency voltages and currents (impedance based principle).
- Time-domain based procedures such as travelling-wave fault locators.
- Non-conventional fault locating procedures such as those based on Artificial Neural Networks [46].

The fundamental frequency based fault locating procedures are the most popular and widely used in real applications. The travelling-wave procedures take into account voltage and current waves that travel back and forth along the line from the point of disturbance. This type of fault locating procedure is typically more costly due

to the high sampling rate requirements. A diagrammatic classification of the various fault locating procedures is shown in Fig. 2.20 [1].

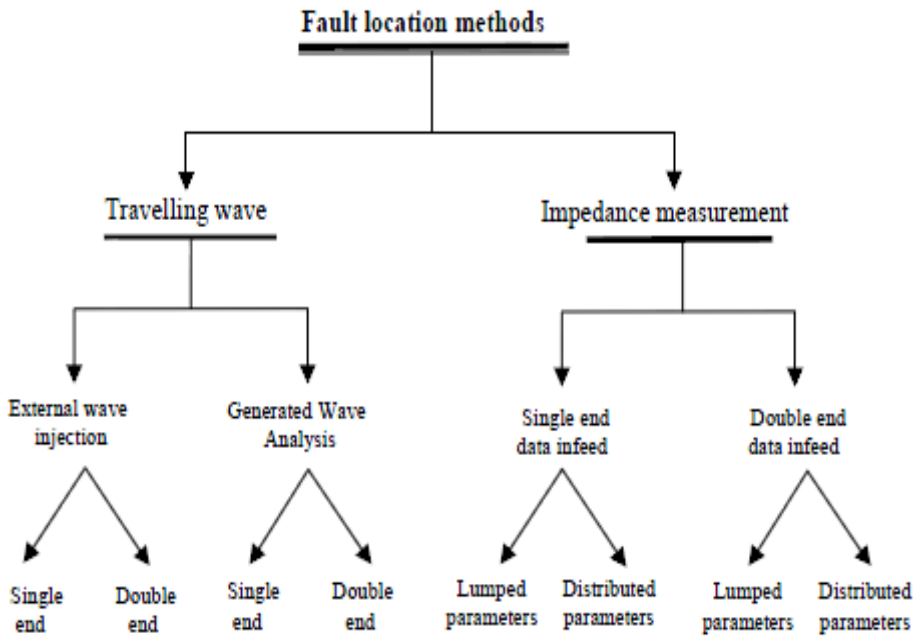

Fig. 2.20 - Fault location methods [1]

2.11.1. Fault Location Schemes.

The gradual development of standardized means of communication between relay line terminals has opened up a new front for improved fault location accuracy. Fault locating algorithms that utilize two-ended measurements can have signal data fed from either synchronized samplers, with aid of Global Positioning System (GPS), or unsynchronized digital fault recorders. Synchronized sampling of data from the two ends of a transmission line facilitates simple and accurate fault location. Modern PMUs can reportedly achieve synchronization accuracy of ±0.5 μs [48]. A schematic diagram of two-ended, synchronized fault locating procedure is shown in Fig. 2.21. Satellite based GPS has the salient ability of providing a common time reference signal. This enables accurate synchronization of geographically separated substations where three-phase data measurements are recorded.

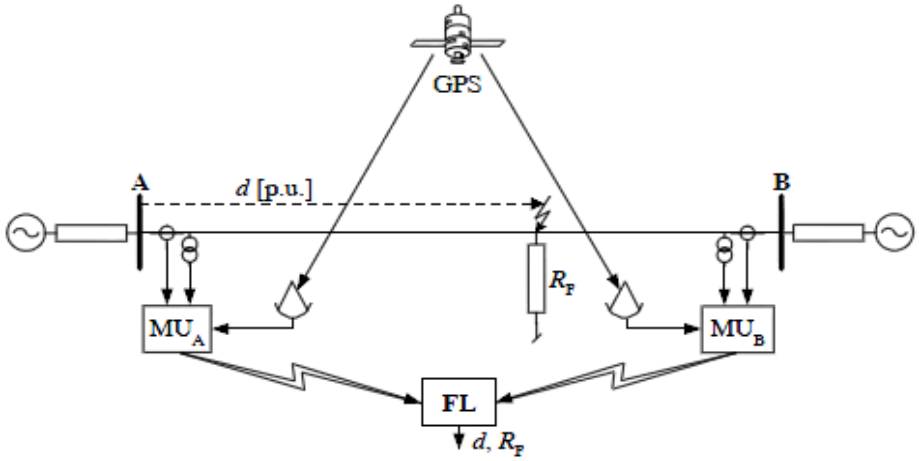

Fig. 2.21 - Fault location using GPS [48]

Where d is the per-unit distance to the point of fault and R_F is the fault resistance.

When the GPS based synchronization mechanism is unavailable, the measurements from the two line terminals are performed asynchronously. Data measurements performed asynchronously do not have a common time reference and consequently, the sampling instants at points *A* and *B* do not coincide. As a result of the mismatched sampling instants, a certain phase shift, δ, exists between the waveforms recorded by the A/D converters on either ends.

In case of unsynchronized sampling of three phase data, the collected measurement data is generally shifted in time. The phase delay can be caused by a number of factors:

- Relays at two terminals of the transmission line detect the presence of a fault at two slightly different instants.
- The lack of a synchronization mechanism such as GPS for harmonizing analog to digital converter clocks.
- Different sampling rates of A/D converters on line terminals.
- Phase shifts introduced due to measurement channels.

Fault locators, compared to protection relays, are expressly designed to pinpoint the exact location of faults on transmission lines to expedite the process of repair and restoration of the power system. Two-ended measurement algorithms collect signals

from both ends of a transmission line and offer far superior performance as opposed to single-end algorithms due to their apparent insensitivity to source impedance, fault resistance and remote-end in-feed [37].

A simple protection approach for multi-terminal transmission lines using synchronized voltage measurements is presented in [35]. The process can be applied to both transposed and un-transposed lines but requires source impedance data. Also, fault distance calculation results in [35] indicate the dependence on the type of fault and the fault resistance involved. Generally, the percentage error in distance calculation increases with higher fault resistance. Fault location algorithms for two-terminal systems using unsynchronized data measurements are presented in [37]-[39] and [59]-[61].

An iterative procedure is developed in [37] where the unknown synchronization angle can be found using the Newton-Raphson technique. A similar iterative procedure is presented in [39] where a modified secant method is used to obtain the value of the unknown synchronization angle. A non-iterative fault location and synchronization procedure is developed in [38] using incremental positive sequence quantities for symmetrical faults, and simultaneously using positive and negative sequence quantities for unsymmetrical faults. All of the procedures presented in [37]-[39] result in multiple pairs of synchronization angle and fault distance values. The multiple solutions must be carefully treated with specially developed conditions to select the correct pair of angle and distance.

The PMU-based fault location schemes provide the advantage of being insusceptible to source impedance behind the relay, fault resistance involved and any remote in-feed from far end terminals [47]. However, the fact remains that GPS assisted PMUs are still not as widely adopted as they could be due to economic considerations.

The common occurrence of compensating elements on transmission lines has made reliable protection of power systems a challenging and difficult task. Series compensation of transmission lines increases the power transfer capability of the network and also improves the overall stability of the system. Despite the obvious

advantage of using series compensation, it has been observed that series capacitors generally result in an increase in the fault current level due to the reduced line impedance and may also cause sub-synchronous resonance. Compensated transmission lines present unique challenges to power system engineers who design protective relays such as differential, directional and distance relays because the transient response of series capacitors cannot be preconceived. The protective relays of a given transmission line are affected by the reactance change and the sub-harmonic frequencies generated by the series capacitor, in addition to the high frequency transients that may also emanate in the event of a short-circuit. Fortunately, the digital filters implemented on micro-processor-based numerical relays have the ability to attenuate these high frequency components to a large extent. Generalized models of compensated transmission lines are shown in the Fig. 2.22.

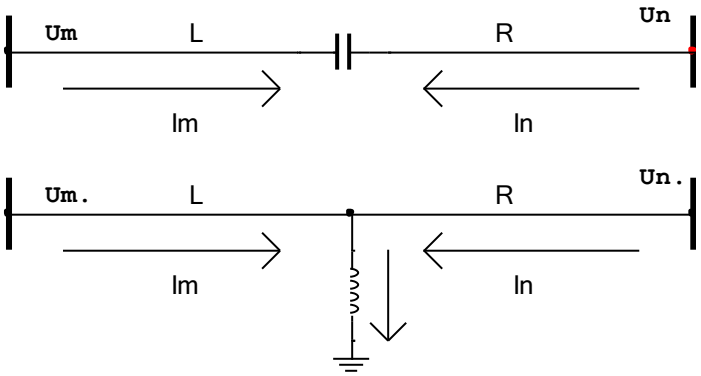

Fig. 2.22 - Compensated transmission lines

Protective relays installed on transmission lines are influenced by a number of factors which need to be carefully considered to mitigate the adverse effects of compensating elements. Protective devices that respond to phase quantities are affected by voltage inversion phenomenon which is a change of 180^{o} in voltage phase angle. This usually occurs for a fault near the series capacitor and when the impedance between capacitor and the fault point is capacitive rather than inductive. Relays that use phase information from the fault side of the line will be able to detect the fault successfully whereas the relays on the adjacent side of the capacitor might not be able to correctly declare the fault location. In addition to the voltage inversion phenomena, series compensated transmission lines also affect directional and

differential type relays and those that respond to sequence voltage and current quantities [51]-[53].

Numerous fault location algorithms have been proposed for series compensated transmission lines that utilize one-ended or two-ended measurements. A one-end fundamental frequency based technique is proposed in [49] where an equivalent model for series capacitor and MOV is utilized and represented as current-dependent variable impedance. The algorithm is tested for short circuit conditions with low fault resistances. The algorithm also requires data on local and remote end sources impedances and any mismatch of the assumed parameters is likely to affect distances estimates. Being a one-end data algorithm, significant current in-feed from remote sources is also likely to exacerbate distance estimation error.

A PMU-based fault location algorithm for series compensated lines that avoids using the series capacitor device model by utilizing a two step algorithm is proposed in [50] and [51]. A pre-location subroutine is designed to first obtain a crude estimate of the fault location. The distance estimate is then refined using a correction subroutine by iteratively calculating the series capacitor voltage drop and hence the fault location and device impedance. The complex algorithms makes use of synchronized data sampling and cannot be used on systems where GPS-assisted data recorders are not present.

Fault location algorithm for double-circuit series compensated lines using unsynchronized data is described in [53]. This solution is a multi-stage algorithm where data synchronization can be achieved using three separate procedures. The algorithm makes use of aggregate sequence voltages and currents to estimate the distance to the point of fault as well as the fault resistance and SC/MOV impedance.

2.11.2. Transmission Line Models.

Over-head transmission lines considered in relation to particular applications are generally of two types:

- Lumped-parameter line models, and
- Distributed-parameter line models.

Lumped parameter models are lines represented by lumped impedance elements. The impedance parameters are calculated using a single frequency, usually the fundamental power frequency. The simplified models are utilized for steady-state fault location calculations or other transient simulations in the vicinity of a particular frequency under study. A simple lumped-parameter model of an over-head line is shown in Fig. 2.23.

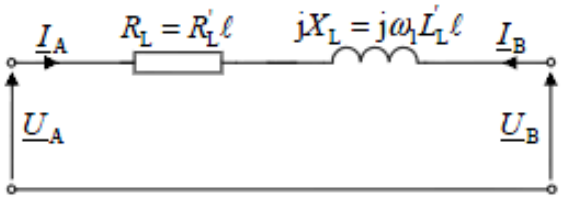

Fig. 2.23 - Lumped parameter model [21]

Where *l* is the per-unit distance and w_1 is the fundamental frequency.

The per-phase self and mutual impedances of the model are dependent on line geometry. For a transmission line with symmetrical impedance matrix, both the diagonal and off-diagonal elements are equal. This is a condition which is satisfied when the line is completely transposed as illustrated in Fig. 2.24.

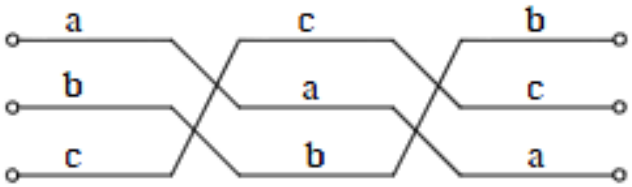

Fig. 2.24 - Section of a three phase transposed line [1]

The method of symmetrical components enables linear transformation of phase components to a set of symmetrical quantities. This allows a three-phase network to be decoupled in to three sequence networks which can be analyzed independently. A short-circuit fault on a typical lumped-parameter transmission line is represented in Fig. 2.25.

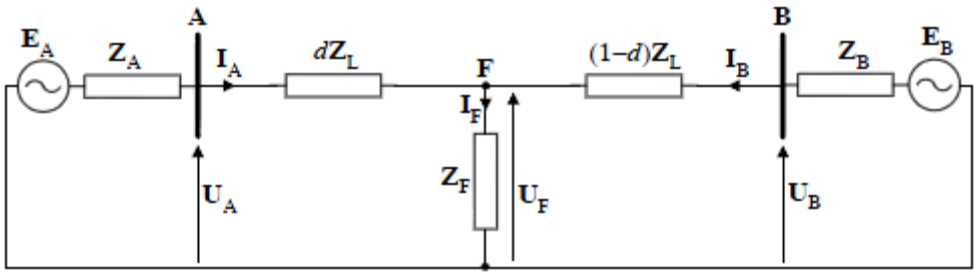

Fig. 2.25 - Fault on lumped-parameter line [16]

Application of sequence transformation on the per-phase voltage, current and impedance quantities allows the system to be resolved into positive, negative and zero sequence networks as shown in Fig. 2.26.

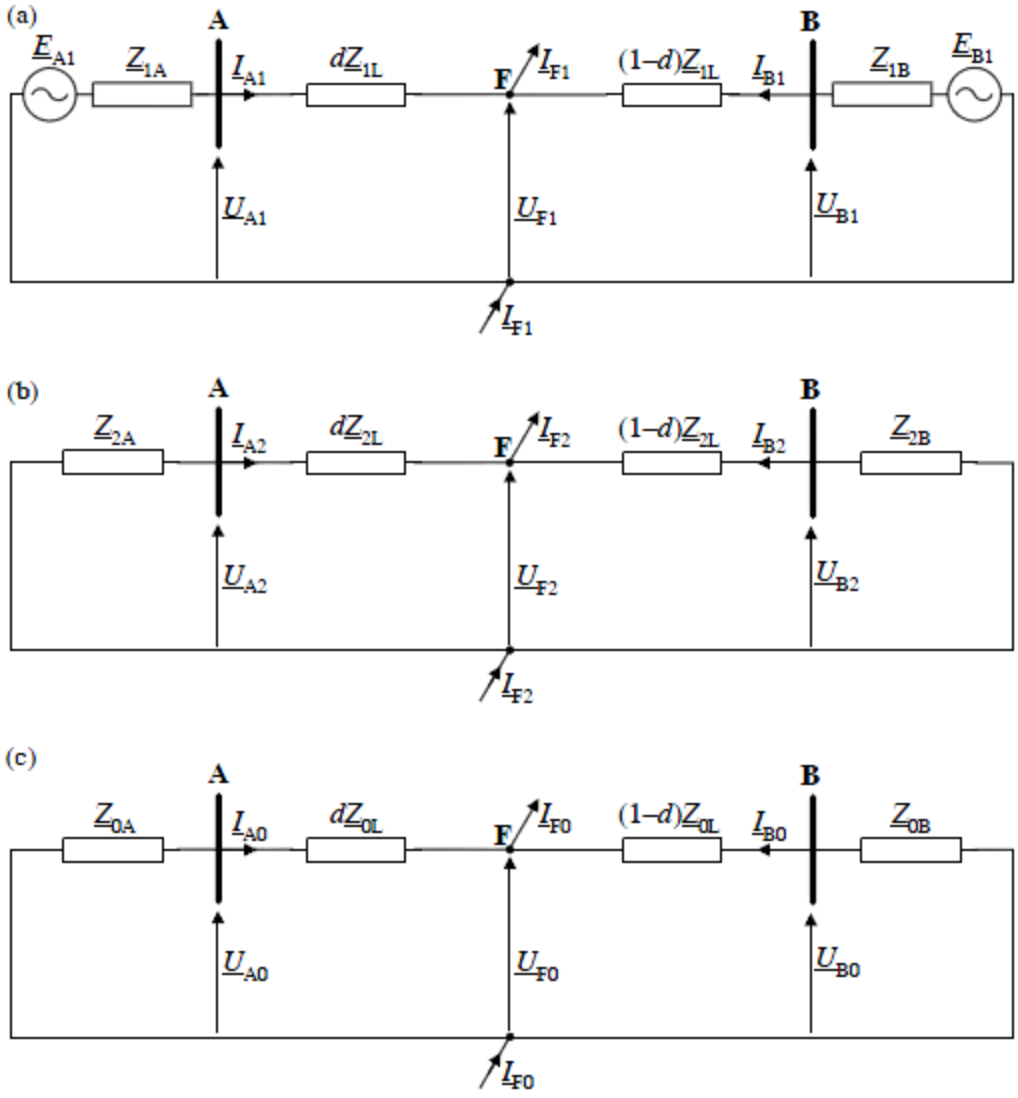

Fig. 2.26 - (a) Positive, (b) Negative and (c) Zero sequence networks [16]

Transformation from symmetrical components into phase components is defined as:

$$\begin{bmatrix} V_a \\ V_b \\ V_c \end{bmatrix} = \begin{bmatrix} 1 & 1 & 1 \\ 1 & a^2 & a \\ 1 & a & a^2 \end{bmatrix} \begin{bmatrix} V_0 \\ V_1 \\ V_2 \end{bmatrix} \tag{2.38}$$

Where a is defined as $e^{j2\pi/3}$.

The distributed-parameter model is a more accurate representation of a transmission line. The distributed model consists of series *RL* impedance along with shunt admittance. For medium to long distance transmission lines, shunt admittance need to be incorporated to account for the leakage current. A generalized distributed-parameter model of transmission line is depicted in the figure below.

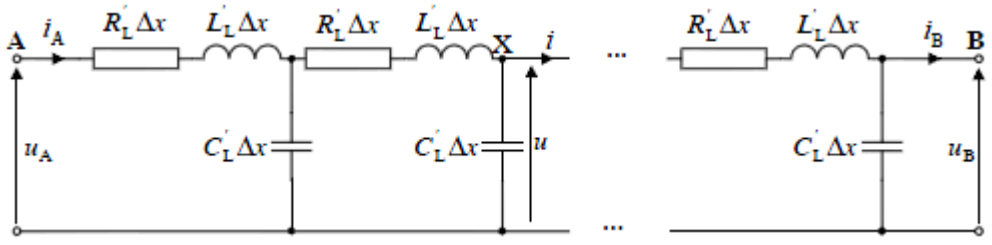

Fig. 2.27 - Distributed-parameter line model [37]

For a distributed-parameter transmission line, the voltage and current along the line are functions of both the distance *x* and time *t*. Since the distributed model can be applied to phasors as well, the equivalent π circuit representation in Fig. 2.28 is used more commonly for impedance-principle based fault locating procedures [53].

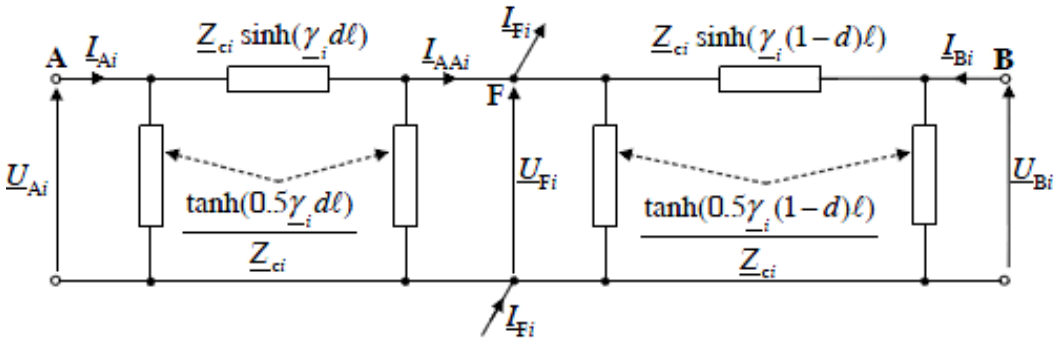

Fig. 2.28 - Distributed π model for i[th] symmetrical component [38]

Where $\gamma_i$and $Z_{ci}$are the ith symmetrical component propagation constant and surge impedance respectively.

Chapter 3

Problem Formulation and System Modeling

In this chapter, the solution to the transmission line protection problem is modeled as a fault locating algorithm. The mathematical models for the proposed systems are developed assuming unsynchronized three-phase voltage and current measurements. Two new fault locating algorithms are formulated in this thesis:

1- *Fault Location Scheme for a Multi-Terminal Transmission Line System Using Unsynchronized Measurements*

A fault location algorithm for multi-terminal transmission lines using unsynchronized measurements from one fault data recorder placed on each voltage source terminal is developed. The multi-terminal system used is a four generator EHV system with five transmission lines that need to be protected. The basic principles of two and three-terminal line protection are extended to a multi-terminal system.

The data synchronization procedure presented here also doubles as a fault detection scheme and is immune to power system transients such as load and capacitive switching. The proposed fault location method is independent of high fault resistance and the variation of source impedance behind the fault. The delivered fault detection and location algorithm is then extensively tested for all major fault types and large fault resistances.

2- *Fault Location on Series and Shunt-Compensated Lines Using Unsynchronized Measurements*

A simple but effective fault location algorithm for both series and shunt compensated transmission lines using unsynchronized two-ended measurements is proposed. The data synchronization is achieved using post-fault data samples which enhance the performance of the delivered algorithm. Fault location is achieved by simultaneously processing the positive and negative sequence fault impedance loops for unsymmetrical faults, and the positive and superimposed-positive sequence fault impedance loops for symmetrical faults. The algorithm is able to deliver accurate

results post power system transients such as abrupt load switching. The algorithm is extensively tested for all major fault types and large fault resistances.

3.1. Fault Location Scheme for a Multi-Terminal Transmission Line System Using Unsynchronized Measurements

Fault location on overhead power transmission lines remains a subject of great interest and has been researched intensively over the years [33]-[47]. Fault location algorithm for teed-feeders that carries out data synchronization by selecting a common reference and equating the voltages at the teed-point is proposed in [33]. Super-imposed component extraction and modal transformation is used for fault distance calculation. However, the authors assume synchronization mismatch of only a few data samples and the delivered algorithm wasn't tested for large or obtuse synchronization angles. The three-terminal protection scheme that uses Clarke transformation to decouple the inter-phase quantities and develop a fault detection index is proposed in [34]. The algorithm offers high-speed response but needs synchronized data measurement from Phasor Measurement Units (PMU) and Global Positioning System (GPS).

The fact remains that GPS assisted PMUs are still not as widely adopted as they could be due to economic considerations. Therefore, data obtained from asynchronous fault recorders need to be corrected by using a complex synchronization operator ($e^{j\delta}$), where δ is the synchronization angle. Moreover, the application of two-end fault location algorithms on multi-terminal lines would require *2n* fault data recorders, where *n* is the number of transmission lines.

In this research, a simple alternative fault location algorithm is developed using unsynchronized measurements from one fault data recorder placed on each voltage source terminal as shown in Fig. 3.1. The multi-terminal system used to apply the developed fault location algorithm is a four generator EHV system with five transmission lines.

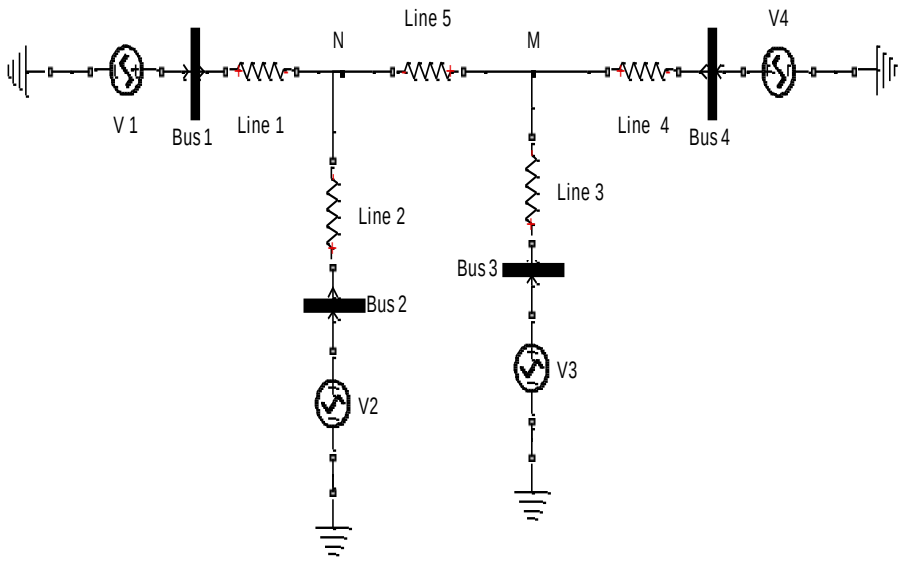

Fig. 3.1 - Five line multi-terminal system

The basic principles of two and three-terminal line protection are extended to multi-terminal systems devising the delivered algorithm. The distributed parameter line model is strictly used to represent high voltage transmission lines such that their behaviors resemble real-life system dynamics.

A non-iterative data synchronization procedure is developed using known pre-fault measurements. Data synchronization can be carried out in a single-shot fashion without any constraints on the amount of synchronization required by the system. Different from algorithms presented in [37]-[39], the data synchronization procedure presented here provides the additional advantage of doubling back as a fault detection method as well, which obviates the need for Clarke transformation based detection methods as described in [33]-[35]. The formulation for the fault locating procedure results in five distance functions, one for each line, which can not only identify the faulted leg but also clearly point out the correct tee-point in the event of a fault evolving at points M or N of the system in Fig. 3.1.

3.1.1. Data Synchronization Procedure.

The synchronization procedure begins with designating one of the buses as the common reference point. In this case, bus 4 is used as the common reference. The technique is designed such that data from other ends can be synchronized without any

restriction on the amount of synchronization needed by the system before the fault location process can be initiated. That is, the synchronization procedure works for both acute and obtuse synchronization angles. The various types of faults differ in the type of sequence component quantities present in voltages and currents during faulted operation. Of all the different fault types, the presence of positive sequence quantities is common for both symmetrical and non-symmetrical faults. Therefore, only positive sequence phasors are used for the data synchronization process and fault location scheme. It should also be noted that the synchronization procedure developed in this section is highly suitable for implementation on a digital micro-processor.

Once the three-phase quantities are decoupled using symmetrical component transformation, the relationship between positive sequence voltage and current at location *x* from any bus can be expressed as [39]:

$$\frac{\partial V_1}{\partial x} = Z_1 I_1$$

$$\frac{\partial I_1}{\partial x} = Y_1 V_1 \tag{3.1}$$

where V_1 and I_1 are the positive sequence voltage and current respectively, Z_1 is the positive sequence impedance and Y_1 is the positive sequence admittance.

The solution of the above two decoupled equations can be written in a two port network form by applying the boundary conditions as follows:

$$\begin{bmatrix} V_{s1} \\ I_{s1} \end{bmatrix} = \begin{bmatrix} \cosh(\gamma_1 l) & Z_{c1}\sinh(\gamma_1 l) \\ \sinh(\gamma_1 l)/Z_{c1} & \cosh(\gamma_1 l) \end{bmatrix} \begin{bmatrix} V_{R1} \\ I_{R1} \end{bmatrix} \tag{3.2}$$

where V_{S1} and I_{S1} are the sending end positive sequence voltage and currents , and V_{R1} and I_{R1} are the receiving end positive sequence voltage and current. γ_1 is the positive sequence propagation constant and *l* is the line length.

It is helpful to express (3.2) in terms of the sending end quantities to calculate voltage and current at a distance *x* from line terminal.

$$\begin{bmatrix} V_{R1} \\ I_{R1} \end{bmatrix} = \begin{bmatrix} \cosh(\gamma_1 l) & -Z_{c1}\sinh(\gamma_1 l) \\ -\sinh(\gamma_1 l)/Z_{c1} & \cosh(\gamma_1 l) \end{bmatrix} \begin{bmatrix} V_{s1} \\ I_{s1} \end{bmatrix} \tag{3.3}$$

The voltage and current phasors calculated from data measurement at buses 1, 2 and 3 need to be corrected by using the synchronization operator [5]-[7]:

$$V_{n1}(\delta_n) = V_{n1}e^{j\delta_n}$$

$$I_{n1}(\delta_n) = I_{n1}e^{j\delta_n} \tag{3.4}$$

where V_{n1} and I_{n1} are the positive sequence voltage and current measured at bus *n* and $\delta_n$is the synchronization required for bus n.

Evaluating the pre-fault positive sequence voltage and current phasors from buses 3 and 4 at the tee-point M results in the following expression:

$$V_{31}e^{j\partial_3}\cosh(\gamma_1 L_3) - I_{31}e^{j\partial_3}Z_{c1}\sinh(\gamma_1 L_3) = V_M^+ = V_{41}\cosh(\gamma_1 L_4) - I_{41}Z_{c1}\sinh(\gamma_1 L_4) \tag{3.5}$$

In general, V_{x1} and I_{x1} represent the positive sequence voltage and current at bus *x*. V_T^+ and I_T^+ represent positive sequence voltage and current at tee-point M or N. L_x represents line length *x*.

The total current at tee-point M from buses 3 and 4 using (3.3) can be expressed as:

$$I_{M(3,4)}^+ = -V_{31}e^{j\partial_3}\sinh(\gamma_1 L_3)\frac{1}{Z_{c1}} + I_{31}e^{j\partial_3}\cosh(\gamma_1 L_3) - V_{41}\sinh(\gamma_1 L_4)\frac{1}{Z_{c1}} + I_{41}\cosh(\gamma_1 L_4) \tag{3.6}$$

The projected voltage at the tee-point M using the reference bus voltage and current in (3.3) gives:

$$V_M^+ = V_{41}\cosh(\gamma L_4) - I_{41}\,Z_{c1}\sinh(\gamma L_4) \tag{3.7}$$

Using the expressions for the positive sequence voltage and current at the tee-point M in (3.6) and (3.7), the positive sequence voltage at the tee-point N can be calculated using the two-port network equation in (3.3).

$$V_N^+ = V_M^+\cosh(\gamma L_5) - I_{M(3,4)}^+ Z_{c1}\sinh(\gamma L_5) \tag{3.8}$$

The positive sequence voltage at tee-point N in (3.8) is also equal to the voltage projected from buses 1 and 2. This can be expressed as:

$$V_N^+ = V_{11}e^{j\partial_1}\cosh(\gamma L_1) - I_{11}e^{j\partial_1}Z_{c1}\sinh(\gamma L_1) \tag{3.9}$$

$$V_N^+ = V_{21}e^{j\partial_2}\cosh(\gamma L_2) - I_{21}e^{j\partial_2}Z_{c1}\sinh(\gamma L_2) \tag{3.10}$$

With some mathematical manipulation, expressions in (3.3), (3.9) and (3.10) can be re-arranged and expressed in a concise matrix form as shown below:

$$e^{j\partial_3}[M_{13}] = b_1 \tag{3.11}$$

$$e^{j\partial_2}[M_{22}] + e^{j\partial_3}[M_{23}] = b_2 \tag{3.12}$$

$$e^{j\partial_1}[M_{31}] + e^{j\partial_3}[M_{33}] = b_3 \tag{3.13}$$

where,

$$M_{13} = V_{31}\cosh(\gamma_1 L_3) - I_{31}Z_{c1}sinh(\gamma_1 L_3)$$

$$M_{22} = -V_{21}\cosh(\gamma_1 L_2) + I_{21}Z_{c1}sinh(\gamma_1 L_2)$$

$$M_{23} = V_{31}\sinh(\gamma_1 L_3)\sinh(\gamma_1 L_5) - I_{31}Z_{c1}sinh(\gamma_1 L_5)\cosh(\gamma_1 L_3)$$

$$M_{31} = -V_{11}\cosh(\gamma_1 L_1) + I_{11}Z_{c1}sinh(\gamma_1 L_1)$$

$$M_{33} = V_{31}\sinh(\gamma_1 L_3)\sinh(\gamma_1 L_5) - I_{31}Z_{c1}sinh(\gamma_1 L_5)\cosh(\gamma_1 L_3)$$

and,

$$b_1 = V_{41}\cosh(\gamma_1 L_4) - I_{41}Z_{c1}sinh(\gamma_1 L_4)$$

$$\begin{aligned} b_2 = {} & -V_{41}\cosh(\gamma_1 L_4)\cosh(\gamma_1 L_5) + I_4 Z_{c1}\sinh(\gamma_1 L_4)\cosh(\gamma_1 L_5) \\ & - V_4\sinh(\gamma_1 L_4)\sinh(\gamma_1 L_5) + I_4 Z_{c1}\cosh(\gamma_1 L_4)\sinh(\gamma_1 L_5) \end{aligned}$$

$$b_3 = b_2$$

Equations (3.11), (3.12) and (3.13) can now be expressed as:

$$\begin{bmatrix} M_{11} & M_{12} & M_{13} \\ M_{21} & M_{22} & M_{23} \\ M_{31} & M_{32} & M_{33} \end{bmatrix} \begin{bmatrix} e^{j\delta_3} \\ e^{j\delta_2} \\ e^{j\delta_1} \end{bmatrix} = \begin{bmatrix} b_1 \\ b_2 \\ b_3 \end{bmatrix} \tag{3.14}$$

where

$$M_{11} = M_{12} = M_{21} = M_{32} = 0$$

The synchronization angle vector δ, required for synchronizing data measured at buses 1, 2 and 3 with respect to bus 4, can now be calculated from (3.14) and is given by the following expression:

$$\delta^{\circ} = \begin{bmatrix} \delta_3 \\ \delta_2 \\ \delta_1 \end{bmatrix} = Arg\left(\begin{bmatrix} M_{11} & M_{12} & M_{13} \\ M_{21} & M_{22} & M_{23} \\ M_{31} & M_{32} & M_{33} \end{bmatrix}^{-1} \begin{bmatrix} b_1 \\ b_2 \\ b_3 \end{bmatrix} \right) \text{x} \frac{pi}{180} \tag{3.15}$$

where the angle vector δ is in degrees given as obtained from (3.15).

The required synchronization operator can be solved for by using (3.15) for each incoming voltage and current data sample after calculating the positive sequence phasors. Equation (3.15) when expressed in the given form makes it possible to calculate all the required synchronization angles at once and is convenient for implementation on a digital computer.

The fault detection schemes described in [33] and [34] utilize Clarke transformation of inter-phase signals to obtain the decoupled ground and aerial mode quantities. A fault detection index is formulated and used with a threshold to detect the faulted leg in the teed system. The fault detection scheme described in [35] evaluates each bus voltage at the tee-point and observes large differences that indicate a faulted leg. The fault detection scheme used in this algorithm is inherent in the data synchronization process. An overview of the complete algorithm which details the various stages involved is shown in Fig. 3.2. The system calculates and records the synchronization angle during the steady-state pre-fault condition. Once a fault occurs on any of the five protected transmission lines, evaluating (3.15) results in a deviation from the steady state synchronization angle values. This deviation is used to determine if the system is operating under a fault condition. The detection scheme is formalized in the pseudo-code below:

if

$$\left|\delta(t) - \delta_{steady-state}\right| \geq threshold$$

$then$

$$locate\ fault$$

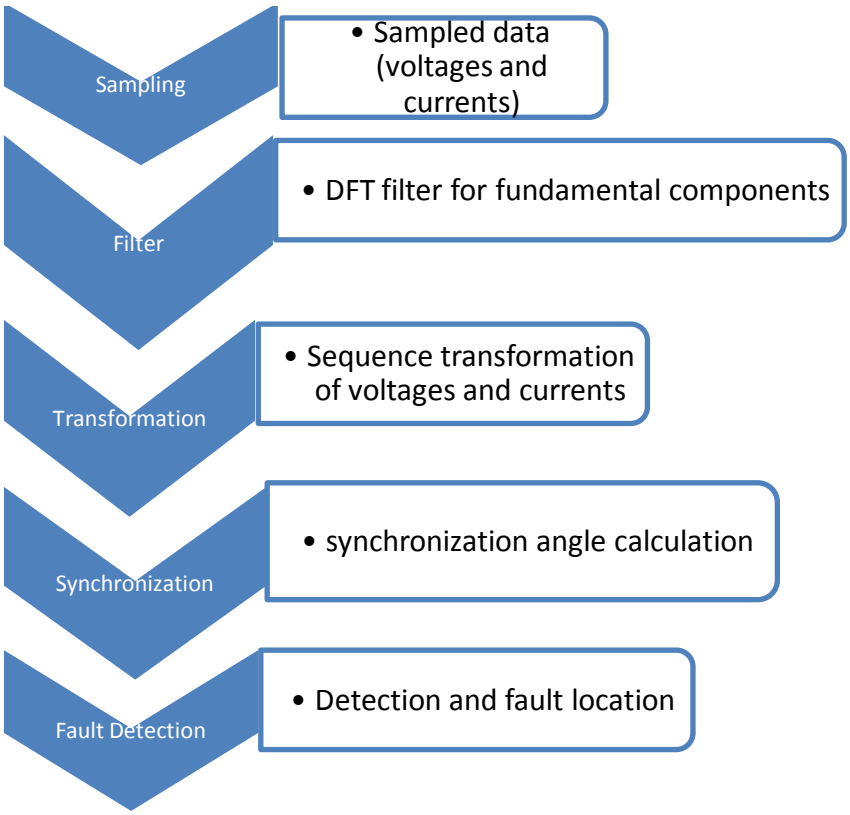

Fig. 3.2 - Fault locator algorithm

3.1.2. Fault Location Scheme.

The fault location scheme involves reducing the multi-terminal system to a two-terminal system such that the faulted leg is contained in the reduced two-terminal line. The fault location function developed here is for the ground fault on line L_1 as shown in Fig. 3.3. The use of positive sequence voltage and current phasors ensure that the scheme would work for other fault types as well.

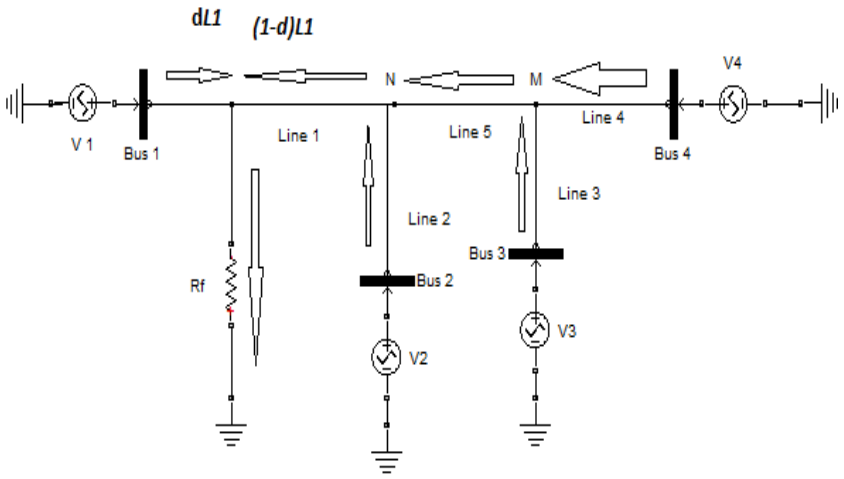

Fig. 3.3 - Fault on line L_1 with assumed current directions

To reduce the four-terminal system that contains a faulted leg to a two-terminal one, the voltage and the total current entering tee-point N need to be calculated. The voltage at N is given by (3.8) and the total current entering N is given by the following expression:

$$I_N^+ = -\frac{V_M^+ \sinh(\gamma_1 L_5)}{\mathrm{Z_{c1}}} + \mathrm{I_{M(3,4)}^+} \cosh(\gamma_1 L_5)$$

$$-V_{21} e^{j\partial_2} \frac{sinh(\gamma_1 L_2)}{Z_{c1}} + I_{21} e^{j\partial_2} \cosh(\gamma_1 L_2) \qquad (3.16)$$

where I_N^+ is the positive sequence current entering N. Using (3.8) and (3.16), let:

$$A_1 = V_N^+$$

$$B_1 = I_N^+$$

The voltage at the fault point is given by the following two equations:

$$V_{F1} = A_1 \cosh(\gamma_1 L_1 (1 - d_1)) - \mathrm{B_1 Z_{c1}} \sinh(\gamma_1 L_1 (1 - d_1)) \qquad (3.17)$$

$$V_{F1} = V_{11} e^{j\partial_1} \cosh(\gamma_1 L_1 d_1) - \mathrm{I_{11}} e^{j\partial_1} Z_{c1} \sinh(\gamma_1 L_1 d_1) \qquad (3.18)$$

where d_1 is the per-unit distance to the fault point from Bus 1.

Subtracting (3.18) from (3.17) and rearranging gives the expression for the per-unit distance to the fault point.

$$d_1 = Real\left[\frac{arctanh\left(\frac{A_1\cosh(\gamma_1 L_1) - \mathrm{B}_1\mathrm{Z}_{c1}\sinh(\gamma_1 L_1) - V_{11}e^{j\partial_1}}{-I_{11}e^{j\partial_1}Z_{C1} + A_1\sinh(\gamma_1 L_1) - \mathrm{B}_1\mathrm{Z}_{c1}\cosh(\gamma_1 L_1)}\right)}{\gamma_1 L_1}\right] \quad (3.19)$$

Using the synchronization operator calculated during steady-state, the per unit distance to the fault point can be calculated using (3.19). Using similar reductions, distance functions for the other four transmission lines can also be derived which would result in a total of five distance functions. The distance functions are evaluated once the fault detection scheme described in the previous section determines a fault condition. Evaluating the five distance functions will result in one function yielding a per-unit value less than one, which would help single out the faulted transmission line. Moreover, if a fault occurs on line 1 then the sequence voltages projected at *M* from buses 3 and 4 should be equal, in additional to satisfying equation (3.8). Hence, logical conditions can be developed to identify faults on line 1 which are presented here as a pseudo-code:

if

$$[M(V_{3i}) = M(V_{4i})]\ \&\ [(3.10) = true]\ \&\ [0 \leq d_1 \leq 1]$$

$then$

$$faulted\ line = line1$$

where *i* is the ith sequence component. Similar logical conditions can be developed to identify other fault legs as well. The compound logical conditions ensure that right fault line is always identified. Additionally, for faults on the tee-point M, distance functions d_3, d_4 and d_5 will indicate a per unit value of 1. Whereas for a fault on the tee-point N, d_5 will indicate a per unit value of zero.

3.2. Fault Location on Series and Shunt-Compensated Lines Using Unsynchronized Measurements

A simple but effective fault location algorithm is proposed for both Fixed Series Compensated (FSC) and shunt compensated transmission lines using unsynchronized two-ended measurements. The data synchronization is achieved using post-fault data samples which enhance the performance of the fault locating procedure. Additionally, the developed algorithm is also able to deliver accurate fault location estimates post power system transients.

Most of the fault-locating algorithms presented in literature are highly complex due to the fact that the voltage drop across the series capacitor or its current-controlled dynamic impedance cannot be predetermined and need to be estimated. A typical Fixed Series Compensation (FSC) and its nonlinear overvoltage protection such as metal-oxide varistor (MOV) have three modes of operation [49]-[51]:

- Large fault current mode – where the series-capacitor is almost completely bypassed and short-circuited by the MOV.
- Low fault current mode – where most of the current flows through the series capacitor due to high impedance faults.
- Intermediate fault current mode – where the device voltage is above the MOV threshold voltage and both the SC and MOV partially conduct the fault current.

A large portion of the computational effort in [49]-[51] and [53] is spent on estimating the behavior of the series compensation device when both the series capacitor and MOV partially conduct. In addition, the presented algorithms do not cater to the situation when alternate compensating elements, such as shunt reactors, are installed on the transmission line, which play a vital role to voltage and system stability. Shunt reactors are installed to absorb reactive power and help reduce the over-voltages during light-load conditions. Moreover, shunt reactors also help reduce over-voltages that occur due to switching and lightening surges. The algorithms presented in literature would do well if a dedicated procedure existed to remove the

dependency on FSC/MOV mode of operation. This would help save the burgeoning computational effort and improve the accuracy of the fault locating procedure.

Fixed Series Compensation (FSC) provides one of the simplest and most cost-effective types of series compensation as compared to Flexible AC Transmission Systems (FACTS). A generalized model of FSC with a parallel connection of series capacitor (SC) and metal-oxide varistor (MOV) is depicted in Fig. 3.4.

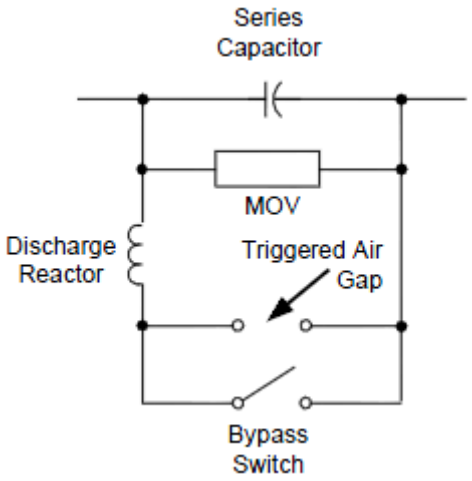

Fig. 3.4 - Generalized SC/MOV model [53]

An FSC device consists of actual three-phase capacitor banks in parallel connection with MOVs. Triggered spark-gaps and circuit breakers (bypass switches) are also part of the construction on FSC devices [53]-[54]. MOVs are non-linear elements that protect the capacitor bank from over-voltages. The triggered-spark gaps are included to protect the MOVs against excess heat dissipation and circuit breakers in turn protect the spark gap. The v-i characteristic of the non-linear MOV is often approximated by an exponential function as [55]-[56]:

$$i_{MOV} = P(\frac{v_x}{V_{REF}})^q \tag{3.20}$$

Where i_{MOV} and v_x are the MOV current and voltage respectively; P and V_{REF} are reference constants and q is the exponent of the characteristic. A typical characteristic curve of an SC/MOV device is shown in Fig. 3.5.

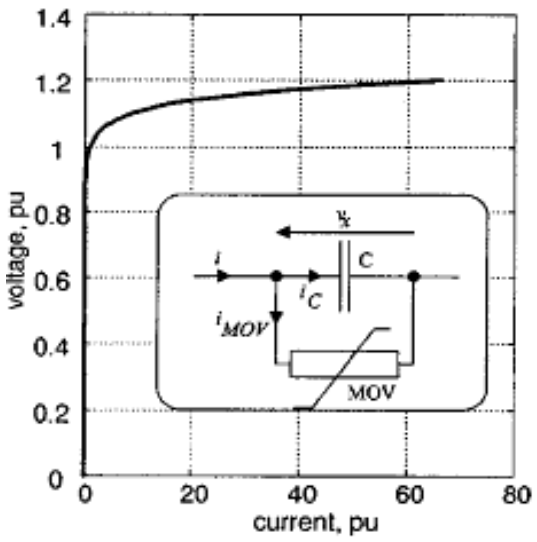

Fig. 3.5 - Sample characteristic curve of an FSC [55]

A lot of effort in literature is focused on calculating the series capacitor voltage using the approximate exponential model which requires a large amount of calculations to get the accurate result. There can also be considerable error when the FSC bank is not close to the relay because the current flowing in the FSC device is different from what is measured at the line terminal due to charging current [56]. In this thesis, the traditional method of approximating the series capacitor voltage from the relay line terminal is abandoned in favor of the state-of-the-art FSC monitoring systems that can accurately measure three-phase current and voltages.

3.2.1. Fixed Series Compensation Monitoring System

Fixed series compensation monitoring systems are expressly designed to gather real-time information on the physical state of FSC devices and have integrated communications capabilities. The use of FSC monitoring systems has been a growing trend since the 1980s to allow programmed maintenance and avoid unnecessary mass power transfer interruptions. A typical FSC monitoring system comprises of data acquisitions units and several other protection, control and supervision systems (PCSS) [56]-[57]. A single line diagram of an integrated FSC platform and monitoring system is shown in Fig. 3.6.

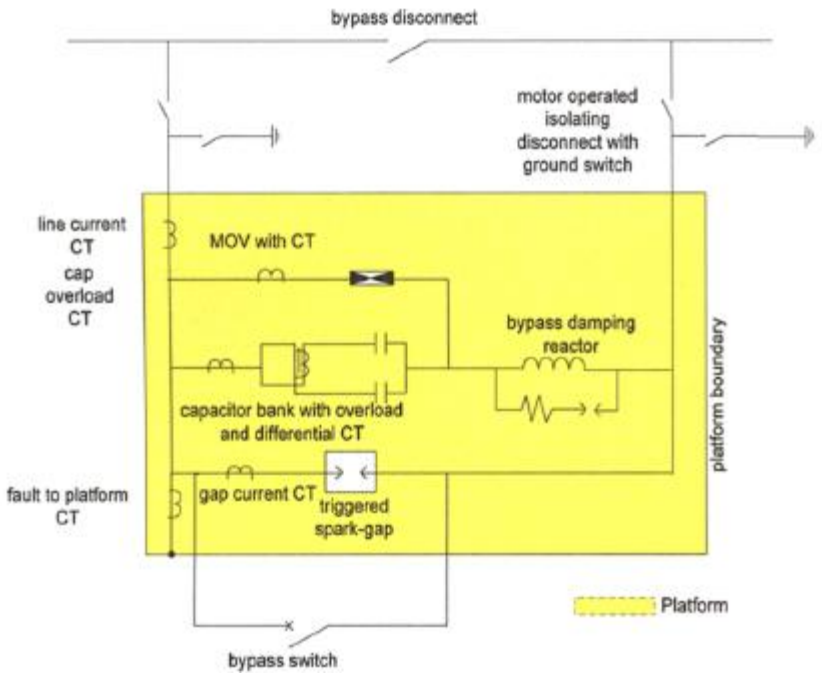

Fig. 3.6 - Single line diagram of FSC platform [57]

The data signal flow from the platform to the monitoring system is illustrated in Fig. 3.7.

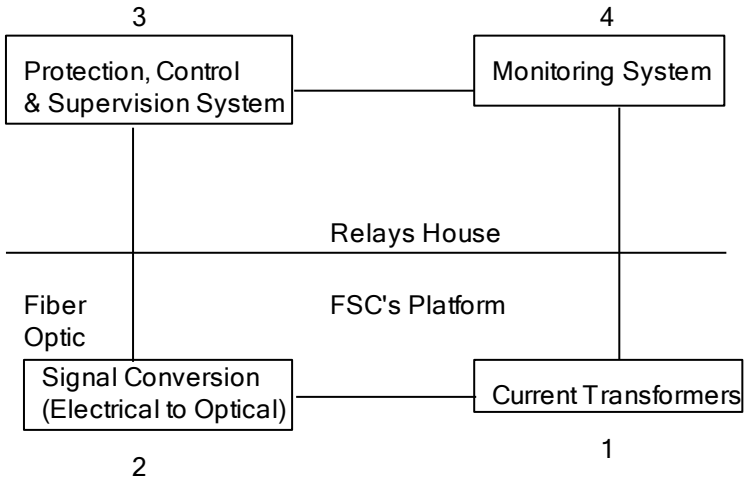

Fig. 3.7 - Data flow between FSC and monitoring system [57]

The data acquisition unit of the monitoring system gathers and transmits data on incoming transmission line current, capacitor bank and MOV leakage current and phase voltages of the FSC device. The MOV element essentially remains in an open-circuit condition as long as the MOV voltage (equal to capacitor voltage) remains

below the threshold reference voltage, usually an 80% margin. Since the series capacitor and MOV leakage current measurements are available through the monitoring system, the phase voltages of the series capacitor can be easily calculated by the onboard processing units with reference to the diagram in Fig. 3.8.

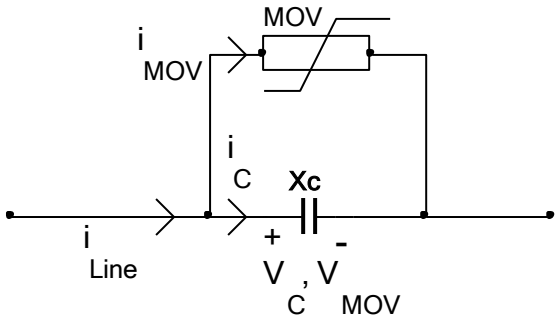

Fig. 3.8 - SC/MOV bank structure

The capacitor voltage is given by:

$$v_C(t) = \frac{1}{C}\int_{t_0}^{t} i_C(t) + v_C(t_0) \tag{3.21}$$

where,

$$i_C(t) = i_{Line}(t) - i_{MOV}(t)$$

The discrete-time solution to the continuous-time differential equation is given by:

$$v_C(n) = \frac{T_s}{2C}\big(i_C(n) + i_C(n-1)\big) + v_C(n-1) \tag{3.22}$$

where,

$$i_C(n) = i_{Line}(n) - i_{MOV}(n)$$

The FSC monitoring system can provide accurate phase voltage and current measurements in real-time and will be used for the fault locating algorithm proposed in this section. Albeit, synchronization between the data measured at the FSC unit and the primary reference bus cannot be guaranteed and is taken into account by the fault locating procedure.

3.2.2. Fault Location Scheme.

The algorithm proposed in this thesis uses unsynchronized measurements from the two ends of the transmission line and the FSC unit. The algorithm works for all fault types and fault impedances. In general, the synchronization required for the data measured at one of the relay terminals and the FSC device may not be equal. As with most other algorithms, information on the type of incident fault and the faulted phases is provided by external diagnostic procedures which are not explicitly detailed here. The proposed algorithm successfully extends the concept presented in [38] to series and shunt compensated transmission lines. The fault locating procedure involving FSC is essentially a three variable problem that has not been addressed before in literature. A single line diagram of a series-compensated line is shown in Fig. 3.9.

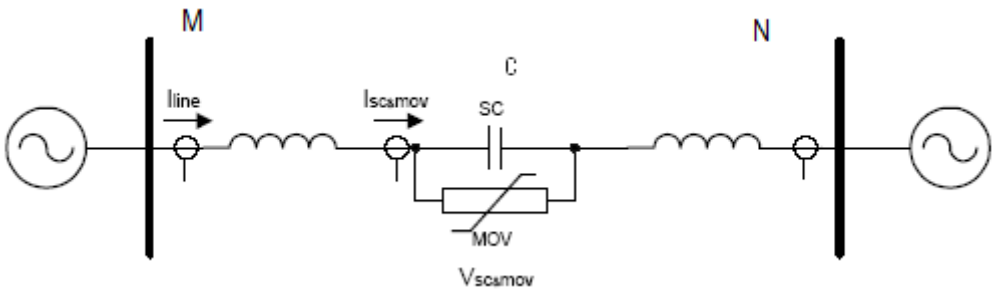

Fig. 3.9 - Series-compensated line

Bus N is selected as the reference terminal for the purpose of data synchronization. The three variables that need to be calculated for a short-circuit fault on a series-compensated line are:

- δ_M, the synchronization angle required for terminal M measurements.
- δ_C, the synchronization angle required for FSC measurements.
- d, the per-unit distance to the point of fault.

A special non-iterative procedure was developed for calculating the synchronization angles and the fault distance. This was achieved by simultaneously processing the positive and negative sequence fault impedance loops for unsymmetrical faults, and the positive and superimposed-positive sequence fault

impedance loops for symmetrical faults. The data synchronization procedure is inherent in the fault location scheme and is carried out using post-fault data samples for enhanced accuracy. A Fault location scheme was also developed for shunt compensated lines along with a novel relay trip-blocking index. The model of shunt-compensated transmission line is shown in Fig. 3.10.

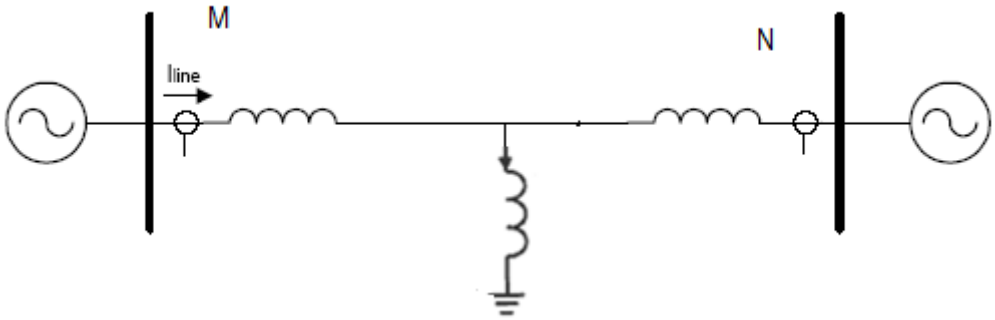

Fig. 3.10 - Shunt-compensated transmission line

The data obtained from the asynchronous data recorders need to be corrected by using a complex synchronization operator($e^{j\delta}$), where δ is the synchronization angle. While deriving the proposed algorithm, the distributed parameter line model is strictly used to represent transmission lines such that their behavior closely resembles real-life system dynamics. The proposed fault locating algorithm does not depend on the mode of operation of the non-linear series compensation devices and can be used for all types of short-circuit faults and fault resistance variations.

With low fault-current levels, none of the phase MOVs or the air-gap conduct and the series capacitor bank is equivalent to its pure nominal reactance value. The phase reactance of the capacitor bank is given by:

$$Z_A = Z_B = Z_C = -jX_c \tag{3.23}$$

Where X_c is given by $\frac{1}{2\pi fC}$. As per the theory of sequence components, the sequence impedances of the series capacitor device is given by

$$Z_{012} = \begin{bmatrix} -jX_c & 0 & 0 \\ 0 & -jX_c & 0 \\ 0 & 0 & jX_c \end{bmatrix} \tag{3.24}$$

When the fault current level exceeds the threshold, the MOVs begin to partially conduct which induces mutual coupling between the sequence impedances of the series capacitor which cannot be accurately predicted. Hence, accurate phase voltage and current measurements are instead utilized by the fault locating procedure. Once the asynchronously measured three-phase quantities are decoupled using symmetric transformation, the relationship between the sequence voltages and currents at location *x* is given by the partial differential equation in (3.1). The solution of the above two decoupled equations can be written in a two port network form and is given by (3.3). The fundamental voltage and current phasors calculated from the data measured at bus *M* need to be analytically synchronized with respect to bus *N*. This can be done using a synchronization operator and applying it to the resulting voltage and current sequence quantities.

$$V_{m1}(\delta) = V_{m1} e^{j\delta_M} \tag{3.25}$$

$$I_{m1}(\delta) = I_{m1} e^{j\delta_M} \tag{3.26}$$

Where V_{m1} and I_{m1} are the positive sequence voltage and current measured at bus *M* and δ_M is the synchronization required for bus *M*.

3.2.2.1. Fault Location for Series Compensated Lines.

An accurate fault locating algorithm is developed using unsynchronized measurements. The sequence voltage drop across the FSC unit can be calculated using the measurements from the monitoring system. Table 3.1 shows the various sequence current and voltage components that emanate in the system for various types of short-circuit faults.

Table 3.1 - Sequence components in various fault types

	Current & Voltage Sequence Components		
Fault Type	Positive Sequence	Negative Sequence	Zero Sequence
SLG	√	√	√
L-L	√	√	
L-L-G	√	√	√
3-phase	√		

Positive sequence quantities are common to all fault types whereas negative sequence quantities evolve in unsymmetrical faults. The fault locating algorithm for an unsymmetrical fault is developed using positive and negative sequence quantities simultaneously. Fig. 3.11 shows the unsymmetrical fault condition which would be common for both positive and negative sequence fault loop impedances. The algorithm is designed to estimate the per-unit distance, *d*, to the fault with respect to location of series device which can be installed at any known arbitrary point from the buses.

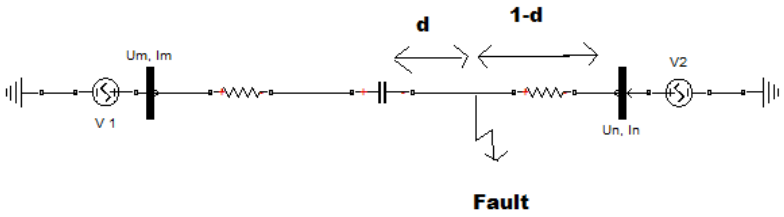

Fig. 3.11 - Unsymmetrical fault on right side of FSC unit

The measurements obtained at the line terminal *M* and the FSC unit are unsynchronized with reference to bus *N* and the synchronization mismatch might not be necessary equal. The required synchronization compensation ($e^{j\delta c}$) for the FSC unit measurements cannot be directly calculated in absolute terms since the fault is between the series compensation and the line terminal *N* at a yet unknown distance *d*. A novel skillful synchronization procedure that calculates the relative synchronization mismatch between bus *M* and FSC measurements is proposed. This is done by introducing a new synchronization operator term, $e^{j\delta r}$, to synchronize bus *M* measurements with respect to the FSC measurements. The subscript *r* stands for relative. At the onset of a short-circuit fault, it was noticed that the positive sequence quantities undergo a period of disturbance before settling to a new steady-state value. Therefore, negative sequence quantities are utilized in the calculation of the synchronization mismatch. Since the line current measurements are available, the negative sequence current entering FSC unit must be equal to the negative sequence current leaving terminal *M* corrected for the charging current. The negative sequence current entering the FSC device is given by:

$$I_{mL}^{-} = I_{mR}^{-} = \left[\frac{-V_m^-}{Z_c}\sinh(\gamma_1 L_1) + I_m^- \cosh(\gamma_1 L_1)\right] e^{j\delta_r} \tag{3.27}$$

In general, V_{xY}^{i} and I_{xY}^{i} represent the positive sequence voltage and current from bus *x* to side *Y* of the compensation device (right *R* or left *L*). '*i*' represents the type of sequence used, '+' indicates positive and '-' indicates negative components. L_1 represents the total line length from Bus *M* to the compensating device. Positive sequence propagation constant, γ_1, is equal to the negative sequence propagation constant γ_2. It is also known that the series compensation device does not affect the through-current and the current leaving the FSC unit is equal to the current entering. Therefore,

$$I_{mL}^{-} = I_{mR}^{-} \tag{3.28}$$

Equation (3.27) can be rearranged to solve for the synchronization operator $e^{j\delta_r}$.

$$e^{j\delta_r} = \frac{I_{mL}^{-}}{\left[\frac{-V_m^-}{Z_c}\sinh(\gamma_1 L_1) + I_m^- \cosh(\gamma_1 L_1)\right]} \tag{3.29}$$

The unsynchronized positive sequence voltage to the left of series device is given by:

$$V_{mL}^{+} = [V_m^{+}\cosh(\gamma_1 L_1) - I_m^{+} Z_c \sinh(\gamma_1 L_1)] \tag{3.30}$$

Since the positive sequence voltage can be calculated from the known FSC measurements, the line voltage on the right side of SC device is then given by:

$$V_{mR}^{+} = [V_{mL}^{+} e^{j\delta_r} - V_c^{+}] \tag{3.31}$$

Where V_{mR}^{+} is the positive sequence line voltage on the right side of the SC device as seen from bus *M* and V_c^{+} is the positive sequence voltage drop across the capacitor.

With reference to Fig. 3.11, the synchronized positive sequence fault voltage is then expressed as:

$$V_{MF}^{+} = V_{mR}^{+} e^{j\delta} \cosh(\gamma_1 L_1 d) - I_{mR}^{+} e^{j\delta} \mathrm{Z_c} \sinh(\gamma_1 L_1 d) \tag{3.32}$$

where V_{MF}^{+} is fault point voltage in terms of the sequence quantities measured at bus *M* and *d* is the per-unit distance to the fault with reference to the SC device. The fault point positive sequence voltage as seen from bus *N* (reference bus) can also be expressed in a similar way yielding the following expression:

$$V_{nF}^{+} = V_{n}^{+} \cosh\big(\gamma_1 L_1 (1-d)\big) - I_{n}^{+} Z_c \sinh(\gamma_1 L_1 (1-d)) \tag{3.33}$$

Where V_{nF}^{+} is the positive sequence fault voltage as seen from bus *N*. Combining (3.32) and (3.33) and rearranging results in the following hyperbolic expression:

$$\begin{aligned} \tanh(\gamma_1 L_1 d)\left[-I_{mR}^{+} e^{j\delta} Z_c + V_{n}^{+} \sinh(\gamma_1 L_1) - I_{n}^{+} Z_c \cosh(\gamma_1 L_1)\right] \\ = V_{n}^{+} \cosh(\gamma_1 L_1) - I_{n}^{+} Z_c \sinh(\gamma_1 L_1) - V_{mR}^{+} e^{j\delta} \end{aligned} \tag{3.34}$$

Equation (3.34) has two variables that need to be solved for, namely the per-unit distance *d* and the synchronization operator $e^{j\delta}$.

Following through the same derivative procedure presented for positive sequence quantities, a second hyperbolic expression in terms of the per-unit distance and synchronization operator can be obtained for negative sequence quantities.

$$\begin{aligned} \tanh(\gamma_1 L_1 d)\left[-I_{mR}^{-} e^{j\delta} Z_c + V_{n}^{-} \sinh(\gamma_1 L_1) - I_{n}^{-} Z_c \cosh(\gamma_1 L_1)\right] \\ = V_{n}^{-} \cosh(\gamma_1 L_1) - I_{n}^{-} Z_c \sinh(\gamma_1 L_1) - V_{mR}^{-} e^{j\delta} \end{aligned} \tag{3.35}$$

Taking the ratio of (3.34) to (3.35) eliminates the function dependency on the fault distance *d* and rearranging yields the following expression:

$$\frac{-I_{mR}^{+}e^{j\delta}Z_c + k_{1p}}{-I_{mR}^{-}e^{j\delta}Z_c + k_{1n}} = \frac{k_{2p} - V_{mR}^{+}e^{j\delta}}{k_{2n} - V_{mR}^{-}e^{j\delta}} \tag{3.36}$$

where the constants k_{1p}, k_{2p}, k_{1n} and k_{2n} are defined as follows:

$$k_{1p} = V_n^{+}\sinh(\gamma_1 L_1) - I_n^{+}Z_c\cosh(\gamma_1 L_1)$$

$$k_{2p} = V_n^{+}\cosh(\gamma_1 L_1) - I_n^{+}Z_c\sinh(\gamma_1 L_1)$$

$$k_{1n} = V_n^{-}\sinh(\gamma_1 L_1) - I_n^{-}Z_c\cosh(\gamma_1 L_1)$$

$$k_{2n} = V_n^{-}\cosh(\gamma_1 L_1) - I_n^{-}Z_c\sinh(\gamma_1 L_1)$$

Simplifying (3.36) and rearranging yields the following quadratic equation with only the synchronization operator as the variable.

$$e^{2j\delta}[A] + e^{j\delta}[B] + C = 0 \tag{3.37}$$

where the constants *A*, *B* and *C* are defined as follows:

$$A = I_{mR}^{-}Z_c V_{mR}^{+} - V_{mR}^{-}I_{mR}^{+}Z_c$$

$$B = V_{mR}^{+}k_{2n} + I_{mR}^{-}Z_c\,k_{1p} - V_{mR}^{-}k_{2p} - I_{mR}^{+}Z_c\,k_{1n}$$

$$C = k_{1p}k_{2n} - k_{1n}k_{2p}$$

Equation (3.37) can now be solved for $e^{j\delta}$ using the quadratic formula given in (3.38).

$$e^{j\delta} = \frac{-B \pm \sqrt{B^2 - 4AC}}{2A} \tag{3.38}$$

The solution to (3.38) yields two complex values for the synchronization angle δ. The criterion for selecting the correct synchronization angle is described below.

$$1 - \varepsilon \leq \left|e^{j\delta}\right| \leq 1 + \varepsilon \tag{3.39}$$

where ε is a small deviation in the magnitude of $e^{j\delta}$. The per-unit distance to the point of fault can then be calculated by using either (3.34) or (3.35) and recording the real value of the complex distance *d*. The distance between the compensating device and bus *N* was taken as per-unit value of 1.0, therefore if total line-length between buses *M* and *N* is rescaled to be 1.0 p.u and the SC device is connected in the center, the per-unit distance from bus *M* is given by:

$$d_M = \frac{Real(d)}{2} + \frac{1}{2} \tag{3.40}$$

Where d_M is the distance with respect to bus *M*. Once the synchronization operators $e^{j\delta}$ and $e^{j\delta_r}$ are known, the absolute synchronization mismatch with respect to the reference bus *N* can then be calculated as follows:

$$e^{j\delta_C} = e^{j\delta} \tag{3.41}$$

$$e^{j\delta_M} = e^{j\delta}.e^{j\delta_r} \tag{3.42}$$

The fault locating procedure for the faults occurring to the left side of the compensating device can be developed in a similar fashion and operated concurrently with the right-sided fault locating procedure. Results show that only one of the procedures results in an acceptable per-unit distance due to the distance selection logic that will be described later. The fault locating procedure for symmetric three-

phase faults can be derived with slight alteration to the previous subroutine meant for unsymmetrical faults. Negative sequence quantities cannot be utilized for symmetrical faults since these are absent as per Table 3.1. Instead super-imposed/incremental positive sequence quantities can be used as described in [58]. This results in a similar quadratic relation for the synchronization operator and is not explicitly derived here.

3.2.2.2. Algorithm for shunt-compensated lines.

The algorithm for shunt reactor compensated lines, shown in Fig. 3.12, is devised by approximating the reactor sequence currents. Positive and negative sequence impedance loops are used for unsymmetrical faults and incremental positive sequence quantities are utilized for balanced three-phase faults. Moreover, the shunt reactor bank installed on the line might have inter-phase coupling and must be taken into account.

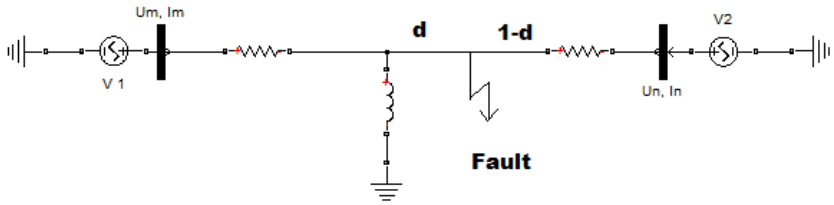

Fig. 3.12 - Fault on shunt-compensated line

Considering a fault on the right side of shunt reactor as shown in Fig. 3.12, the unsynchronized positive sequence voltage at the reactor tie-in point as seen from bus *M* is given by:

$$V_{mR}^{+} = V_{mL}^{+} = [V_m^{+}\cosh(\gamma_1 L_1) - I_m^{+} Z_c \sinh(\gamma_1 L_1)] \tag{3.43}$$

The sequence current to the left of the shunt reactor from bus *M* is given by:

$$I_{mL}^{+} = [\frac{-V_m^{+}}{Z_c}\sinh(\gamma_1 L_1) + I_m^{+}\cosh(\gamma_1 L_1)] \tag{3.44}$$

The positive sequence current flowing in to the shunt reactor can be approximated as:

$$I_{Xl}^{+} = \frac{V_{mR}^{+}}{X_L} \tag{3.45}$$

where I_{Xl}^{+} is the inductor current and $X_L$is the reactor impedance defined as:

$$X_L = jw(L_s - L_m)$$

L_s and L_m are self and mutual inductances respectively. The current to the right of the shunt reactor can then be expressed as:

$$I_{mR}^{+} = (I_{mL}^{+} - I_{Xl}^{+}) \tag{3.46}$$

Similarly, the unsynchronized negative sequence voltage and current to the left of the shunt reactor can be defined by:

$$V_{mR}^{-} = V_{mL}^{-} = [V_m^{-} \cosh(\gamma_1 L_1) - I_m^{-} Z_c \sinh(\gamma_1 L_1)] \tag{3.47}$$

$$I_{mR}^{-} = (I_{mL}^{-} - I_{Xl}^{-}) \tag{3.48}$$

Where V_{mR}^{-} and $I_{mR}^{-}$are the negative sequence voltage and current to the left of the shunt reactor, respectively. Once the former two quantities are available, the procedure developed using equations (3.32) through (3.39) can be used to calculate the synchronization operator and the per-unit distance with respect to the compensating device. The procedure for the three-phase balanced phase faults is similar to the one used for FSC device using both positive and super-imposed positive sequence quantities.

The fault locating algorithm for faults occurring on either side of the compensating device consists of the two subroutines developed in the previous section. The two procedures are run concurrently and only one will yield an acceptable value for the per-unit fault distance. The procedure for selecting the

appropriate distance value is developed here. While selecting the correct per-unit distance d from the right-sided and the left-sided fault locating procedures, both the real and imaginary components of d need to be carefully considered.

The correct solution for the complex fault distance d will abide with the following two conditions:

$$0 - \varepsilon \leq Real(d) \leq 1 + \varepsilon \tag{3.49}$$

$$0 - \varepsilon \leq Imag(d) < 0 + \varepsilon \tag{3.50}$$

where ε is a small tolerance taken to be of the order 10^{-1} for this system. The real value of the fault distance d will need to lie between 0.0 and 1.0 whereas the imaginary value will ideally be zero.

The next chapter comprises of extensive performance evaluation of the fault locating algorithms for multi-terminal lines and series and shunt-compensated transmission lines.

Chapter 4

Performance Evaluation and Simulation Results

In this chapter, the solution to power system protection is modeled as a fault location problem. The four-terminal system shown in Fig. 3.1 is simulated first using unsynchronized measurements and tested for various types of faults and fault impedances. Series and shunt-compensated systems shown in figures 3.9 and 3.10 were also simulated using unsynchronized measurements and tested for various types of faults on either side of the compensation device. Results of fault location and impedance trajectory are presented in this chapter. The results verify the efficacy of the proposed solutions.

4.1. Algorithm Evaluation for Multi-terminal System.

The four-terminal line shown in Fig. 3.1 is simulated in MATLAB SIMULINK. The transmission lines simulated have different lengths but similar impedance characteristics for simplicity. The transmission line parameters are shown in Tables 4.1 and 4.2. The system was simulated with 735 kV voltage sources at different angles as shown in Table 4.3.

Table 4.1 - Line Impedance Parameters

Parameter	Positive sequence / Km	Zero sequence / Km
R	0.011223 Ω	0.30079 Ω
L	0.00086848 H	0.002988 H
C	1.34E-08 F	8.59E-09 F

Table 4.2 - Line lengths

Line	Length / Km
1	100
2	140
3	180
4	200
5	50

Table 4.3 - Voltage sources in simulated system

Source	Angle / Degrees
1	15
2	10
3	5
4	0

4.1.1. Synchronization and Fault Detection

The signals obtained from the SIMULINK simulations are naturally synchronized. In order to evaluate the performance of the proposed algorithm, the signals obtained from buses 1, 2 and 3 were delayed by 96, 30 and 45 degrees, respectively. Signals from bus 1 was delayed by 96 degrees to show that the algorithm works for large synchronization angles as well. Fig. 4.1 shows a comparison of delayed phase-A voltage and current waveforms for line 1 against the original un-delayed versions. This holds true for the rest of the phases and transmission lines as well.

The calculated synchronization angles during steady-state operation, using (3.15), are shown in Fig. 4.2. A phase-to-ground, 50Ω fault was placed on line 1 at 0.1s and at a distance of 0.5 per-unit. As a safety measure, the algorithm registers a fault condition only if the synchronization angle deviation persists for more than three data samples. The apparent deviation of synchronization angles from their steady state value is shown in the Fig. 4.3.

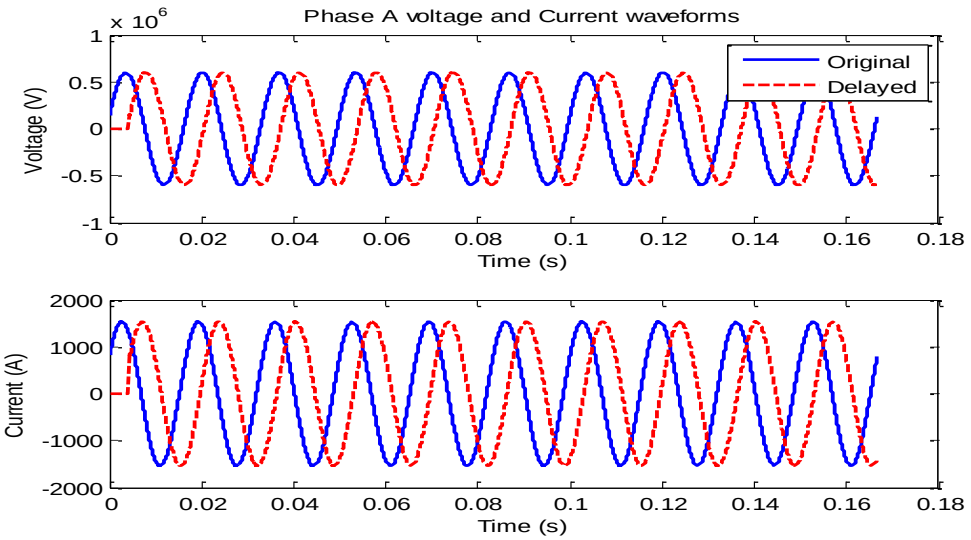

Fig. 4.1 - Phase-A voltage and current waveforms

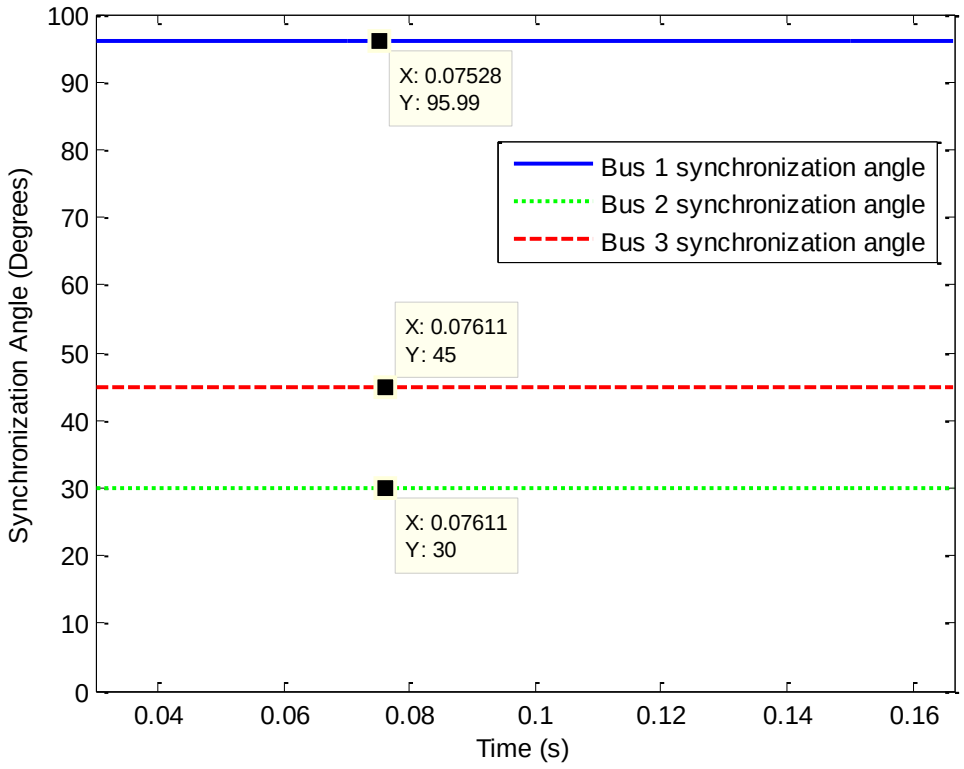

Fig. 4.2 - Calculated synchronization angles

The calculated steady-state synchronization angles precisely reflect the sample delays introduced in each of the bus measurements. All synchronization angles can be

calculated at once using (3.15) instead of sifting through numerous permutations of signal data shifts as proposed in [33] to achieve synchronization. The apparent deviation of synchronization angles from their steady-state values during a fault condition is shown in the Fig. 4.3.

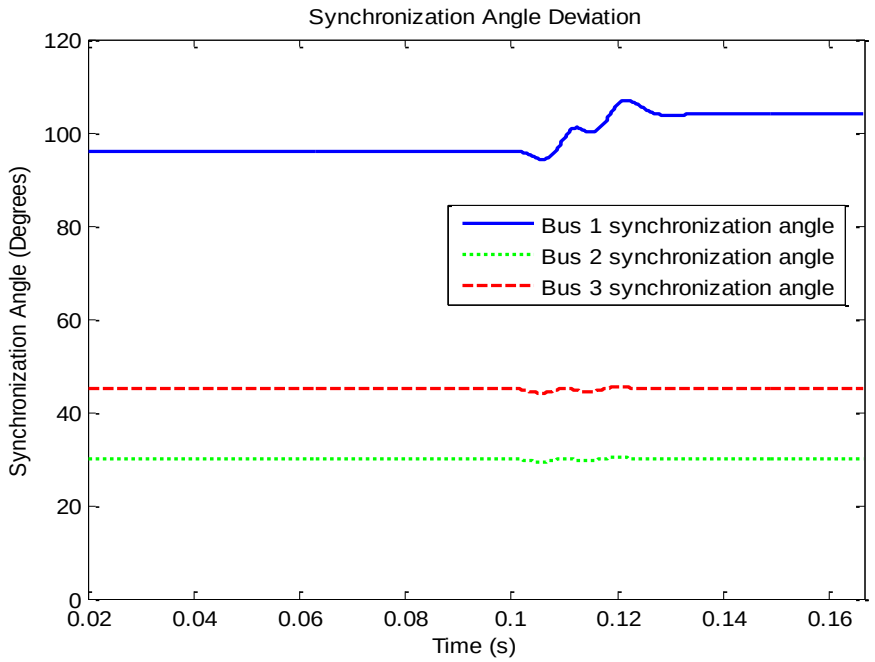

Fig. 4.3 - Apparent deviation of synchronization angles

4.1.2. Evaluation of Fault Locating Procedure.

Different types of faults with varying fault resistances were simulated on different sections of the five transmission lines and the performance of the fault locating functions was evaluated for all the fault types to cover all possibilities. The fault resistance was varied from 1 to 200 Ω which covers a large variance and captures high resistance faults. Performance plots for three of the test cases are presented here.

4.1.2.1. Single Line to Ground Fault on Line 1.

A single line to ground fault was placed on line 1 at 0.1 seconds (6^{th} cycle), 0.5 per-units away from bus 1 with a fault resistance of 120Ω. The real and imaginary values of the calculated per-unit distance, *d*, are plotted in Fig. 4.4 and agree well with the expected theoretical results. The trajectory of the actual positive sequence

impedance is also plotted in Fig. 4.5 against the three zones of an MHO relay set to cover 85, 120 and 150 percent of line 1. The current wave-forms from measurements at bus 1 are shown in Fig. 4.6.

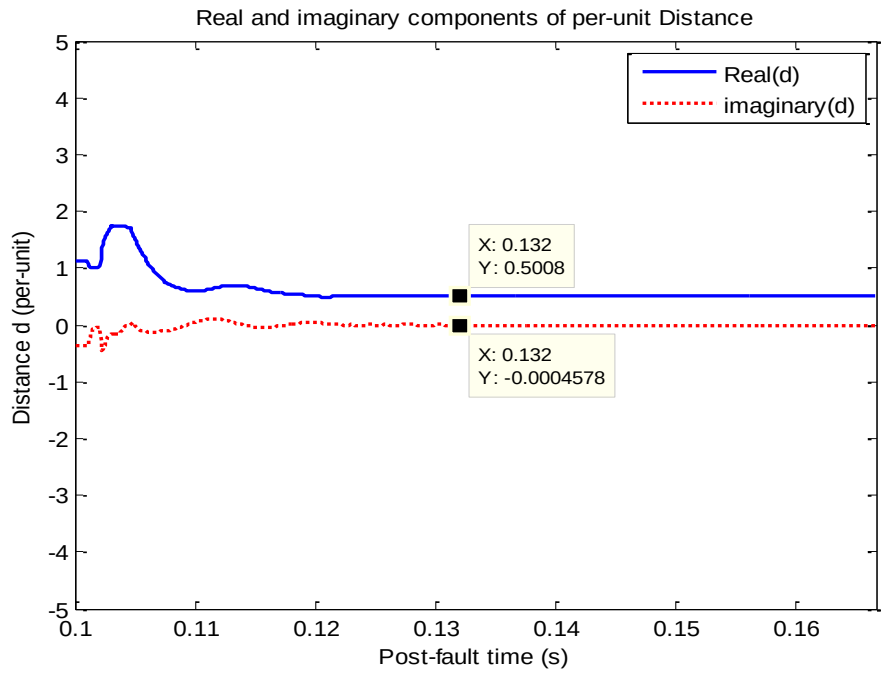

Fig. 4.4 - Distance *d*, phase-A, SLG fault

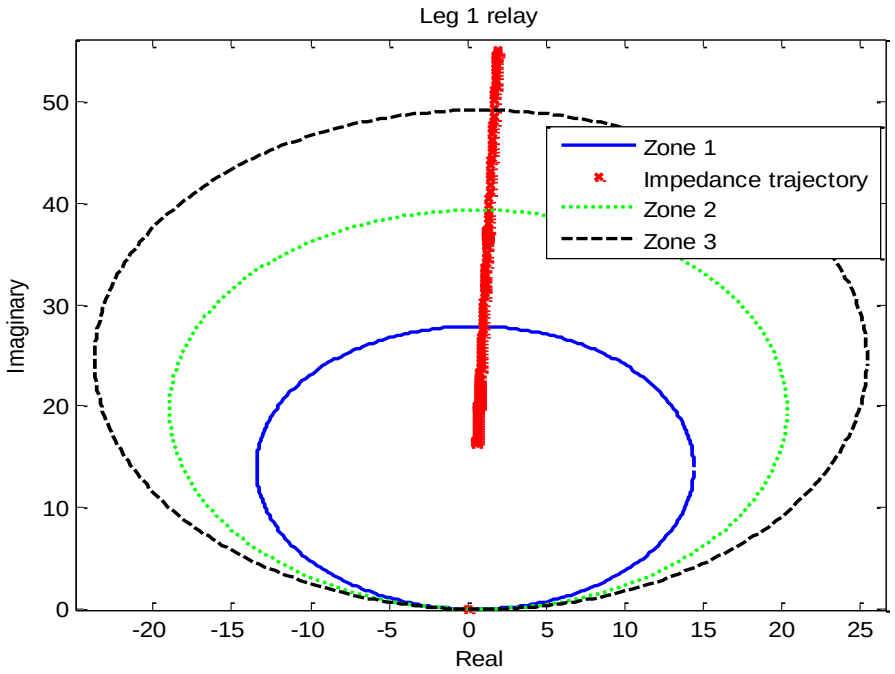

Fig. 4.5 - Actual Impedance Trajectory, SLG fault

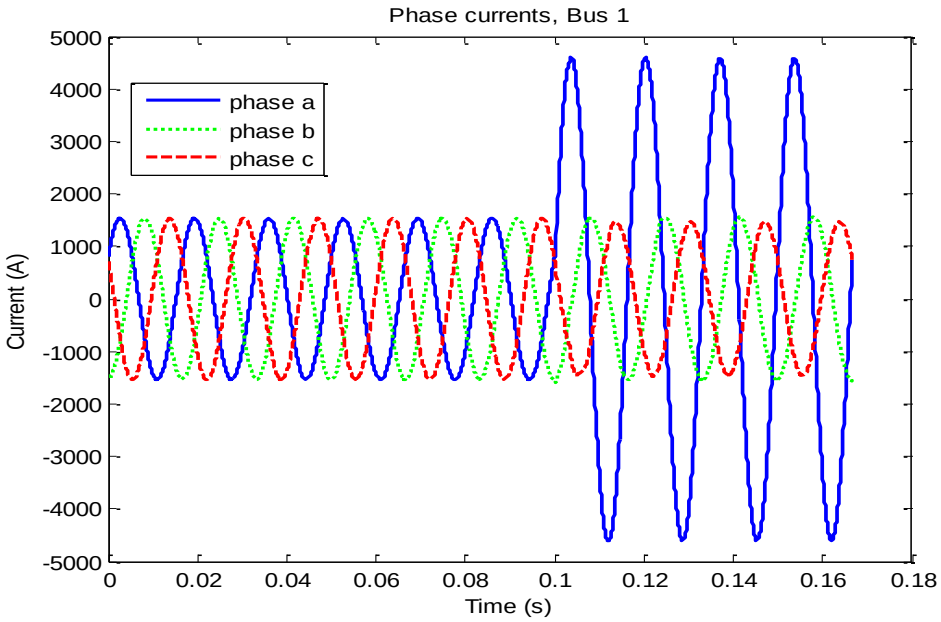

Fig. 4.6 - Bus 1 Phase Currents

4.1.2.2. Phase A-B-Ground Fault on Line 2

A phase-to-phase-to-ground fault was placed on line 2 at 0.1 seconds (6^{th} cycle), 0.5 per-units away from bus 2 with a fault resistance of 10Ω. The real value and imaginary value of the calculated per-unit distance *d* are plotted along with the actual impedance trajectory and current waveforms in Figures 4.7, 4.8 and 4.9 respectively.

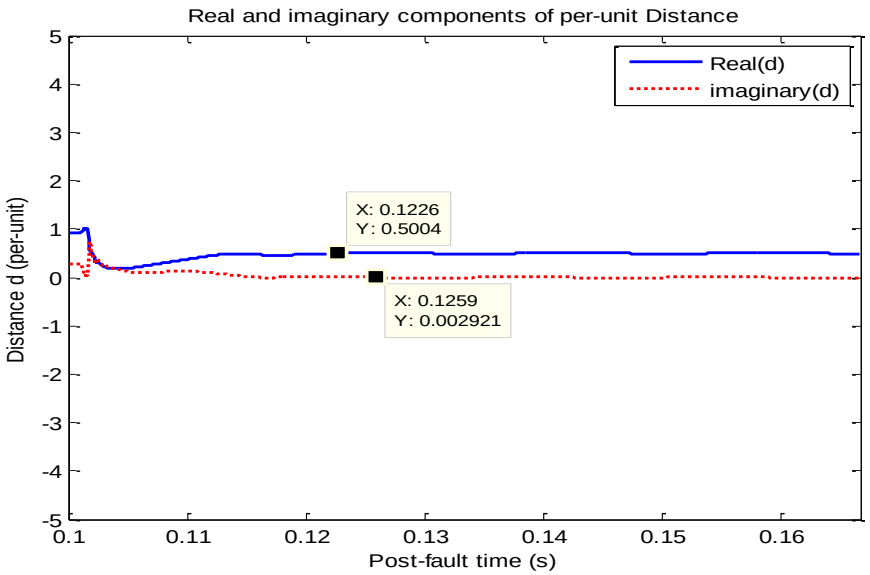

Fig. 4.7 - Distance *d*, A-B-G fault

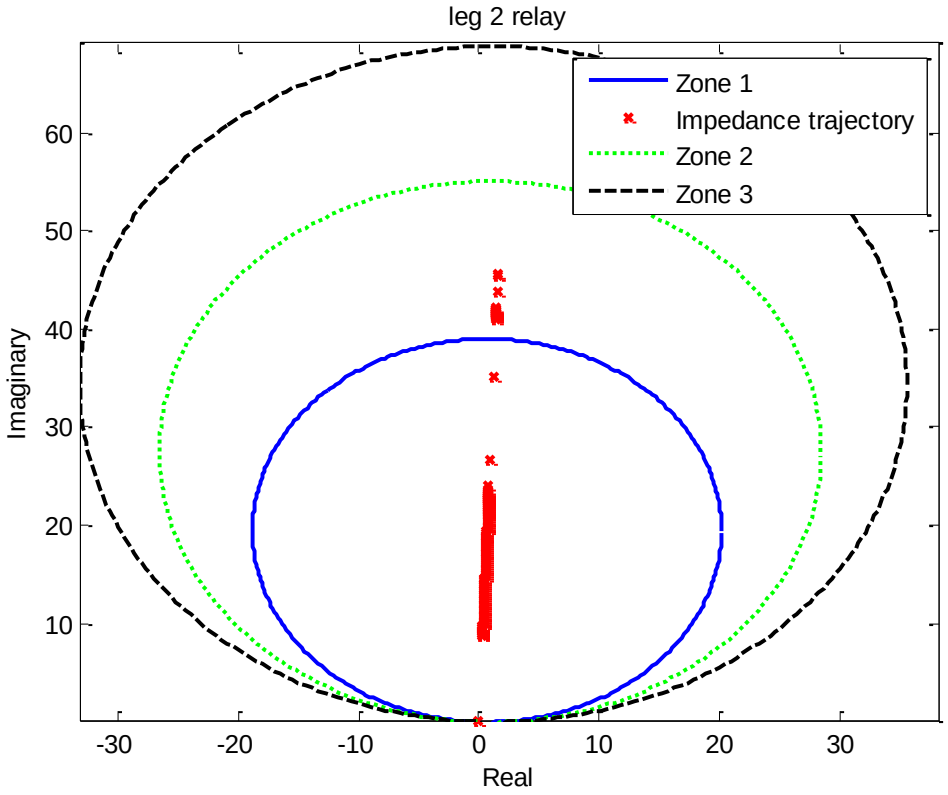

Fig. 4.8 - Actual Impedance trajectory, L-L-G fault

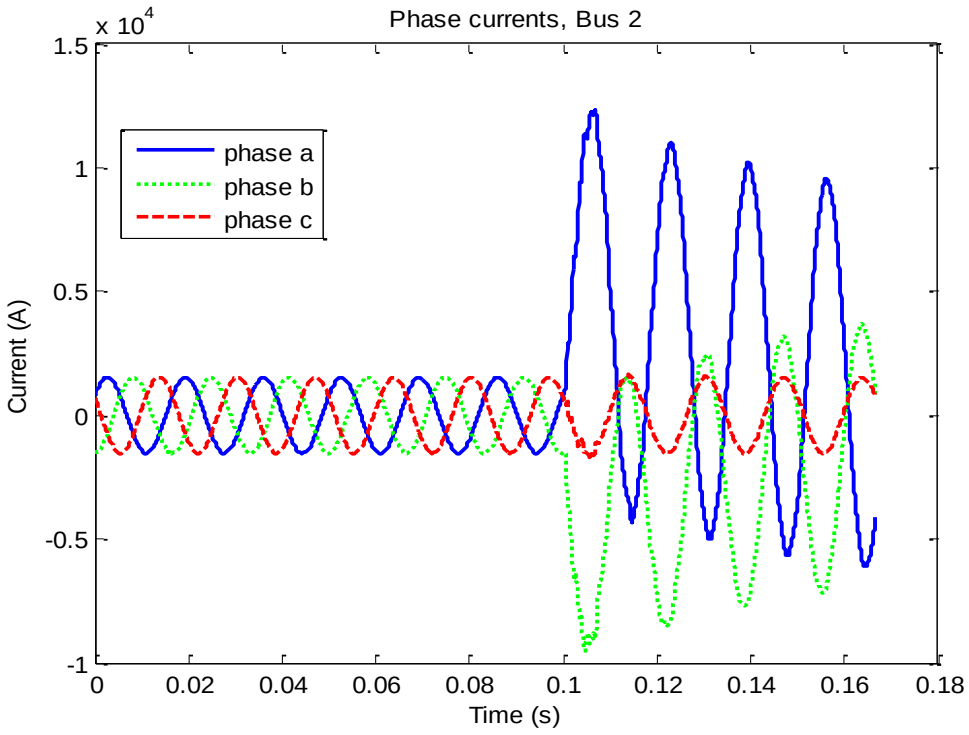

Fig. 4.9 - Phase currents, bus 2

4.1.2.3. Three-phase Fault on Line 3.

A symmetrical three-phase fault was placed on line 3 at 0.1 seconds (6th cycle), and 0.7 per-units away from bus 3. The real and imaginary components of the calculated per-unit distance *d* are plotted along actual impedance trajectory and current waveforms in Figures 4.10, 4.11 and 4.12 respectively.

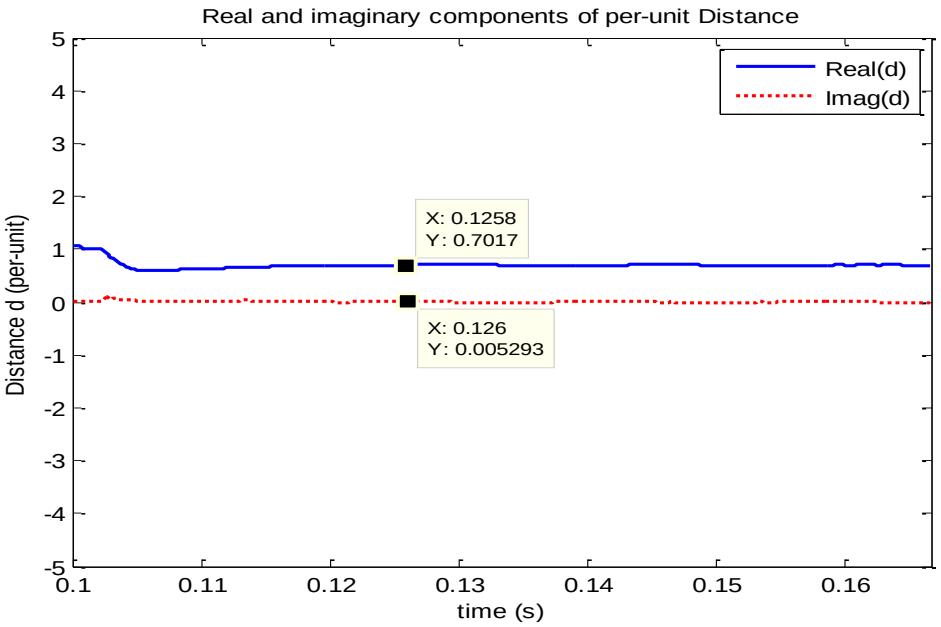

Fig. 4.10 - Distance *d*, 3-phase fault

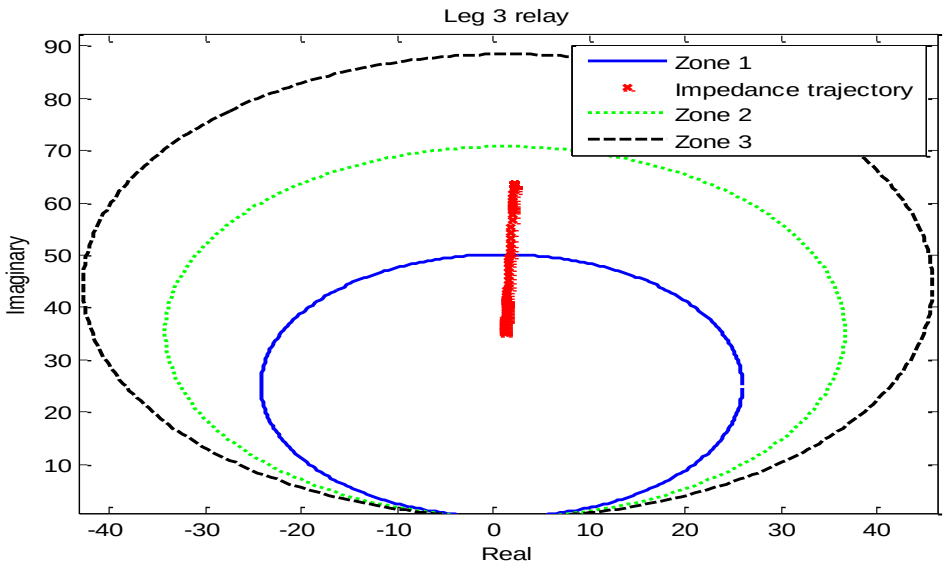

Fig. 4.11 - Actual Impedance, 3-phase fault

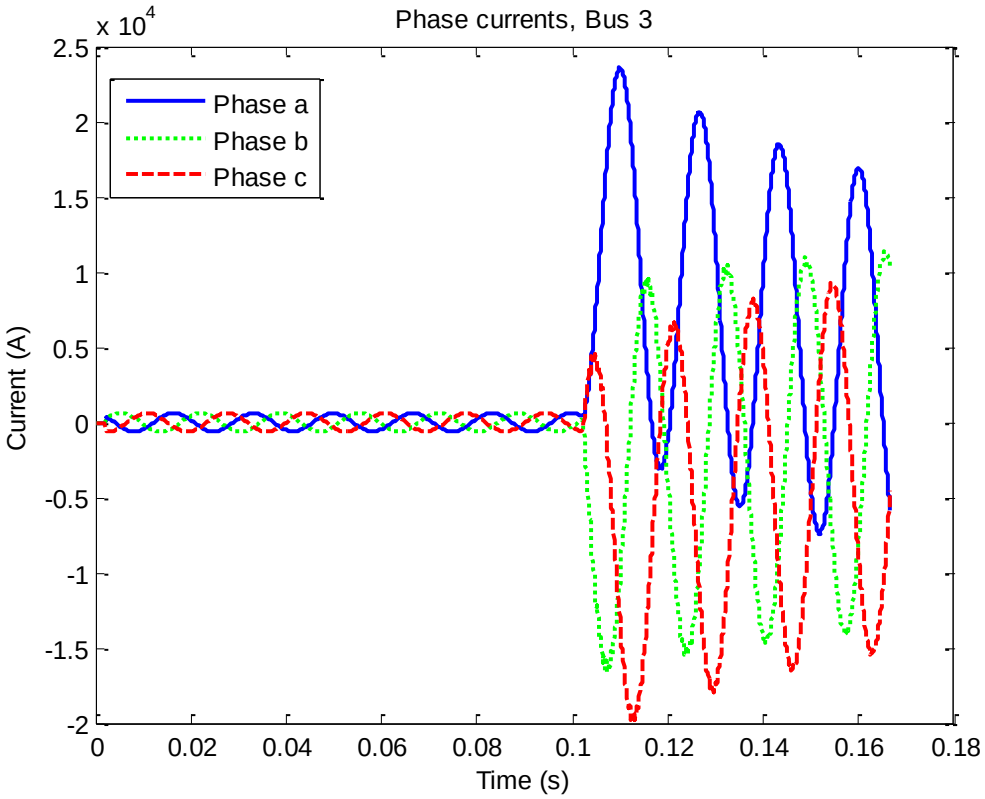

Fig. 4.12 - Three phase currents, bus 3

The results show that the percentage error of fault location for all fault types is well within the 1% margin and do not exhibit any particular trend. In all cases the algorithm is able to identify the faulted transmission line since real value of the calculated per-unit distance was less than 1 using the method previously described in Chapter 3. The fault locating algorithm is tested for various combinations of fault types and distances and the summarized results are presented in Table 4.4.

Table 4.4 - Performance of fault locating scheme

Faulted Line	Fault			% Error
	Type	Location	$R_F(\Omega)$	
Line 1	AG	10% from Bus 1	1	0.012
	BC	30% from Bus 1	50	0.024

	ABG	50% from Bus 1	100	0.015
	ABC	85% from Bus 1	200	0.019
Line 2	AG	10% from Bus 2	1	0.045
	BC	30% from Bus 2	50	0.031
	ABG	50% from Bus 2	100	0.014
	ABC	85% from Bus 2	200	0.016
Line 3	AG	10% from Bus 3	1	0.041
	BC	30% from Bus 3	50	0.019
	ABG	50% from Bus 3	100	0.039
	ABC	85% from Bus 3	200	0.028
Line 4	AG	10% from Bus 4	1	0.052
	BC	30% from Bus 4	50	0.017
	ABG	50% from Bus 4	100	0.027
	ABC	85% from Bus 4	200	0.021
Line 5	AG	10% from N	1	0.021
	BC	30% from N	50	0.019
	ABG	50% from N	100	0.026
	ABC	85% from N	200	0.038

4.1.3. Power System Transients and Fault Detection.

Power systems are often subjected to high-speed transients that fade away within the span of a few fundamental power cycles. Studying the response of protective devices to transient conditions is crucial for avoiding malfunctioning and false tripping of relays. The fault locating scheme developed in this thesis is highly robust and can provide accurate fault distance estimates if a fault closely follows a power system transient event.

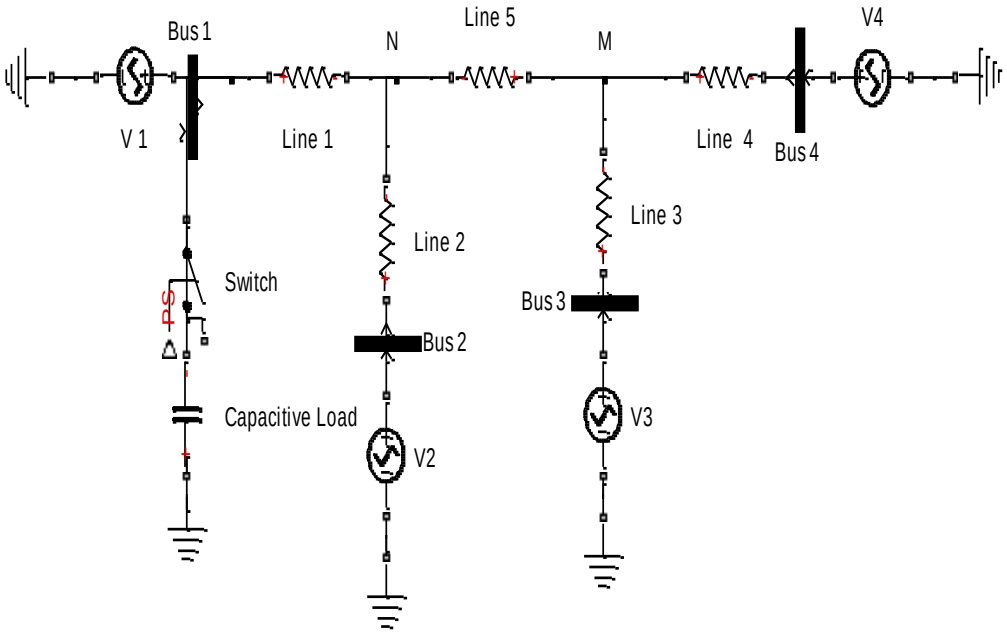

Fig. 4.13 - Multi-terminal line with load

The algorithm presented in Chapter 3 was tested with the system subjected to load switching transients. A 50 MVAR capacitive load was attached to bus 1 as shown in Fig. 4.13 and the fault detection scheme was analyzed for erroneous false-positive response. The attached load was switched on after the fourth power cycle (0.0667 seconds) and its effect on the voltage and current waveforms measured at bus 1 was observed.

Figures 4.14 and 4.15 clearly show the effect of load switching on the voltage and current waveforms at bus 1, respectively. Despite the waveform distortion, the fault detection scheme is able to correctly ignore the altered system operating condition without giving a false positive response.

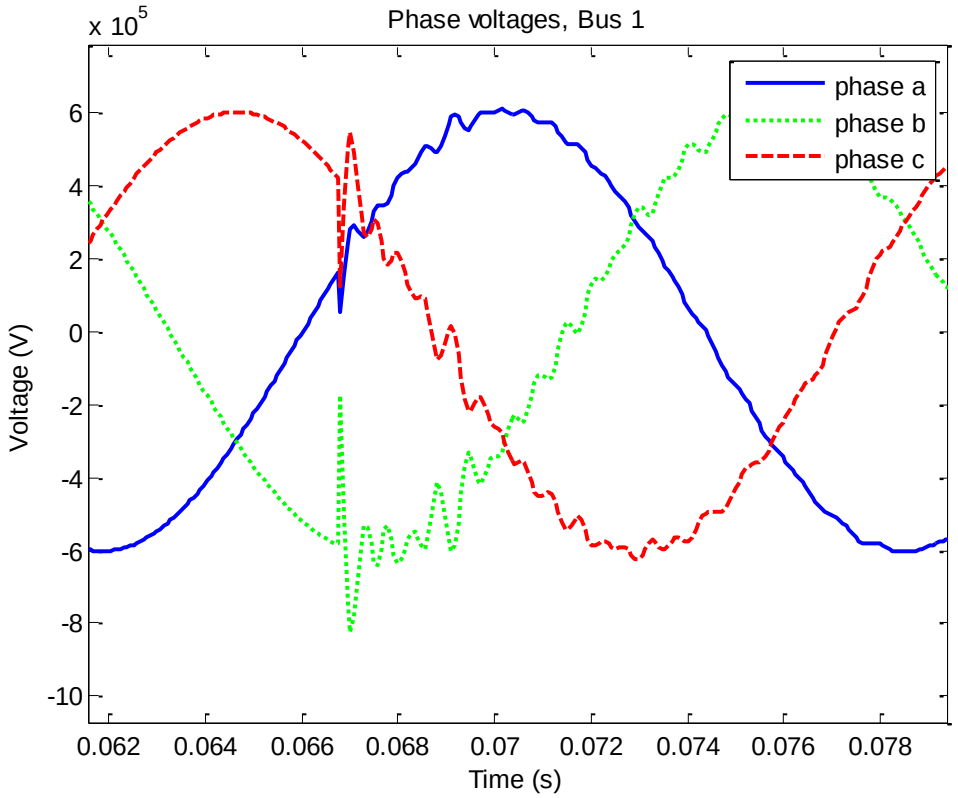

Fig. 4.14 - Bus 1 phase voltage waveforms during transients

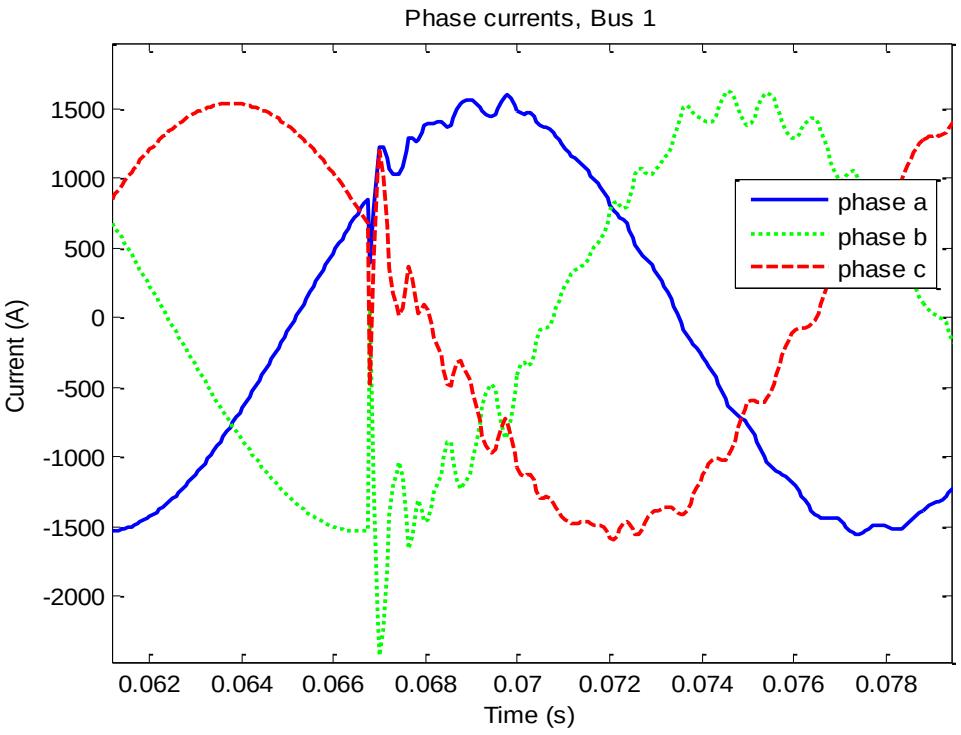

Fig. 4.15 - Bus 1 phase current waveforms during transients

The performance of the fault detection scheme is shown in Fig. 4.16. The calculated synchronization angles do not show any discernible deviation from their steady state values.

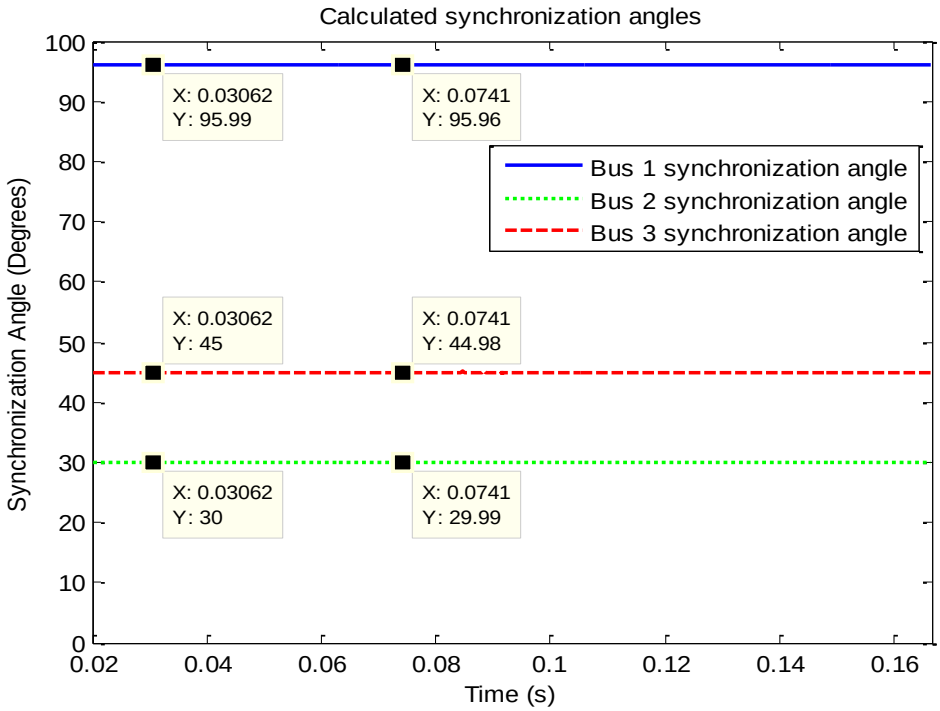

Fig. 4.16 - Synchronization angles during transients

The utility of the detection scheme is obvious from the fact that the algorithm was able to carry out data synchronization during power system transients. The test was repeated with varying load levels and by placing the load at buses 2, 3 and 4. It is worth noting that the fault detection scheme performed well consistently. The algorithm was tested more stringently by placing a high resistance phase-a to phase-b phase fault on line 1 shortly after a load switching transient occurred. The attached load was switched on after cycle number five (0.0833 seconds), whereas the fault was initiated one cycle later at 0.1 seconds.

Table 4.5 - Fault location estimate after transients

Faulted Line	Fault			% Error
	Type	Location	$R_F(\Omega)$	
Line 1	AB	50% from Bus 1	100	0.08

The fault location estimate for the test is shown is Table 4.5 and is consistent with the results shown in Table 4.4.

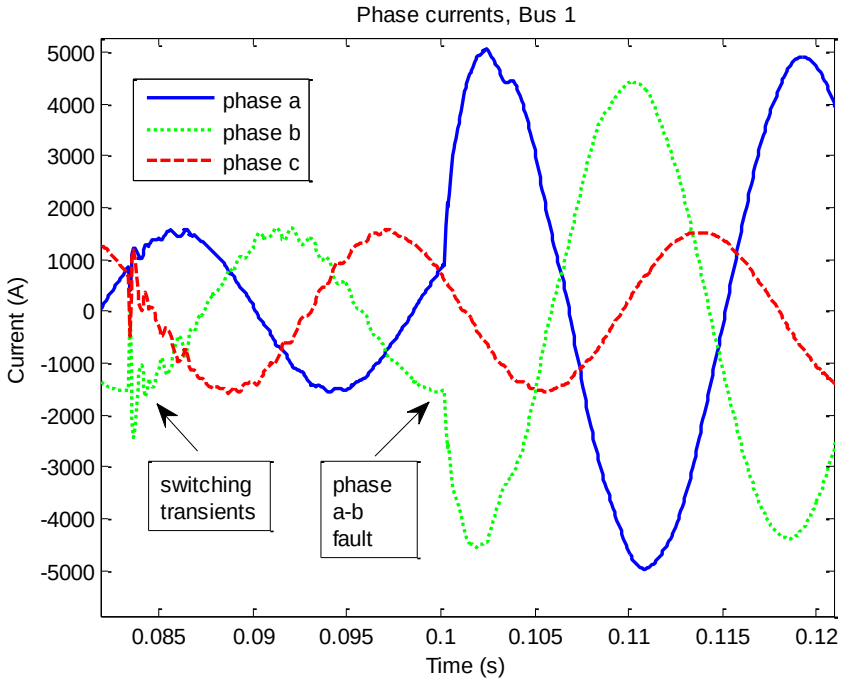

Fig. 4.17 - Bus 1 phase current waveforms during transients and fault

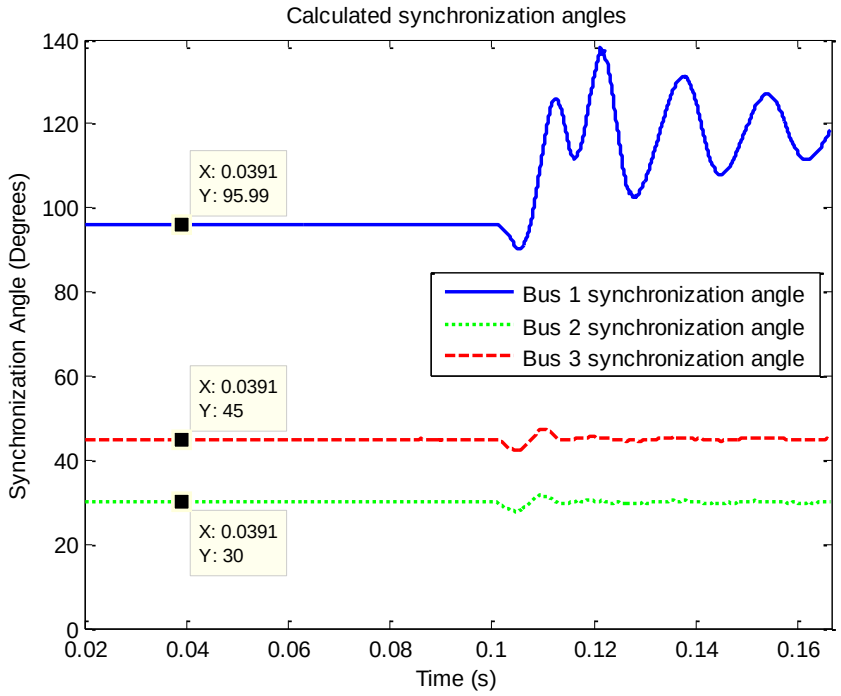

Fig. 4.18 - Synchronization angles during transients and fault

The current waveforms measured at bus 1 during transients and post-fault are shown in Fig. 4.17. The synchronization angles calculated during transients and post-fault are shown in Fig. 4.18. The fault detection scheme was able to successfully differentiate and identify the fault that was placed just one power cycle after initializing switching transients on line 1. This clearly indicates the robustness of the proposed algorithm.

4.2. Algorithm Evaluation for Series and Shunt Compensated Lines.

The two-terminal compensated line system was tested using MATLAB SIMULINK. The 735 kV transmission line used has a length of 200 Km with the compensation devices installed at the mid-point of the line. The transmission line sequence parameters are shown in Table 4.6.

Table 4.6 - Line sequence parameters

Parameter	Positive sequence / Km	Zero sequence / Km
R	0.011223	0.30079
L	0.00086848	0.002988
C	1.34E-08	8.59E-09

The data signals collected from SIMULINK are naturally synchronized. In order to test the performance of the algorithm, the data signals from bus *M* were deliberately delayed by a few samples equivalent to a lag of 30^{o}, whereas data measurement from the FSC device were delayed by a lag of 15^{o}.

The total line positive sequence reactance as per the table above is 65.5Ω. The FSC device simulated with the system is setup to provide 65 percent compensation. Series capacitor and MOV parameters are summarized in Table 4.7. The MOV protection level required to protect the capacitor is set at 2.5 the nominal capacitor voltage. The FSC device is also equipped with damping elements and spark gaps to protect the capacitor against excess heat dissipation with a set point of 30 MJ. Fig.

4.19 shows the SIMULINK model used to simulate series compensation on transmission lines.

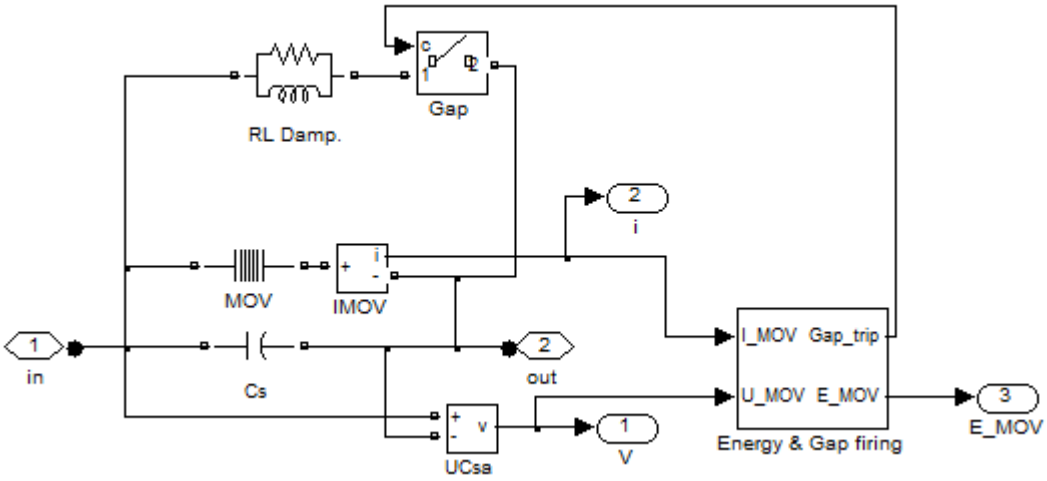

Fig. 4.19 - FSC model in Simulink

Table 4.7 - FSC/MOV parameters

Device	Impedance	MOV protection level
Series Capacitor	42.24Ω (62.8 F)	411840 V

4.2.1. Evaluation of Synchronization and Fault Locating Procedure

The algorithm was first tested with a series compensated device for variable fault impedance and both symmetrical and unsymmetrical faults. A single-phase fault on phase-A with a ground resistance of 150 Ω was placed on the system at 0.1 seconds and at a distance of 0.5 p.u to the right of the FSC. The synchronization angles calculated using post-fault data samples were recorded. The right and the left-sided fault locating procedures were run concurrently each yielding two sets of values. The synchronization angles calculated from the left-sided fault locating procedure are completely rejected by the algorithm due to the conditions described in (3.39), (3.49) and (3.50). At the onset of a fault, the relative synchronization angle δ_r was calculated first and is shown in Fig. 4.20. Only one solution from the two

synchronization angles calculated using the right-sided fault locating subroutine, is corresponding to the actual synchronization angle needed as shown in Fig. 4.21.

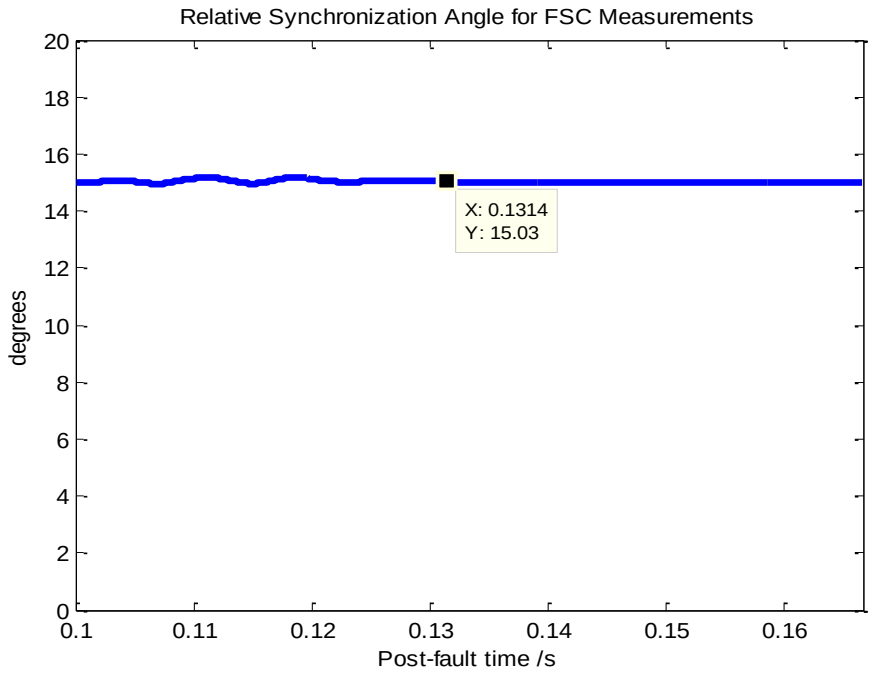

Fig. 4.20 - Relative synchronization angle $\boldsymbol{\delta_r}$, for fsc device

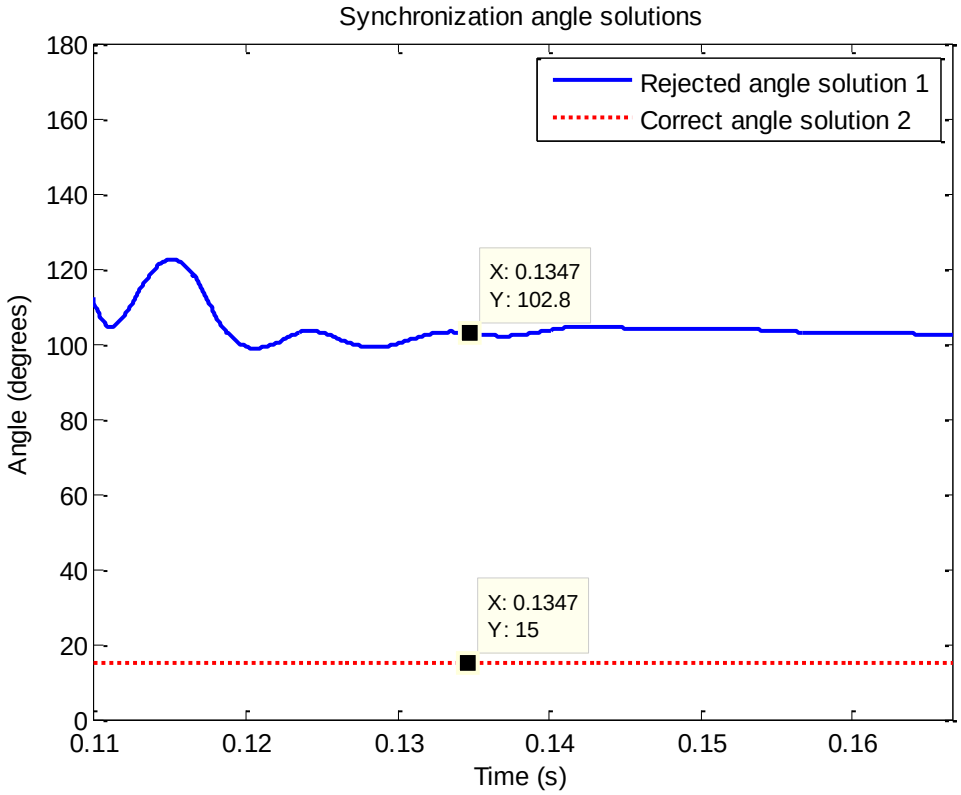

Fig. 4.21 - Synchronization angle solutions for $\boldsymbol{\delta}$

One of the two solutions shown in Fig. 4.21, is again rejected as it does not conform to the conditions described earlier. Using the correct solutions, the absolute synchronization mismatch with respect to bus *N* can be calculated using (3.41) and (3.42).

$$e^{j\delta_C} = e^{j\delta} = e^{j15^o}$$

$$e^{j\delta_M} = e^{j\delta}e^{j\delta_R} = e^{j30^o}$$

The calculated per-unit distance with respect to the location of the SC device using the two angle solutions from the right-sided subroutines is plotted in Fig. 4.22a and Fig. 4.22b. The wrong synchronization angles can be easily rejected based on the conditions described in (3.39), (3.49) and (3.50). The actual real and imaginary components of the per-unit distance to the fault are plotted in the Fig. 4.22b.

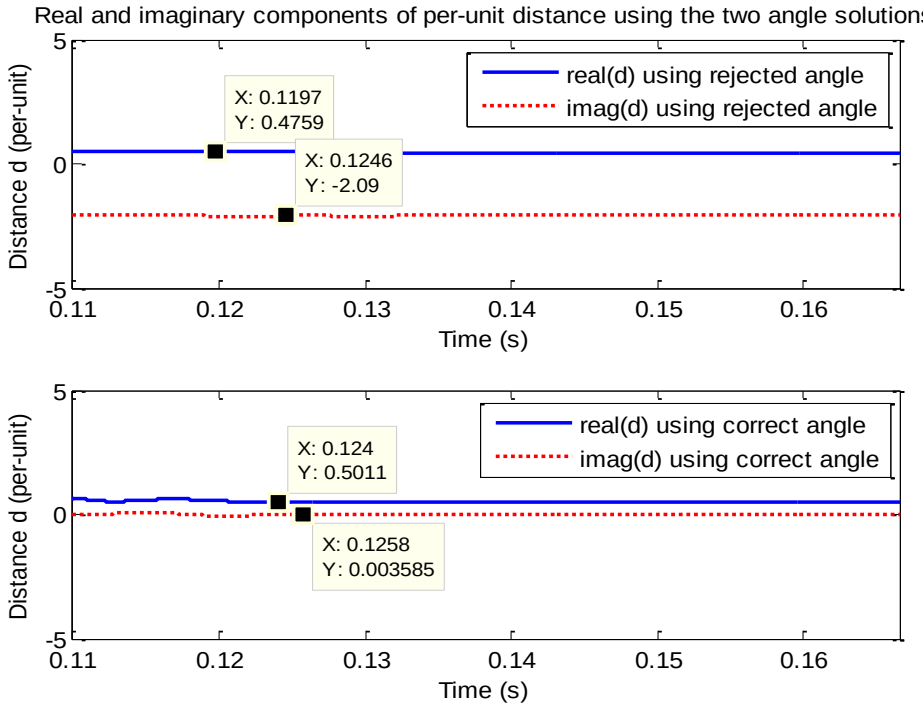

Fig. 4.22 – a) Rejected distance estimate, b) Correct distance estimate

As can be seen from Fig. 4.22, the distance estimates using the first angle can be easily discarded since the imaginary component of distance d exceeds the bounds established in (3.50). The distance estimate using the second angle solution is the actual solution to the fault location problem and complies with the selection procedure.

A similar test was carried using the transmission line compensated with shunt reactor installed midway. The system was tested with a single phase to ground fault on the right side of the shunt reactor and the correct synchronization angle was selected based on the required criteria. Fig. 4.23 shows the correct synchronization angle (δ_M) calculated after the onset of the fault.

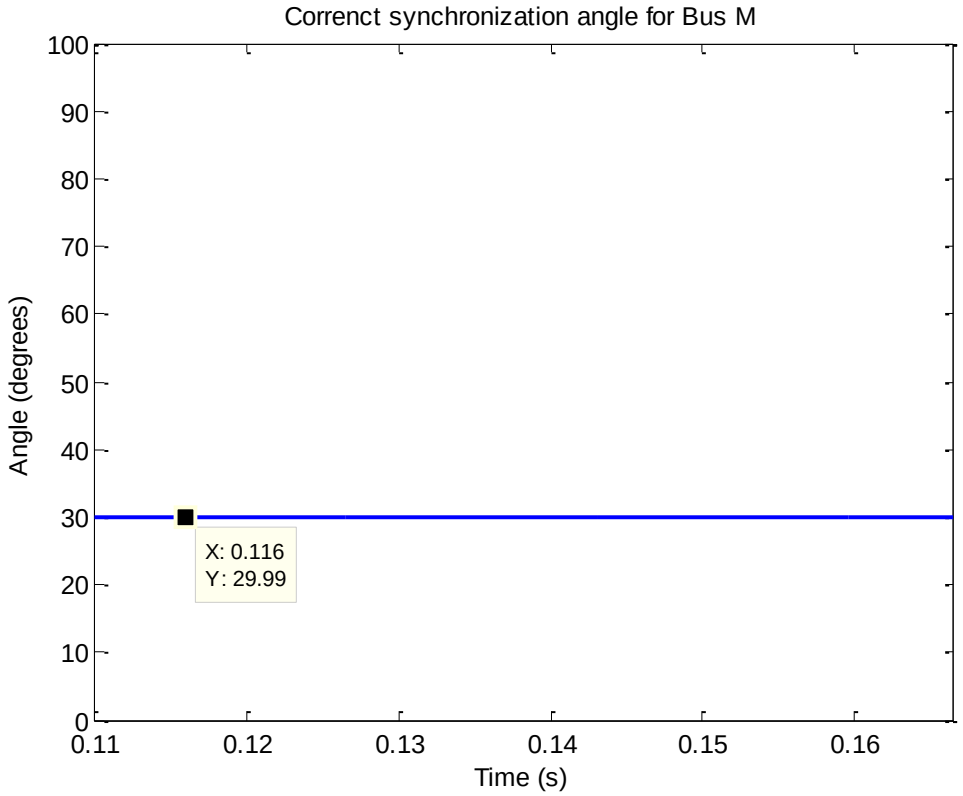

Fig. 4.23 - Correct synchronization angle solution for Bus M

It can be seen from the previous plots that the delivered algorithm can accurately calculate the synchronization angles and pick out the appropriate one with the aid of strong exclusion conditions developed in the earlier section

The corresponding per-unit distance to the fault tested with shunt compensation is plotted in the Fig. 4.24.

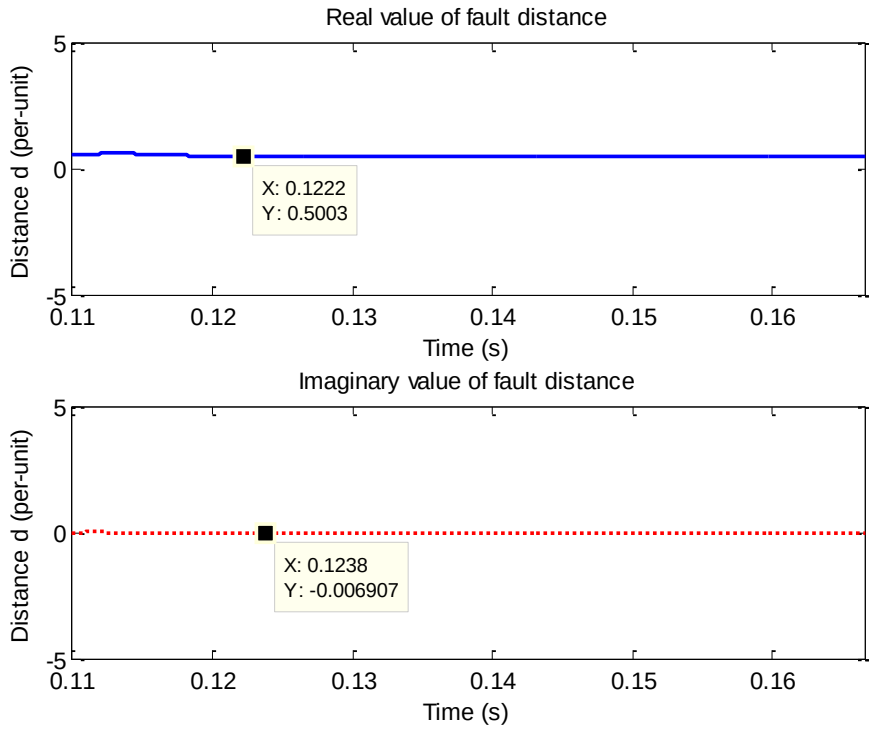

Fig. 4.24 - Real and imaginary values of correct fault distance estimate, shunt compensated lines

Fig. 4.24 clearly shows that the actual per-unit distance to the fault abides by the criteria devolved in (3.49) and (3.50). Different types of faults with various fault resistances were simulated on the transmission line at various distances with respect to the compensating device. For faults occurring on the right side of the device, the distance calculated is with respect to the device itself. For faults occurring on the left side of the compensating device, the distance calculated is with respect to bus *M* in Fig. 3.12. Results from two of the test cases are presented in this section. For each of the fault test cases presented, the phase current waveforms, series capacitor voltage and MOV leakage current waveforms, if applicable, and distance estimates are plotted.

4.2.2. Two-phase-to-ground Fault with FSC Device Installed.

A two-phase-to-ground (A-B-G) was placed on the transmission line with the FSC device installed. The fault was initiated at 0.1 s with a ground resistance of 50Ω and at a distance of 0.5 per-units to right of the compensating device. The resulting waveforms and distance estimate are shown in Figures 4.25 and 4.26.

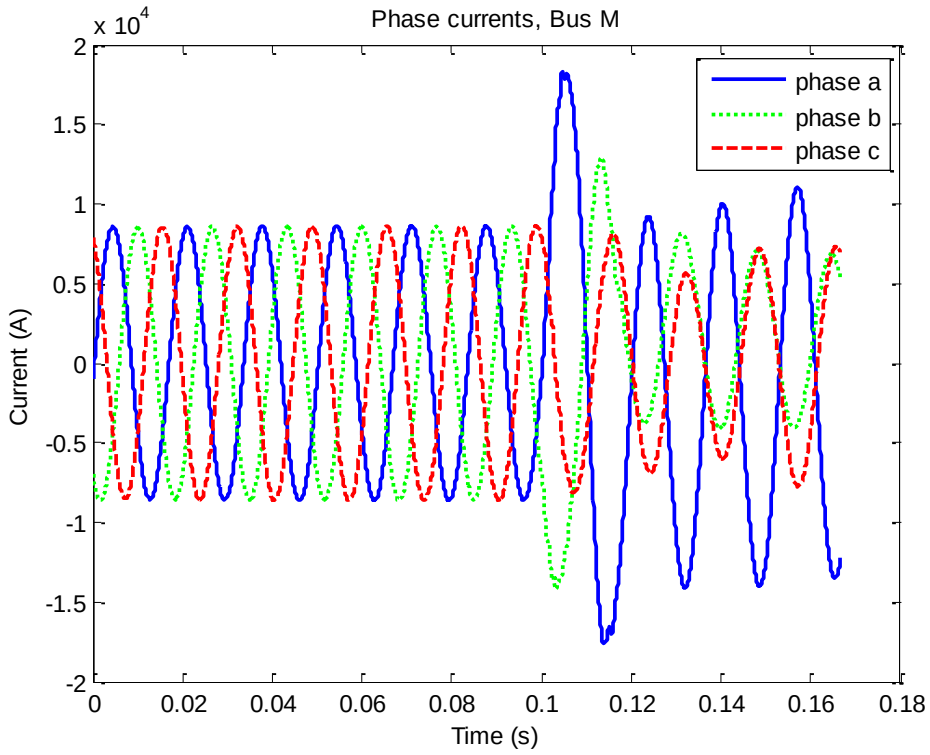

Fig. 4.25 - Phase currents, bus M

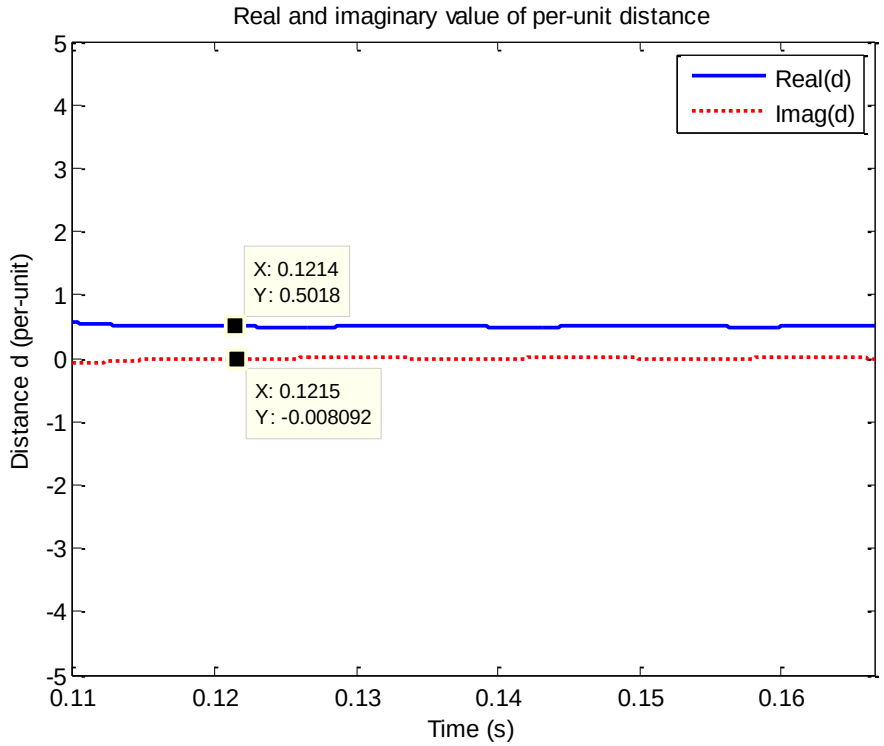

Fig. 4.26 - Real and imaginary components of distance *d*

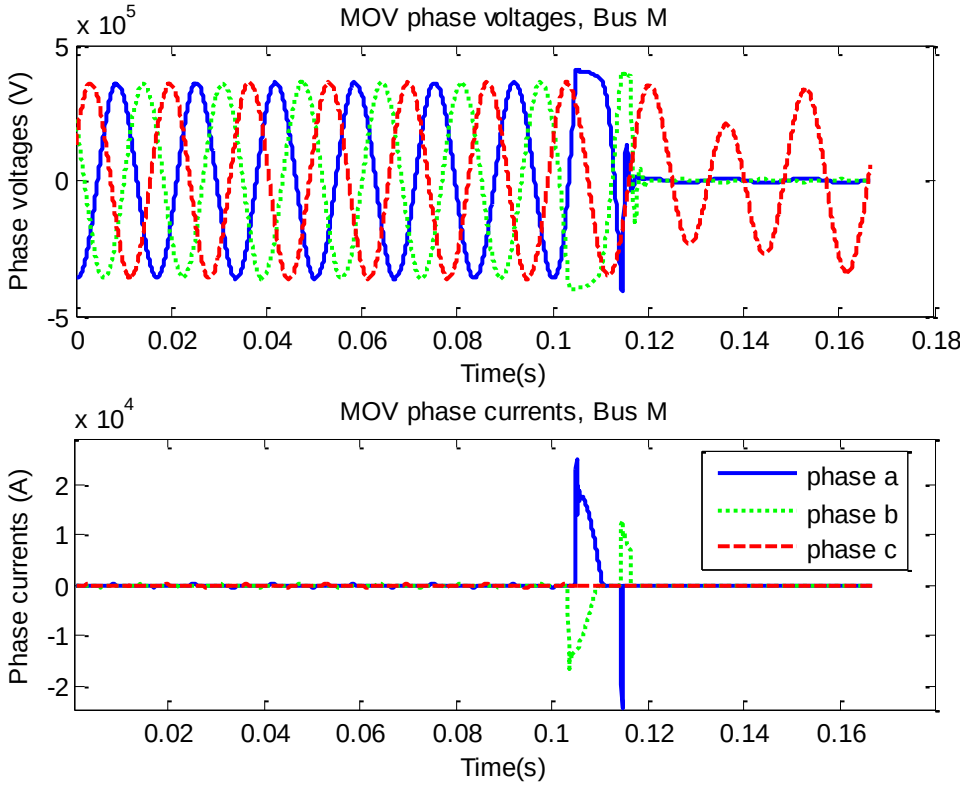

Fig. 4.27 – SC/MOV phase voltages and MOV phase currents

Fig. 4.25 clearly shows the turbulence in phase current wave-forms after the onset of the fault due to the harmonic distortion caused by the FSC device. Despite the turbulence, the fault locating scheme was able to accurately pin-point the distance to the fault in Fig. 4.26 where the solution complies with the selection criteria described in (3.49) and (3.50). Fig. 4.27 shows collapse in phase A and phase B voltages as expected along with the MOV leakage phase currents.

4.2.3. Symmetric Three-phase Fault with Shunt Reactor Installed.

A symmetric three-phase fault at 0.1 s was placed on the line with the shunt reactor installed. The fault was placed at a distance of 0.6 per-unit from the shunt reactor. The resulting phase current waveforms measured at bus *M* and the distance estimates are plotted in the Figures 4.28 and 4.29, respectively. The distance estimate is again consistently accurate.

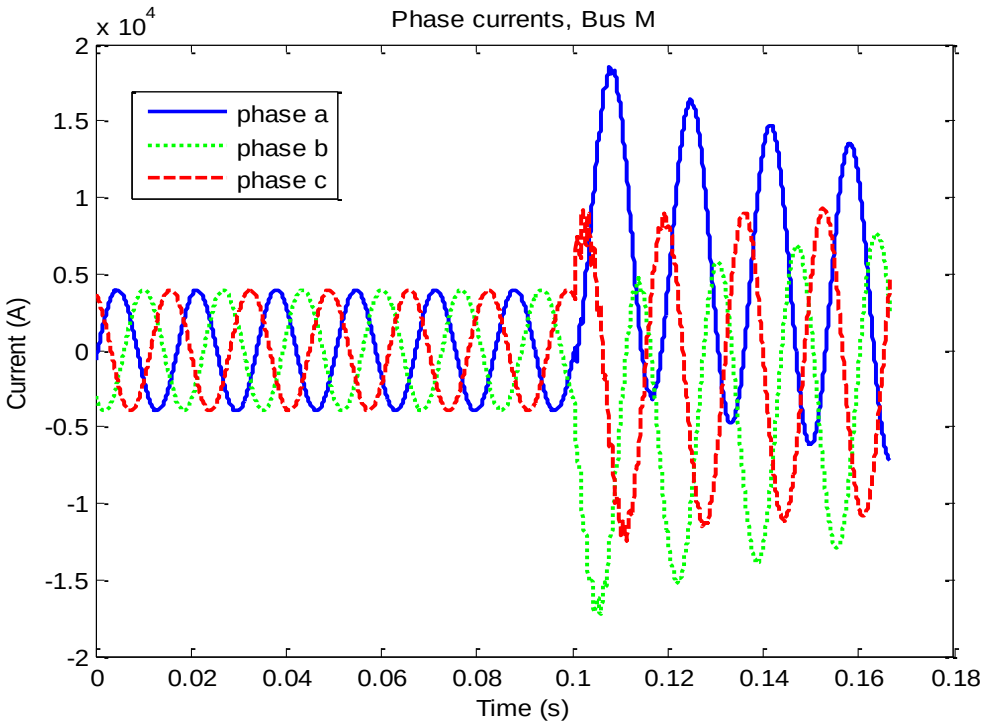

Fig. 4.28 - Phase currents, bus *M*

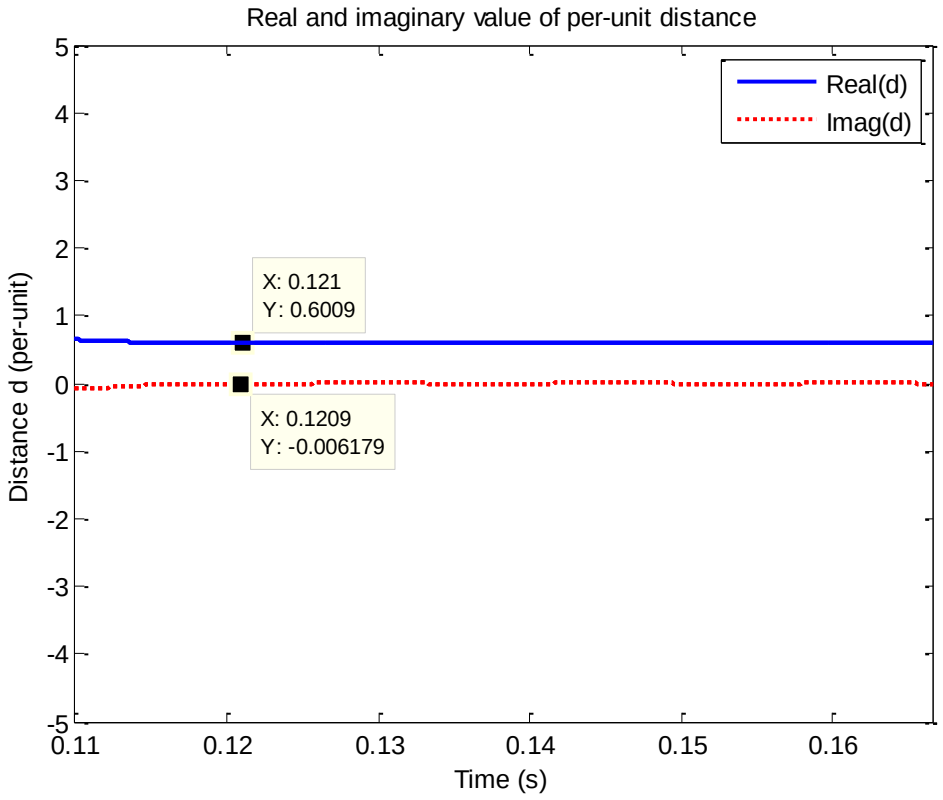

Fig. 4.29 - Fault distance estimate

More tests were carried out including all major fault types with a wide variance of fault resistances. In all cases, the algorithm was able to accurately calculate and pick the appropriate synchronization angle and the corresponding fault distance. The test data is summarized in the Table 4.8.

Table 4.8 - Performance of fault location scheme

Compensation Device	Fault			% Average Absolute Error
	Type	Location (p.u)	$R_F(\Omega)$	
Shunt compensation	AG	+0.2	1	0.012
	BC	-0.3	50	0.024
	ABG	+0.4	100	0.015
	ABC	-0.25	200	0.019
Series Compensation	AG	+0.2	150	0.045
	BC	-0.3	200	0.031
	ABG	+0.4	120	0.014
	ABC	-0.25	250	0.016

Locations with a positive sign indicate faults occurring on the right side of the device and those with a negative sign indicate that faults were placed on the left side of the compensation device.

Chapter 5

Conclusion and Recommendations for Future Work

This Thesis proposes an alternative simple fault detection and location scheme for multiple-terminal transmission lines which can, in principle, be extended to any N-terminal system. The algorithm carries out data synchronization using the known steady-state measurements and utilizes the apparent deviation in synchronization angles to determine a faulted state of operation. The fault location scheme gives accurate estimates for fault distances which are well within the one percent margin. The transmission lines are modeled using distributed-parameter line model to mimic real life system dynamics as closely as possible and substantiate the efficacy of the proposed algorithms. Additionally, the method remains unaffected by power system transients and high fault resistances.

An accurate, non-iterative fault detection and location scheme for series and shunt compensated transmission lines is also proposed in this thesis that utilizes unsynchronized measurements from the two terminals of a transmission line and from the monitoring system if a fixed series compensating (FSC) device is installed. The algorithm carries out data synchronization using the measured post-fault data samples for both symmetrical and unsymmetrical faults. The fault location scheme gives accurate estimates for fault distances which are well within the one percent margin. In principle, the two-end fault locating algorithm can be easily adapted for operation on any standard interconnected power bus system; as long as the transmission line that needs to be protected is enveloped by fault data recorders on line terminals. In case of transmission lines operated with series compensation for enhanced power delivery, the solution to line protection is defined as a three-variable problem that has not been addressed by solutions presented in the literature. Moreover, the fault locating algorithm also caters to scenarios where the system might have alternative compensating devices installed such as shunt reactors.

The main contributions of this thesis can be summarized as:

- Transmission line protection as a fault locating problem: The problem of efficient transmission line protection is modeled as a fault locating procedure that work with unsynchronized measurements.
- Two new fault locating algorithms are developed: A fault locating algorithm for multi-terminal transmission line with an in-built fault detection mechanism; and a fault locating scheme for series and shunt compensated transmission lines.
- The accuracy of the proposed fault locating schemes is not affected by fault location, fault type and the level of pre-fault power flow. Neither is it affected by source impedance variations behind the relay terminals.
- The works done in this thesis has been presented in two journal papers submitted to *IEEE Transactions on Power Delivery* and are currently under review. The third research paper submitted to *IEEE Power & Energy Society General Meting 2013* has been accepted for publication.

The fault locating algorithms also perform well in the vicinity of power system transients as well as in the presence of non-linear over-voltage protection devices such as metal oxide varistors (MOVs) that are commonly installed with series compensating capacitors.

Future work on the topic of transmission line fault location could focus on designing algorithms to work with un-transposed transmission lines. Transposition of transmission lines ensure that the sequence components of the line's impedance are not mutually coupled which enables the circuit sequence networks to be dealt with independently, as was shown in the literature review. Un-transposed lines have the effect of inducing inter-network coupling between sequence impedances which convolutes the fault location process. It would be necessary to resort to phase voltage, current and distributed impedance parameters when designing fault locators for un-transposed lines.

Most of the fault locating schemes designed to work with series-compensated lines utilize the exponential function described earlier to approximate the phase-voltage drop across the capacitors. The use of FSC monitoring devices for fault locating algorithms obviates the need for predictive impedance functions and

enhances the accuracy of fault distance estimations. The error in the calculated phase-voltage drop using the current mathematical model accentuates as the FSC device is placed further away from the reference line terminal. This is due to the fact that the dynamic impedance of the FSC device is a function of the through-current which cannot be pre-determined analytically for various short-circuit conditions. The problematic issue of dynamic FSC impedance can be tackled by designing an accurate predictive impedance function which can track the behavior of series-compensated devices more closely.

References

[1] Johns, A.T. and Salman S.K., *Digital Protection for Power Systems*, Peter Peregrinus Publications, 1995.

[2] General Electric. (undated). Distance Relay Fundamentals. [Online]. Viewed 2011 December. Available: http://store.gedigitalenergy.com/faq

[3] Phadke, A.G., Ibrahim, M. and Hlibka, T., "Fundamental basis for distance relaying with symmetrical components," *Power Apparatus and Systems, IEEE Transactions on* , vol.96, no.2, pp. 635- 646, Mar 1977.

[4] Erezzaghi, M.E. and Crossley, P.A., "The effect of high resistance faults on a distance relay," *Power Engineering Society General Meeting, 2003, IEEE* , vol.4, no., pp. 4 vol. 2666, 13-17 July 2003.

[5] Pipes, Louis A., "Transient Analysis of Symmetrical Networks by the Method of Symmetrical Components," *American Institute of Electrical Engineers, Transactions of the* , vol.59, no.8, pp.457-459, Aug. 1940.

[6] Zou Gui-bin and Gao Hou-lei, "The current differential and travelling wave based algorithm for ultra high speed hybrid protection," *Electric Utility Deregulation and Restructuring and Power Technologies, 2008. DRPT 2008. Third International Conference on* , vol., no., pp.1693-1697, 6-9 April 2008.

[7] Arnborg, S., Andersson, G., Hill, D.J. and Hiskens, I.A., "On influence of load modelling for undervoltage load shedding studies," *Power Systems, IEEE Transactions on* , vol.13, no.2, pp.395-400, May 1998.

[8] Osman, A.H., Abdelazim, T. and Malik, O.P., "Transmission line distance relaying using on-line trained neural networks," *Power Delivery, IEEE Transactions on* , vol.20, no.2, pp. 1257- 1264, April 2005.

[9] Osman, A.H. and Malik, O.P., "Protection of parallel transmission lines using wavelet transform," *Power Delivery, IEEE Transactions on* , vol.19, no.1, pp. 49-55, Jan. 2004.

[10] Chengzong Pang and Kezunovic, M., "Fast Distance Relay Scheme for Detecting Symmetrical Fault During Power Swing," *Power Delivery, IEEE Transactions on* , vol.25, no.4, pp.2205-2212, Oct. 2010.

[11] AlFuhaid, A.S. and El-Sayed, M.A., "A recursive least-squares digital distance relaying algorithm," *Power Delivery, IEEE Transactions on* , vol.14, no.4, pp.1257-1262, Oct 1999.

[12] Cook, V., "Fundamental aspects of fault location algorithms used in distance protection," *Generation, Transmission and Distribution, IEE Proceedings C* ,

vol.133, no.6, pp.359-368, September 1986.

[13] Shateri, H. and Jamali, S., "Distance relays ideal tripping characteristic in presence of directly connected load to transmission lines," *Power Systems Conference and Exposition, 2009. PSCE '09. IEEE/PES* , vol., no., pp.1-6, 15-18 March 2009.

[14] Abidin, A.F. and Shareef, H., "Adaptive Distance Relay During Voltage Collapse", *International Review of Electrical Engineering*, May-June 2010.

[15] P. Pawelczak, K. Nolan, S. Oh, and D. Cabric, "Cognitive Radio: Ten Years of Experimentation and Development," *IEEE Communications Magazine*, vol. 55, pp. 523-531, March 2011.

[16] Izykowski, J., Rosolowski, E. and Saha, M., "Post-fault analysis of operation of distance protective relays of power transmission lines," *Power Tech, 2005 IEEE Russia* , vol., no., pp.1-7, 27-30 June 2005.

[17] Sidhu, T.S., Baltazar, D.S., Palomino, R.M. and Sachdev, M.S., "A new approach for calculating zone-2 setting of distance relays and its use in an adaptive protection system," *Power Delivery, IEEE Transactions on* , vol.19, no.1, pp. 70- 77, Jan. 2004.

[18] Chul-Hwan Kim, Jeong-Yong Heo and Aggarwal, R.K., "An enhanced zone 3 algorithm of a distance relay using transient components and state diagram," *Power Engineering Society General Meeting*, 2004. IEEE , vol., no., pp. 99 Vol.1, 6-10 June 2004.

[19] Seong-Il Lim, Chen-Ching Liu, Seung-Jae Lee, Myeon-Song Choi and Seong-Jeong Rim, "Blocking of Zone 3 Relays to Prevent Cascaded Events," *Power Systems, IEEE Transactions on* , vol.23, no.2, pp.747-754, May 2008.

[20] Farid Bin Abidin, Ahmad and Mohamed, Azah, "On the use of voltage stability index to prevent undesirable distance relay operation during voltage instability," *Environment and Electrical Engineering (EEEIC)*, 2010 9th International Conference on , vol., no., pp.384-387, 16-19 May 2010.

[21] Abdlrahem, A.A. and Sherwali, H.H., "Modelling of numerical distance relays using MATLAB," Industrial Electronics & Applications, 2009. ISIEA 2009. *IEEE Symposium on* , vol.1, no., pp.389-393, 4-6 Oct. 2009.

[22] Chi-Shan Yu, "A discrete Fourier transform-based adaptive mimic phasor estimator for distance relaying applications," *Power Delivery, IEEE Transactions on* , vol.21, no.4, pp.1836-1846, Oct. 2006.

[23] Smith, C.M. and Nair, N.-K.C., "Evaluation of Discrete Wavelet Transform implementation for protective relaying," TENCON 2009 - 2009 IEEE Region 10

Conference , vol., no., pp.1-5, 23-26 Jan. 2009.

[24] Chi-Shan Yu, Yi-Sheng Huang and Joe-Air Jiang, "A Full- and Half-Cycle DFT-based technique for fault current filtering," Industrial Technology (ICIT), *2010 IEEE International Conference on* , vol., no., pp.859-864, 14-17 March 2010.

[25] Sidhu, T.S., Xudong Zhang and Balamourougan, V., "A new half-cycle phasor estimation algorithm," *Power Delivery, IEEE Transactions on* , vol.20, no.2, pp. 1299- 1305, April 2005.

[26] Ha Heng-xu, Zhang Bao-hui, Yuan Wen-guang and Li Wei-shuo, "Novel algorithm of variable-window Fourier transform based high-speed distance relay for EHV transmission lines," Power System Technology, 2004. PowerCon 2004. *2004 International Conference on* , vol.1, no., pp. 6- 11 Vol.1, 21-24 Nov. 2004.

[27] Jun-Zhe Yang and Chih-Wen Liu, "Complete elimination of DC offset in current signals for relaying applications," *Power Engineering Society Winter Meeting*, 2000. IEEE , vol.3, no., pp.1933-1938 vol.3, 23-27 Jan 2000.

[28] Ching-Shan Chen, Chih-Wen Liu and Jiang, J.-A., "Application of combined adaptive Fourier filtering technique and fault detector to fast distance protection," *Power Delivery, IEEE Transactions on* , vol.21, no.2, pp. 619- 626, April 2006.

[29] Kundur, P., Paserba, J., Ajjarapu, V., Andersson, G., Bose, A., Canizares, C., Hatziargyriou, N., Hill, D., Stankovic, A., Taylor, C., Van Cutsem, T. and Vittal, V., "Definition and classification of power system stability IEEE/CIGRE joint task force on stability terms and definitions," *Power Systems, IEEE Transactions on* , vol.19, no.3, pp. 1387- 1401, Aug. 2004.

[30] Costas, V. and Cutsem, T. V.; *Voltage stability of Electric Power Systems*, Kluwer Academic Publishers, 1998.

[31] Esmaeilian, A., Mohseninezhad, M., Doostizadeh, M. and Khanabadi, M., "A precise PMU based fault location method for multi terminal transmission line using voltage and current measurement," Environment and Electrical Engineering (EEEIC), *2011 10th International Conference on* , vol., no., pp.1-4, 8-11 May 2011.

[32] Kase, T., Kurosawa, Y. and Amo, H., "Charging Current Compensation for Distance Protection," *Power Delivery, IEEE Transactions on* , vol.23, no.1, pp.124-131, Jan. 2008.

[33] Aggarwal, R.K., Coury, D.V., Johns, A.T. and Kalam, A., "A practical approach to accurate fault location on extra high voltage teed feeders," *Power Delivery, IEEE Transactions on* , vol.8, no.3, pp.874-883, July 1993.

[34] Ching-Shan Chen, Chih-Wen Liu and Joe-Air Jiang, "Three-terminal transmission line protection using synchronized voltage and current phasor measurements," *Transmission and Distribution Conference and Exhibition 2002: Asia Pacific*. IEEE/PES , vol.3, no., pp. 1727- 1732 vol.3, 6-10 Oct. 2002.

[35] Brahma, S.M., "Fault location scheme for a multi-terminal transmission line using synchronized Voltage measurements," *Power Delivery, IEEE Transactions on* , vol.20, no.2, pp. 1325- 1331, April 2005.

[36] Brahma, S.M., "New Fault Location Scheme for a Two- Terminal Transmission Line Using Synchronized Phasor Measurements," *Transmission and Distribution Conference and Exhibition*, 2005/2006 IEEE PES , vol., no., pp.853-857, 21-24 May 2006.

[37] Izykowski, J., Molag, R., Rosolowski, E. and Saha, M.M., "Accurate location of faults on power transmission lines with use of two-end unsynchronized measurements," *Power Delivery, IEEE Transactions on* , vol.21, no.2, pp. 627-633, April 2006.

[38] Izykowski, J. and Rosolowski, E., "Accurate non-iterative fault location algorithm for three-terminal line," Electrical and Electronics Engineering, 2009. ELECO 2009. *International Conference on* , vol., no., pp.I-154-I-158, 5-8 Nov. 2009.

[39] Chi-Shan Yu, "An Unsynchronized Measurements Correction Method for Two-Terminal Fault-Location Problems," *Power Delivery, IEEE Transactions on* , vol.25, no.3, pp.1325-1333, July 2010.

[40] Sanderson, J.V.R., Santana, R.G.R. and Al-Fakri, B., "Improved directional comparison based algorithm for protection of multi-terminal transmission lines," Developments in Power System Protection, 1993., *Fifth International Conference on* , vol., no., pp.153-156, 1993.

[41] Dalcastagne, A.L., Filho, S.N., Zurn, H.H. and Seara, R., "An Iterative Two-Terminal Fault-Location Method Based on Unsynchronized Phasors," *Power Delivery, IEEE Transactions on* , vol.23, no.4, pp.2318-2329, Oct. 2008.

[42] Kizilcay, M. and La Seta, P., "A new unsynchronized two-terminals fault location method on series compensated lines," *Power Tech, 2005 IEEE Russia* , vol., no., pp.1-7, 27-30 June 2005.

[43] Ching-Shan Chen, Chih-Wen Liu and Jiang, J.-A., "Application of combined adaptive Fourier filtering technique and fault detector to fast distance protection," *Power Delivery, IEEE Transactions on* , vol.21, no.2, pp. 619- 626, April 2006.

[44] Chi-Shan Yu, "A discrete Fourier transform-based adaptive mimic phasor estimator for distance relaying applications," *Power Delivery, IEEE Transactions on* , vol.21, no.4, pp.1836-1846, Oct. 2006.

[45] Ha Heng-xu, Zhang Bao-hui, Yuan Wen-guang and Li Wei-shuo, "Novel algorithm of variable-window Fourier transform based high-speed distance relay for EHV transmission lines," Power System Technology, 2004. PowerCon 2004. *2004 International Conference on* , vol.1, no., pp. 6- 11 Vol.1, 21-24 Nov. 2004.

[46] Osman, A.H., Abdelazim, T. and Malik, O.P., "Transmission line distance relaying using on-line trained neural networks," *Power Delivery, IEEE Transactions on* , vol.20, no.2, pp. 1257- 1264, April 2005.

[47] Esmaeilian, A., Mohseninezhad, M., Doostizadeh, M. and Khanabadi, M., "A precise PMU based fault location method for multi terminal transmission line using voltage and current measurement," Environment and Electrical Engineering (EEEIC), *2011 10th International Conference on* , vol., no., pp.1-4, 8-11 May 2011.

[48] Saha, M.M., Izykowski, J. and Rosolowski, E., "Fault Location on Power Networks", *Springer-Verlag London Limited Publications*, 2010.

[49] Saha, M.M., Izykowski, J., Rosolowski, E. and Kasztenny, B., "A new accurate fault locating algorithm for series compensated lines," *Power Engineering Society 1999 Winter Meeting*, IEEE , vol.2, no., pp. 956 vol.2, 31 Jan-4 Feb 1999.

[50] Chi-Shan Yu, Chih-Wen Liu and Joe-Air Jiang, "A new fault location algorithm for series compensated lines using synchronized phasor measurements," *Power Engineering Society Summer Meeting*, 2000. IEEE , vol.3, no., pp.1350-1354 vol. 3, 2000.

[51] Chi-Shan Yu, Chih-Wen Liu, Sun-Li Yu and Joe-Air Jiang, "A new PMU-based fault location algorithm for series compensated lines," *Power Delivery, IEEE Transactions on* , vol.17, no.1, pp.33-46, Jan 2002.

[52] Xu, Z.Y., Du, Z.Q., Ran, L., Wu, Y.K., Yang, Q.X. and He, J.L., "A Current Differential Relay for a 1000-kV UHV Transmission Line," *Power Delivery, IEEE Transactions on* , vol.22, no.3, pp.1392-1399, July 2007.

[53] Izykowski, J., Rosolowski, E., Balcerek, P., Fulczyk, M. and Saha, M.M., "Fault Location on Double-Circuit Series-Compensated Lines Using Two-End Unsynchronized Measurements," *Power Delivery, IEEE Transactions on* , vol.26, no.4, pp.2072-2080, Oct. 2011.

[54] de Oliveira, A.L.P., "Fixed series compensation monitoring system," *Transmission and Distribution Conference and Exposition: Latin*

America, 2008 IEEE/PES , vol., no., pp.1-5, 13-15 Aug. 2008.

[55] Rosolowski, E., Izykowski, J., Pierz, P., Fulczyk, M., Balcerek, P. and Saha, M.M., "High voltage series-compensated transmission line - evaluation of new distance protection," High Voltage Engineering and Application (ICHVE), *2010 International Conference on* , vol., no., pp.513-516, 11-14 Oct. 2010.

[56] Su, B., Dong, X.Z. and Sun, Y.Z., "A Simplified Accurate Algorithm For The Calculation Of Series Capacitor Voltage," *Study Committee B5 Colloquium* , Calgary, Canada, Sep. 2005.

[57] Mulder, M.C., Erickson, D.C. and Courts, A.L., "A Microprocessor Based Monitoring and Protection System for a Series Capacitor Zn0 Nonlinear Bypass Resistor," *Power Apparatus and Systems, IEEE Transactions on* , vol.PAS-99, no.5, pp.1879-1885, Sept. 1980.

[58] Izykowski, J., Rosolowski, E., Balcerek, P., Fulczyk, M. and Saha, M.M., "Accurate Noniterative Fault-Location Algorithm Utilizing Two-End Unsynchronized Measurements," *Power Delivery, IEEE Transactions on* , vol.26, no.2, pp.547-555, April 2011.

[59] Hussain, S. and Osman, A.H., "Fault Location on Series-Compensated Lines Using Unsynchronized Measurements," *IEEE Power & Energy Society General Meeting*, 21-25 July 2013.

[60] Hussain, S. and Osman, A.H., "Series and Shunt-Compensated Transmission Line Fault Location Using Unsynchronized Measurements," *Power Delivery, IEEE Transactions on* , April. 2013 (Under review).

[61] Hussain, S. and Osman, A.H., "Fault Location Scheme for a Multi-Terminal Transmission Line System Using Unsynchronized Measurements," *Power Delivery, IEEE Transactions on* , June. 2012 (Under review).

Vita

Shoaib Hussain was born in 1986 in Karachi, Islamic Republic of Pakistan. He completed O-levels from the Westminster School, and A-levels from Arab Unity School in Dubai. He received his Bachelor of Science in Electrical Engineering from American University of Sharjah in Fall 2010. In Spring 2011, Shoaib joined the Masters of Science program in Electrical Engineering at American University of Sharjah where he worked as a Graduate Teaching Assistant. During this time, he pursued his research interests which include digital protection relaying and application of computer technology in power system protection. Currently, Shoaib is employed as a Lab Engineer at Abu Dhabi Polytechnic (Institute of Applied Technology) in the Department of Electro-Mechanical Engineering Technology.